ÉCOLE CENTRALE MARSEILLE
UNIVERSITÉ PAUL CÉZANNE (AIX-MARSEILLE III)

N° attribué par la bibliothèque
XXXX

TITRE :

DÉTECTION ET CARACTÉRISATION DE CONTOURS DANS DES IMAGES PAR LES MÉTHODES À SOUS-ESPACES

THÈSE
pour obtenir le grade de DOCTEUR

délivré conjointement par L'ÉCOLE CENTRALE MARSEILLE
et UNIVERSITÉ PAUL CÉZANNE (AIX-MARSEILLE III)

Discipline : Optique, Photonique et Traitement d'Image

Effectuée à l'INSTITUT FRESNEL
Présentée et soutenue publiquement par :

Haiping JIANG

le 27 Septembre 2011

Directeurs de thèse : Pr. Salah Bourennane
Co-Directeurs de thèse : Mme. Caroline Fossati
École Doctorale : Physique et Sciences de la Matière

JURY :

Rapporteurs :	Pr. Yide WANG	Ecole Polytechnique de l'Université de Nantes
	M. Karim ABED-MERAIM	Télécom ParisTech
Examinateurs :	M. Jean-Pierre SESSAREGO	DR CNRS, Lab. de Mécanique et d'Acoustique -CNRS
	M. Julien MAROT	Université Paul Cézanne (Aix-Marseille III)
Directeurs de thèse :	Pr. Salah BOURENNANE	École Centrale Marseille, Institut Fresnel
	Mme. Caroline FOSSATI	École Centrale Marseille, Institut Fresnel

ANNEE : 2011

ÉCOLE CENTRALE MARSEILLE
UNIVERSITÉ PAUL CÉZANNE (AIX-MARSEILLE III)

TITLE :

DETECTION AND CHARACTERIZATION OF CONTOURS IN IMAGES BY SUBSPACE-BASED METHODS

THESIS
to obtain the degree of DOCTOR

issued jointly by ÉCOLE CENTRALE MARSEILLE
and UNIVERSITÉ PAUL CÉZANNE (AIX-MARSEILLE III)

Discipline : Optics, Photonics and Image Processing

Carried out at INSTITUTE FRESNEL
Presented and defended publicly by :

Haiping JIANG

on September 27th 2011

Thesis advisor : Pr. Salah Bourennane
Thesis co-advisor : Mme. Caroline Fossati
Doctoral school : Physics and Material Sciences

COMMITTEE :

Reviewers :	Pr. Yide Wang	Ecole Polytechnique de l'Université de Nantes
	Mr. Karim ABED-MERAIM	Télécom ParisTech
Examiners :	Mr. Jean-Pierre SESSAREGO	DR CNRS, Lab. de Mécanique et d'Acoustique -CNRS
	Mr. Julien Marot	Université Paul Cézanne (Aix-Marseille III)
Thesis advisors :	Pr. Salah Bourennane	École Centrale Marseille, Institut Fresnel
	Mme. Caroline Fossati	École Centrale Marseille, Institut Fresnel

YEAR : 2011

Résumé

LA description de formes est un objectif important de la vision par ordinateur et du traitement d'image. Les contours linéaires, triangulaires et circulaires sont les plus recherchés en traitement d'images. En partant de ce constant, l'objectif visé par cette thèse est d'aboutir à des méthodes de détection et de caractérisation de contours tels que des lignes droites, des cercles, des lignes et des cercles flous, des triangles flous. Ceci en exploitant les méthodes haute résolution du traitement d'antenne, qui sont fondées sur des méthodes à sous-espaces.

Dans le contexte des méthodes de type "contour", il a été prouvé que le transfert de méthodes provenant du domaine du traitement d'antenne, et dédiées à l'origine à l'estimation de fréquences, est très profitable. Ces méthodes sont fondées sur une approche par sous-espaces et visent à retrouver les paramètres de sources tels que la direction d'arrivée sur une antenne des fronts d'onde qu'elles émettent. Ainsi, nous adaptons un formalisme original pour générer des signaux qui suivent un modèle du traitement d'antenne en simulant la propagation d'une onde. Un modèle pour une image conduit à un modèle adéquat pour le signal généré à partir de cette image sur des capteurs virtuels, et les méthodes haute résolution du traitement d'antenne sont adaptées pour estimer les paramètres de contours, tels l'orientation et l'offset pour une ligne droite, ou le centre et le rayon pour un cercle. En particulier, le cas où l'image est dégradée par un bruit corrélé est considéré, et des statistiques d'ordre supérieur sont adaptées pour estimer les paramètres des contours.

Ensuite, nous considérons l'estimation de contours étoilés en émettant l'hypothèse que les coordonnées radiales des pixels du contour s'expriment comme une somme de sinusoïdes amorties ; nous exploitons pour cela une méthode de génération de signal sur une antenne virtuelle circulaire. En partant d'un cercle d'initialisation, la méthode proposée estime les déviations des coordonnées radiales des pixels autour du cercle d'initialisation, avec une méthode qui est robuste au bruit et aux fortes concavités. Nous adoptons une méthode de caractérisation qui fournit les paramètres caractéristiques des sinusoides amorties qui composent le contour. En particulier, nous incluons une étape de raffinement fondée sur une méthode d'optimisation, qui améliore l'adéquation des signaux générés au modèle proposé. On effectue une comparaison des résultats obtenus avec la méthode gradient et la méthode GVF (Gradient Vector Flow).

Finalement, des contours flous sont étudiés. Ils sont modélisés par une distribution Gaussienne de niveaux de gris. Un modèle de signal correspondant à un contour flou est calculé.

Ainsi, nous proposons une approche nouvelle pour détecter des contours flous. En particulier, nous proposons des méthodes par sous-espaces du traitement d'antenne qui sont dédiées à l'origine à la caractérisation de sources incohérentes, pour estimer l'orientation et l'étendue de contours flous linéaires et triangulaires. Des algorithmes d'optimisation sont aussi adaptés pour estimer certains paramètres des contours, tels que l'étendue.

Mots clés : Contour, Détection, Caracterisation, Haute résolution, Cumulants, Contour flou, Traitement d'antenne, Optimisation, Contour linéaire, Contour triangulaire, Contour circulaire, Approximation.

Abstract

SHAPE description is an important goal of computational vision and image processing. Linear, triangular and circular features are most commonly sought in image processing. Based on these facts, this thesis aims mainly at detecting and characterizing contours, such as straight line, circle, blurred line, blurred circle, blurred triangle in images, by exploiting high resolution subspace-based methods.

In the frame of contour-based methods, it has been proved that the transfer of array processing and frequency retrieval are profitable. They rely on subspace approaches to retrieve source parameters such as direction of arrival. Therefore, we adapt an original formalism to generate array signals from an image by simulating wave propagation. After modelling the image data, subspace-based high-resolution methods are used for estimating the parameters, for example, the angle and the offset (for straight line), the radius and center (for circle). In particular, the environment with correlated Gaussian noise is considered, and higher-order statistics methods are proposed to estimate contour's parameters.

Then, we discuss the problem of recovering a star-shaped contour with the assumption that the contour coordinates can be decomposed into damped sinusoids. We continue to exploit the same signal generation method derived from the array processing paradigm. Starting from an initialization circle, the proposed method estimates the deviations of the pixel coordinates around an initialization circle with a method which copes with noise and strongly concave contours. We adopt a signal characterization method which provides the parameters of damped sinusoids. In particular, we include a refinement step based on an optimization method which improves the adequation of the collected signals to the proposed model. The novel proposed method is compared with another signal characterization approach using gradient method, and with GVF (Gradient Vector Flow) method.

At last, blurred contours with Gaussian distribution of grey level value are also investigated. We derive a signal processing model out of an image which contains a blurred contour, and provide a new viewpoint to detect blurred contours for the first time. Especially, we propose subspace-based methods of array processing which are originally dedicated to multiple incoherently distributed sources, to retrieve the orientation and spread parameters of blurred linear and triangular-like contours. Optimization algorithms are also adapted to estimate the parameters.

Key words : Contour, Detection, Characterization, High-resolution, Cumulants, Blurred contour, Array processing, Optimization, Linear contour, Triangular contour, Circular contour, Approximation.

Acknowledgement

THE work in this thesis was carried out at GSM Group (Groupe Signaux Multidimensionnels) of Institut Fresnel, in Marseille, France. I am greatly indebted to many people, who have provided endless support and help.

First, I wish to express my sincerest gratitude to the China Scholarship Council and Ecole Centrale Marseille. They have offered me the great opportunity to come to France and start a new step in my life.

Coming to the work's environment, I am deeply grateful to my supervisors Prof. S. Bourennane and Dr. C. Fossati who welcomed me to the GSM team and gave me their significant guidance and constant encouragement during these three years. Their vast knowledge, unfailing trust have been instrumental in shaping my attitude toward research.

I would like to take this opportunity to express my sincere gratitude to Dr. J. Marot. I am grateful for having had the privilege of working with him on a number of technical results presented in his dissertation and elsewhere. Thanks to his ready assistance, I could have more progress of the thesis and complete this research work.

Special gratitude goes to Prof. Yide Wang from Ecole Polytechnique de l'Université Nantes, and M. Karim Abed-Meraim, working in Ecole Nationale Superieure de Telecommunications for doing me the honor to constructively report my thesis. I wish also to thank Prof. Jean-Pierre Sessarego, the research director of CNRS, from Laboratory of Machine and Acoustics for examining my thesis, as well as for his interest in my work and his constructive remarks and suggestions.

I would also like to thank the researchers of GSM at Institut Fresnel. I would like to thank Dr. Mireille Guillame, Dr. Mouloud Adel, Dr. Mohammad-Ali Khalighi, Dr. Stephone Derrode for their support of my work. Having in mind the memorable time I have spent in GSM group, many thanks go to all my lab colleagues for their sincere help, both former and current ones, including Fang Xu, Alexis Huck, Damien Letexier, Dong Han, Yi Yin, Riad Khelifi, Sylvain Jay, Xuefeng Liu, Alexis Cailly, Yi Zhang, et al.

Finally, I am extremely grateful to my parents and other family members who live in my home country China, for their unfailing love to me from childhood to now. In addition, I also express my thanks to my friends in China.

Table of contents

Introduction

IMAGE segmentation has been continuously improved in the past few decades. The purpose of a general image understanding system is to recognize objects in a complex scene or a document image. In general, when humans are asked to describe a contour, they generally give a list of objects within the picture as well as their relative positions. Thereby, one of the first steps in image understanding is edge detection [1, 2, 3, 4]. Once the edges of an object are detected, other processing such as region segmentation, text finding, and object recognition can take place.

Contour detection consists in producing a new image which is in some way more desirable. In general, contour detection methods have to be robust to noise impairment. Image data come from more and more application fields, due to the progress in numerical computing, video, and acquisition systems such as sensors.

We can distinguish two types of contour detection methods : the regions-based and the contour-based methods. Firstly, region-based segmentation methods aim at distinguishing between set of pixels of the image, referring to properties such as color, texture, or object repartition with mathematical morphology tools. The unsupervised classification of pixels into subsets can also be performed with Hidden Markov Random Fields (HMRF) [5, 6]. Secondly, contour-based methods aim at detecting the set of pixels which delimitate regions. Several methods belong to this category : Ordinary or total least-squares methods for circle fitting seek to minimize the squares sum of error-of-fit with respect to measures. One of the major limitations of most of least-squares approaches is their sensitivity to outliers. Other methods support line or circle retrieval, even in a noisy environment. The Hough transform and the generalized Hough transform (GHT) provide estimation of lines or circle center coordinates (when their radius is known) [7, 8]. The main drawback of the Hough type methods is the computational load, although fast versions have been proposed. Contour-based snakes methods [9], such as Gradient Vector Flow (GVF) [10, 11], were largely used, to retrieve concave and weak edges with blurred boundaries. GVF limitations can be observed when the expected contour exhibits a high curvature. Levelset type methods [12, 13] enhance blindly all contours in images. Levelset does not provide explicitly the characteristics of contours with particular predefined parameters such as the radius of circles or the orientation of lines. On the contrary, some original methods which are parametric such as Subspace-based Line Detection (SLIDE) method [14, 15, 16, 17, 18] have been proposed. They are based on the transfer of array processing methods to the contour detection domain.

An array is composed of a set of sensors. Each sensor receives signals which are assumed to be centered around one frequency.

Array processing methods have been widely studied to solve the problems such as the detection of directions-of-arrival, correlated sources, and the case where correlated noise impairs the image [14, 19, 20, 21, 22, 23]. We associate an array of sensor to an image, and a particular signal generation method consists of adapting an array of sensors to the processed image, a bidimensional image data representation is transferred to a unidimensional array signal. The array is either linear or circular, depending on the shape of the expected object. In another framework, a method reconstructing polygons from moments has established an explicit connection to array processing [24, 25, 26]. It is profitable to transfer the estimation of the parameters of contours in images to the array processing. From this, we exploit the array processing methods to estimate the expected parameters. When the expected contours, such as lines or circles, are present in the image, the generated signals follow an array processing model : the contours correspond to source emitters, the image background corresponds to the propagation medium, the contour characteristics, such as line orientation or circle radius, are the parameters to be estimated. The signal generated on the array sensors can be splitted into several overlapping sections considered as several realizations of a single random signal. This type of data processing relies, in general, on second-order or higher-order statistics computation. In the case where white Gaussian noise impairs the image, the most common processing is to perform the SVD (Singular Value Decomposition) on the covariance matrix of the received signals. Performing SVD is the first step of subspace-based methods, which can be used to extract the desired parameters from the array signals. In the case where correlated noise impairs the image, higher-order statistics can be performed to suppress this noise. In particular, the cumulants of an order higher than three remove all Gaussian components, such as Gaussian noise.

Images suffer other impairments than noise. Owing to object movements, light transmission environment, illumination changes, defocus, etc, edges may not be the sharp transitions of intensity and/or color within an image, so blurred contours occur very often in images. These transitions are characteristics of object edges. Most edge detection methods will lose the necessary information of contour blur. To characterize the contour more precisely, it would make sense, therefore, to try to develop more accurate methods to improve the accuracy of contour characterization by quantifying the contour blur.

The key observation while computing second-order or higher-order statistics is that a low-dimensional subspace permits to extract useful information, in particular the parameters of the expected contours. The knowledge, or the estimation by statistical criteria, of the useful signal subspace dimension permits to partition the measurement space into a signal subspace that contains the desired information, and a noise subspace, that contains all undesired contributions.

In a noisy environment, the algebraic methods can also be performed. There is an interest in combining subspace-based methods and optimization methods to obtain an optimal estimation of either a set of parameters or expected features from the generated signals. Optimization methods mean to retrieve a set of unknown parameters, by optimizing a criterion. One of the effective global optimization methods is DIviding RECTangles (DIRECT) method, and a classical local optimization method for the resolution of nonlinear and non-constrained optimization problems is the gradient or Newton method, which can be accelerated as a variable step gradient method.

Thesis objective and contributions

As we will explain in the following chapters, in practice, we face several practical problems, which consider the different cases of contour characterization in an image. The objective of this thesis is to detect and characterize the contours in images by subspace-based methods of array processing. The detected contours can be divided into two kinds : one-pixel wide contour, and blurred contour which we describe by an actual model. More specifically, the main contributions are summarized as follows :

• In the field of array processing, the direction-of-arrival (DOA) problem has been extensively studied. By making a link between contour characterization in image data and the DOA estimation problem in array processing, we achieve the transfer of the powerful tools of array processing, and show that the derived methods can improve contour detection, in both computational load and estimation accuracy.

• We consider the detection of rectilinear contours in a correlated Gaussian noise environment by adopting the linear antenna model, and provide an improved high-resolution method based on higher-statistics.

• We propose an approach to estimate circle parameters by linear and circular antenna models. We also exploit the higher-statistics to estimate the radii of concentric circles in the correlated noise case.

• We study the problem of recovering a star-shaped contour, and propose a new signal generation model derived from the array processing paradigm. Then the generated signals are decomposed into damped sinusoids. We estimate all frequencies of the signal by a frequency estimation method and recover the contour edge.

• We propose a model for blurred linear contours, and derive the signal model which holds when signals are generated out of the image on a linear antenna. We propose a subspace-based method to retrieve the orientation and offset of the linear contours, and an optimization strategy to estimate the spread parameters.

• For the first time, we derive a signal processing model for the signals generated out of an image which contains a blurred triangular contour. We exploit array processing methods which are originally dedicated to multiple incoherently distributed sources to retrieve the orientation and spread parameters, and estimate the offsets by variable speed generation scheme.

• We provide a model for a blurred circular contour by a few parameters, which characterize its mean position and the gray level variation around. To characterize blurred circular contours, we propose an array processing method to find out the mean position of the contour and estimate the spread parameters by Newton optimization method.

Thesis outline

This thesis is organized in four chapters.

Chapter 1 overviews the basic concept of image segmentation and edge detection in image processing, and present several existing methods. Then array processing is introduced : we present the DOA estimation problem by second-order statistics and higher-order statistics methods, respectively. Based on this theoretical background, we show how image processing and array processing can be connected to each other. Then, we present three prominent mathematical optimization methods : Newton optimization method, Gradient descent method and DIRECT (DIviding RECTangles) method.

Chapter 2 is devoted to the characterization of lines in a correlated Gaussian noise environment. We present a special principle to transpose the image processing problem to an array processing problem. The existing line characterization method called SLIDE leads to models with orientations and offsets of straight lines as the desired parameters. From this, a unidimensional array signal is generated, which consists of the parameters characterizing the rectilinear contour. It has been proven that the cumulant is very effective to solve the correlated Gaussian noise. To suppress the noise, we improve the existing SLIDE method by exploiting higher-order statistics. For this, fourth-order cumulant-based MUSIC-like (Multiple Signal Classification) and improved TLS-ESPRIT (Total Least Square Estimation of Signal Parameters via Rotational Invariance Techniques) algorithm for non-Gaussian signals are presented to estimate the orientations of lines, while the offsets of lines are estimated by the "Extension of the Hough Transform". Specially, we also consider the cumulant slice matrix instead of the whole cumulant matrix, which evidently accelerates the algorithms. The whole proposed methods work blindly for the estimation of both angle and offset.

Chapter 3 introduces a new circular antenna model and adapts the variable speed propagation scheme, which yields from an image containing a circle a generated signal with linear phase. From this, we can estimate close radii of concentric circles by high-resolution methods in white noise environment and in color noise environment, as in **Chapter** 2. Using the linear antenna model, we compute the center coordinates of all circles. Then, for the more general case of strongly concave contours, we exploit a damped sinusoid model, and then a frequency estimation method is used to retrieve the polar coordinates of the contour pixels. Furthermore, we additionally refine the generated signals by STLN (Structured Total Least Norm) optimization method so that they better fit the proposed model, in order to improve the estimation when the noise level is high.

Chapter 4 solves the issue of blurred linear contour, blurred triangular contour and blurred circular contour characterization. For the first time, we propose an innovative model for these contours, involving few parameters. For blurred linear and triangular contour, they are main orientation, center offset and spread parameter ; for blurred circular contour, they are center coordinates, radius and spread parameter, which characterize the contour's mean position and gray level variations aside the contour mean position. Then, we derive appropriate signal generation schemes on either linear or circular antenna, and obtain the corresponding signal models in each case, which fit the subspace-based methods coming from array processing. A signal preprocessing and subspace-based methods yield either the orientation and offset for blurred linear contours, or the radius of a blurred circular contour. Then, appropriate criteria and an optimization strategy yield the contour spread : we adapt the global optimization method DIRECT to characterize blurred linear contours and Newton method to characterize a blurred circle. For blurred triangular contour, a subspace-based method named DSPE (Distributed Source Parameter Estimator) is applied to estimate the orientation and spread parameter for blurred triangular contour, and we adopt a variable speed generation scheme to estimate all offset values. The proposed methods are successfully applied to handmade and real-world images and compared with a level set approach, leading to low parameter bias.

CHAPITRE 1

Research overview and mathematical methods

In this chapter, we firstly present the basic concept of image segmentation and edge detection, then we describe the wave propagation model in array processing, which is derived as a function of the parameters of considered array processing issue, such as the number of sensors, the directions of arrival. Moreover, we introduce the direction of arrival estimation problem, and second-order and higher-order statistical methods are analyzed, respectively to estimate the directions of sources. In the end, to make the following chapters understood easier, we present the mathematical optimization methods, including Newton optimization, Gradient optimization, DIRECT method, which will be adopted in the following.

1.1 Image segmentation

1.1.1 Overview of edge detection

Image segmentation is one of important research fields in computer vision, by which we can partition a digital image into multiple regions or sets of pixels, and simplify and/or change an image to analyze more easily. The segmentation process can be viewed as separating the image into disjoint, or nonoverlapping collectives. Each of the pixels in the segmentation collective should have some similar characteristic or computed property, such as pixel digitalized value, color or intensity. Image segmentation can be approached from three different philosophical perspectives : region approach, boundary approach and edge approach. After image segmentation, a set of regions or a set of contours can be differentiated and recognized, so that the objects and the boundaries (lines, circles, curves, etc.) in image can be located. These results can be further used as the input for another image processing, such as face recognition, intelligent monitoring, medical diagnosis, mechanical part detection. Various of algorithms and techniques have been developed for image segmentation. Since there is no general solution to the image segmentation problem, these methods perform differently, depending on the applications and are not universally applicable to all images.

Edge detection is one of the most frequently used techniques in image segmentation. The boundaries of object surfaces in a scene often lead to oriented localized changes in intensity of an image, called edges. This observation combined with a commonly held belief that edge detection is the first step in image segmentation, has fueled a long search for a good edge detection algorithm to use in image processing. As a fundamental tool, edge detection may filter out the less relevant information and retain important information about object shapes. This leads to significantly reduce the amount of data to be processed, so that the subsequent image processing may be substantially simplified. However, it is not always possible to obtain such ideal edges from real-world images of moderate complexity. For example, detected edges may not be continuous, even not the real one as expected. An important property of the edge detection method is its ability to provide a set of edges potentially forming primitive objects, such as lines, circles, arcs, and so on. Line edges correspond to local maxima of intensity function and are of great use in the identification of image features, such as roads and rivers in remote sensing images. Most of line edge detectors are confined to binary images and a few for grey images. The main problem is that they usually yield edges which are not located accurately enough and the do not perform well in complex images such as remote sensing images.

1.1.2 Existing work

In the last decades, a lot of researches have been made to detect contour edges in various cases, including classic methods, Gaussian based methods, multi-resolution methods, wavelet based methods, statistical methods, machine learning based methods, contextual methods, etc. In point of technical view, most of these methods can be categorized into two categories, search-based and zero-crossing based. In point of conceptual view, these methods are grouped into contextual and non-contextual approaches. Examples of edge detectors are operators that incorporate linear filtering [27, 28], or local energy [29]. Other more original edge detection tools include anisotropic diffusion [30]. We can distinguish two categories of edge detection methods : region-based methods, and contour-based methods. We do not extend to discuss each of these method, this is beyond the scope of this these. We only confine our discussion to a partial list of what we believe to be the leading contribution in these fields, namely, [7, 8, 9, 10, 31, 32, 33].

- **Hough transform methods**

The well known Hough transform [7, 34] is the standard approach for detecting parametric curves or other predefined shapes in a planar set of points. The strength of the Hough transform is in fitting curves to a set of points that can include many outliers, often an order of magnitude more than good data points. On the other hand, pure Hough algorithms rely on an assumption that the good data points are error free. This is the complete opposite to least squares fitting techniques that handle data point location errors very well but collapse in the presence of outliers.

In Hough transform method, each of N data points (x_i, y_i) is transformed to a sinusoidal voting pattern for the detection of straight lines [36],

$$\rho = x_i cos\theta + y_i sin\theta \tag{1.1}$$

in the (θ, ρ) normal parameter plane. This brings that, the points in parameter space will correspond to the lines in picture, and sinusoids corresponds to co-linear points intersect at an unique point. The original collinearity detection problem is thus transformed to the problem of finding the global maximum in the whole accumulator array. Hough transform method was also extended to detect more general shapes. In these cases, a shape is described by a list of template vectors which record the distance and orientation of each point from an arbitrary localization point.

Its generalized version (GHT) [8] retrieves the center of multiple circles, knowing their radius. GHT is robust to partial or slightly deformed shapes and tolerant to noise in terms of estimation accuracy, but a well-known limitation of the Hough transform during the implementation is the huge storage and elevated computational load, which increase when the number of outliers in image increases. That is because the method has to store too many elements in an accumulator array to make the final vote and determine the contour edge, although some of variants of the Hough transform have been proposed in the literature [8, 34].

- **Least-squares methods**

In [33], several algorithms are presented to fit circles and ellipses to given points in some least squares sense in the plane. Circles and ellipses are represented algebraically by a formulation $F(\mathbf{x}) = 0$. If a point is on the curve then its coordinates $\mathbf{x}$ are a zero of the function F. For each point, the algorithms fit it by solving iteratively the nonlinear least squares problem. To solve the nonlinear least squares problem, several algorithms can be used, including : Gauss-Newton method, Newton method, variable projection, orthogonal distance regression, etc.

Active contour model has been widely applied to contour detection. The primary purpose of active contour model is to locate the boundaries of an object. The active contour evolves by the defined energy function. Different researchers have proposed energy based formulations, such as snake model based method and Chan-Vese active contour method.

- **Snake model based methods**

Active contour model was firstly proposed in [9], known as "snake". A snake can be represented as a set of points $\mathbf{v}(s) = (x(s), y(s))$, where $s \in [0, 1]$. These points are linked together to form an active contour. This method requires the initial location of the boundary, and this initialized snake will dynamically converge towards the object boundary by minimizing iteratively the defined energy function, which associates to the current contour as a sum of an internal and external energy. The energy function can be expressed as :

$$E^*_{snake} = \int_0^1 E_{snake}(\mathbf{v}(s))ds = \int_0^1 (E_{int}(\mathbf{v}(s)) + E_{image}(\mathbf{v}(s)) + E_{con}(\mathbf{v}(s)))ds \tag{1.2}$$

where E_{int} denote the internal energy of the spline due to bending, E_{image} represents the image forces acting on spline and E_{con} serves as external constraint forces introduced by the user. The combination of E_{image} and E_{con} can be represented as $E_{external}$, that denote the external energy acting on the spline.

The internal spline energy can be written

$$E_{int} = (\alpha(s))|\mathbf{v}_s(s)|^2 + \beta(s)|\mathbf{v}_{ss}(s)|^2)/2 \tag{1.3}$$

where $\mathbf{v}_s(s)$ and $\mathbf{v}_{ss}(s)$ are the first derivative and the second derivative of $\mathbf{v}(s)$, called elastic forces and bending forces. The elastic force controls the tension of the active contour and is responsible for shrinking the contour. The bending force controls the rigidity of the snake, only the curvature, not the length of the contour. $\alpha(s)$ and $\beta(s)$ control the internal energy and the external energy of the snake.

To handle broken object edges and subjective contours, Xu and Prince [10] proposed a new type of external force, coming from gradient vector flow (GVF) of image.

This computation causes diffuse forces to exist far from the object, and crisp force vectors near the edges. Combining these forces with the usual internal forces yields a powerful computational object. GVF snake is insensitive to initialization and is able to move into boundary concavities. Although GVF snake method handles better the contour with concavities and weak edges with blurred boundaries, its limitations can be observed when the expected contour exhibits strongly concave contours, that is, a strong curvature : it was then improved to cope with concave regions [37].

- **Level set methods**

Level set segmentation is based on a model for active contours by techniques of curve evolution [38]. To avoid some irregularities in the active contour evolution, a recent improved version [39] proposes a new variational level set formulation in which the regularity of the level set function is intrinsically maintained during the level set evolution. A drawback of the level set approach is still the tuning of numerous parameters. In [31], a new model for active contour without edges was proposed based on techniques of curve evolution, Mumford-Shah functional for segmentation and level sets. Assume that the image u_0 is divided by a closed curve C, that is, inside of C and outside of C, the basic model is to minimize the following energy :

$$F_1(C) + F_2(C) = \int_{inside(C)} |u_0(x,y) - c_1|^2 dxdy + \int_{outside(C)} |u_0(x,y) - c_2|^2 dxdy \tag{1.4}$$

where C is any other variable curve, and the constants c_1, c_2 depend on C, are the averages of u_0 inside C and outside C.

The first term can be interpreted as the force to shrink the contour, and the second term is the force to expand the contour. When the evolutional curve reaches the boundary of the expected object, these two forces get balanced. It can be seen that this model is not based on an edge-function to stop the evolving curve on the desired boundary, and the edges of the detected objects are not necessarily defined by gradient or with very smooth boundaries.

In [32], a new multiphase level set framework for image segmentation still adopting Mumford and Shah model. The generalization of [31] based 2-phase segmentation was developed. With level set formulation, $C = \{(x, y)|\phi(x, y) = 0\}$, and thus a formulation similar to Eq. (1.4) is used :

$$\begin{aligned} F(c_1, c_2, \phi) = \; & \int_{inside(C)} (u_0(x, y) - c_1)^2 H(\phi) dxdy \\ & + \int_{inside(C)} (u_0(x, y) - c_2)^2 (1 - H(\phi)) dxdy + \nu \int_{inside(C)} | \bigtriangledown H(\phi)| \end{aligned} \tag{1.5}$$

where $H(\cdot)$ is Heaviside function and ν is a constant.

- **Subspace-based contour detection methods**

In the frame of contour-based methods, it has been proved that array processing and frequency retrieval are profitable to image segmentation, either by a region-based approach [40], or a contour-based approach [18, 22, 24]. Array processing and frequency retrieval are based on algebra tools. They rely in particular on subspace approaches [41], to retrieve source parameters such as direction of arrival [42, 43]. These subspace-based methods have been recently improved in terms of computational load by avoiding eigendecomposition [44, 45]. Algebraic subspace-methods are also used for frequency estimation purposes [46, 47, 48, 49, 50]. Algebraic methods coming from array processing have been transposed to image segmentation. In [40], a region approach is adopted. The authors present a sensor array processing approach to detect the number of object regions. This number provides the necessary information for unsupervised image segmentation. In [14, 16, 17, 18, 22, 24, 51, 52], a contour based approach is adopted, and particular features are expected : either polygons [24], straight lines [16, 17, 18, 51], or circles [16, 22].

Firstly, in [24], binary polygons are reconstructed from a finite number of their complex moments. As pointed out, the formulation of the shape-from-moments problem is very similar to several other fields, such as the estimation of sinusoidal components in speech signal processing [49], and direction of arrival (DOA) in array processing [23, 53, 54]. In a noisy case, the problem of reconstruction becomes an estimation one. The recovered binary polygonal vertices are refined by Generalized Pencil of Function (GPOF), Hankel Total Least Squares (HTLS) method and Structured TLS (STLS) method. Other numerical procedures are presented for the shape-from-moments reconstruction problem in [25, 55]. It turns out that all of these have established the explicit connection between the binary polygonal object reconstruction problem and the field of array processing, and the moment-based polygonal reconstruction represents one of several instantiations of this connection.

Secondly, a similar analogy is made in [18] between a straight line in an image and a planar propagating wavefront impinging on an array of sensors to obtain an array processing formulation for the detection of line parameters within an image, replacing the classic Hough transform approach. The Subspace-based Line Detection (SLIDE) algorithm applied a propagation (phase-preserving projection) scheme on the image pixels. A further benefit of the analogy comes from that an efficient statistical technique from the field of sensor array processing can be used to provide an objective estimate of the number of lines in an image. The whole estimation of line parameters is accomplished in two phases. First, the angles of the lines are estimated by high resolution method, for example, TLS-ESPRIT method, and then the estimates of the offsets are obtained. SLIDE method yields closed-form and high-resolution estimates of the line parameters, as opposed to the Hough transform method. The computational complexity of SLIDE is an order of magnitude less than that of the Hough method. Also, SLIDE does not require a large memory space. SLIDE takes advantage of the spatial coherence existing in the image between the locations of the line pixels on different rows both to reduce the size of the problem to a one-dimensional problem and to introduce a structure into the data that can be exploited for efficient estimation of the desired parameters.

Thirdly, several extensions of this analogy have been developed to recover linear [56], and circular contours [22, 57]. Especially, a different signal generation scheme is proposed in [22], which yields an array processing linear phase signal model out of a binary image containing a circle. In the linear and circular cases, high resolution methods [23, 53] could then be applied to distinguish possibly very close contours by considering them as punctual sources.

1.2 Array processing

In this section, we describe the fundamental wave propagation model and estimation methods that are applied when a sensor array is employed to spatial problems such as DOA estimation.

Array processing are used in a wide range of applications such as wireless communications, radar, sonar, medical diagnosis, seismic exploration, etc, and has been studied extensively during the past decades [58, 59, 60, 61].

1.2.1 Wave propagation model

To introduce the standard signal model, we consider the narrow-band signal emanated by each source. The propagating waves may emanate from sources such as antenna or acoustic sources (underwater SONAR). The traveling wave equation holds for any application of

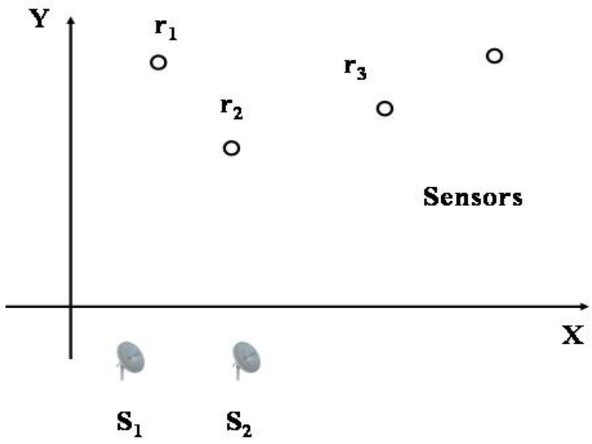

Figure 1.1 — General two dimensional array

interest to the estimation methods.

Assume that a model of an exponential traveling wave signal is as follows,

$$s(t, \mathbf{p}) = s(t - \boldsymbol{\alpha}^T \mathbf{p}) = e^{j(\omega t - \mathbf{k}^T \mathbf{p})} \tag{1.6}$$

where $\boldsymbol{\alpha}$ is the spatial slowness vector which determines the direction of the wave propagation, $\mathbf{p}$ is the position vector, $\omega = 2\pi f$ is the temporal frequency and $\mathbf{k} = \boldsymbol{\alpha}/\omega$ is the wave-vector. The length of $\mathbf{k}$ is the spatial frequency (also referred to as the wavenumber), and equals $2\pi\lambda$, with λ being the wavelength of the carrier, and $'T'$ is the transpose operation.

Equation (1.6) shows that the phase variation of the signal $s(\cdot)$ is temporal as well as spatial. An isotropic point source results in spherical traveling waves, and all the points lying on the surface of a sphere of radius R share a common phase and are referred to as a wavefront. Far-field receiving conditions imply that the radius R of propagation is so large (compared to the physical size of the array) that a flat plane can be considered, resulting in a plane wave.

Assume that the array is planar and has L sensors and their transfer functions are flat over the signal bandwidth, each of which has coordinates $r_l = (x_l, y_l)$ (see Fig. 1.1) and an impulse response

$$h_l(t, \mathbf{p}_l) = a_l(\theta)\delta(t)\delta(\mathbf{p}_l)$$

When there are M signals impinging on an L-dimensional array, the impulse response matrix $\mathbf{H}(t, \boldsymbol{\theta})$ from the impinging emitter signals with parameters $\boldsymbol{\theta} = [\theta_1, \theta_2, \ldots, \theta_M]$, to the sensor outputs can be defined. The lm-th element of $\mathbf{H}(t, \boldsymbol{\theta})$ is as follows :

$$\mathbf{H}_{lm}(t, \boldsymbol{\theta}) = a_l(\theta_m)\delta(t)\delta(\mathbf{p}_l), l = 1, 2, \cdots, L, \quad m = 1, 2, \cdots, M.$$

So the sensor outputs denoted $x_l(t)$ can be written as,

$$x_l(t) = \sum_{m=1}^{M} a_l(\theta_m) e^{j(\omega_m t - \mathbf{k}_m^T \mathbf{r}_l)}$$

The vector representation of the received signal $\mathbf{x}(t)$ is expressed as

$$\mathbf{x}(t) = [\mathbf{a}(\theta_1), \mathbf{a}(\theta_2), \cdots, \mathbf{a}(\theta_M)]\mathbf{s}(t) + \mathbf{n}(t) = \mathbf{A}\mathbf{s}(t) + \mathbf{n}(t), \tag{1.7}$$

where $\mathbf{a}(\theta_m) = [a_1(\theta_m)e^{j\mathbf{k}_m^T \mathbf{r}_1}, a_2(\theta_m)e^{j\mathbf{k}_m^T \mathbf{r}_2}, \cdots, a_L(\theta_m)e^{j\mathbf{k}_m^T \mathbf{r}_L}]^T$, $\mathbf{s}(t) = [e^{j\omega_1 t}, \cdots, e^{j\omega_M t}]^T$, and $t = 1, \cdots, N$.

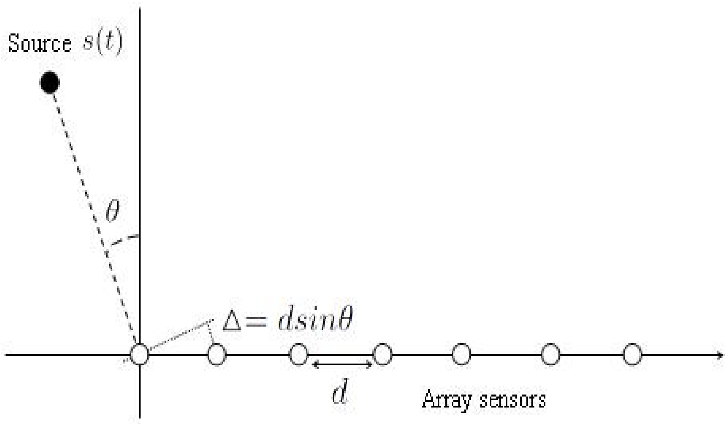

Figure 1.2 — A uniform linear array

When there is a linear sensor array (see Fig. 1.2), the steering vector $\mathbf{a}(\theta)$ has the following form :

$$\mathbf{a}(\theta) = [1, e^{j\phi}, \cdots, e^{j(L-1)\phi}]^T,$$

where $\phi = -\frac{\omega}{c} dsin(\theta)$.

1.2.2 DOA estimation problem

From the previous model, the key interesting issue is to estimate the directions of arrival of sources, that is, find the way to obtain the parameters $\theta_i,\ i = 1, \cdots, M$ given a finite data vector $\mathbf{x}(t)$ observed over $t = 1, 2, \cdots, N$.

The covariance matrix of the signals can be written as :

$$\mathbf{R} = \mathrm{E}\{\mathbf{x}(t)\mathbf{x}^H(t)\} = \mathbf{A}\mathrm{E}\{\mathbf{s}(t)\mathbf{s}^H(t)\}\mathbf{A}^H + \mathrm{E}\{\mathbf{n}(t)\mathbf{n}^H(t)\} \tag{1.8}$$

where $(\cdot)^H$ represents Hermite transpose.

Assume that the white Gaussian noise with variance σ^2 in all sensors, is uncorrelated. This yields $\mathrm{E}\{\mathbf{n}(t)\mathbf{n}^H(t)\} = \sigma^2\mathbf{I}$, and Eq. (1.8) can be expressed as :

$$\mathbf{R} = \mathbf{A}\mathbf{P}\mathbf{A}^H + \sigma^2\mathbf{I} = \mathbf{U}_s\mathbf{\Lambda}_s\mathbf{U}_s^H + \mathbf{U}_n\mathbf{\Lambda}_n\mathbf{U}_n^H, \tag{1.9}$$

where $\mathbf{P} = \mathrm{E}\{\mathbf{s}(t)\mathbf{s}^H(t)\}$, $\mathbf{U}_s$ contains the signal subspace and $\mathbf{U}_n$ spans the noise subspace [14, 19, 20, 53, 62, 63, 64], $\mathbf{\Lambda}_s = diag(\lambda_1, \cdots, \lambda_M)$ is a diagonal matrix of real and positive signal eigenvalues, and $\mathbf{\Lambda}_s = diag(\lambda_{M+1}, \cdots, \lambda_{L-M})$ contains the noise eigenvalues.

Remark :

(1) the discussion earlier is based on second-order statistics of data. When we consider the higher-order statistics, the expression that will be discussed later is different.

(2) the discussion earlier assumes that the acquired data is infinite and leads to the perfect estimation of covariance matrix. However, in practice, it is only estimated by finite sample of data. That means Eq. (1.8) is obtained by maximum-likelihood estimate.

$$\hat{\mathbf{R}} = \frac{1}{N}\sum_{t=1}^{N}\mathbf{x}(t)\mathbf{x}^H(t) \tag{1.10}$$

1.2.2.1 Methods based on second-order statistics

• Spectral-based methods

One should form some spectrum-like function of the parameter of interest. The locations of the highest peak of the function are taken as the estimation of interest. The spectral-based methods consist of the beamforming approaches and the subspace-based methods, where beamforming approaches attempt to automatically localize signal sources using antenna arrays by beamforming techniques. Subspace-base methods stemming intrinsically from eigen-structure properties provide the solutions to the estimation of parameters. The classical methods include MUSIC (multiple signal classification) algorithm and ESPRIT algorithm.

• Parametric methods

This kind of methods requires a simultaneous search for all parameters of interest, for example, maximum likelihood (ML) technique. Comparing with the previous methods, this type of methods usually requires a higher computational load. Parametric methods always yield more sufficient accuracy comparing with spectral-based methods. In particular, the parametric methods have the ability to resolve the problem of highly correlated signals, although these methods have to increase the computational complexity.

1.2.2.2 Methods based on higher-order statistics

Higher-order statistics based methods, which have been extensively studied and applied in array processing [62, 67, 68, 69], are able to handle the colored Gaussian noise environment, and many real-world applications are truly not coherent. This is a valid assumption for most applications. This assumption is essential for higher-order statistics based techniques. In general, fourth-order cumulants are often adopted.

If the signals are real-valued, for a signal sample $\mathbf{x} = [x_1, x_2, \cdots, x_N]$, the second-, third-, and fourth-order cumulant can be defined as :

$$\mathrm{cum}_2(x_1, x_2) = E\{x_1, x_2\} \tag{1.11a}$$

$$\mathrm{cum}_3(x_1, x_2, x_3) = E\{x_1 x_2 x_3\} \tag{1.11b}$$

$$\begin{aligned}\mathrm{cum}_4(x_1, x_2, x_3, x_4) = \quad & E\{x_1 x_2 x_3 x_4\} - E\{x_1 x_2\}E\{x_3 x_4\} - E\{x_1 x_3\}E\{x_2 x_4\} \\ & -E\{x_1 x_4\}E\{x_2 x_3\}\end{aligned} \tag{1.11c}$$

where $E\{\cdot\}$ denotes the expectation.

For complex signals, the fourth-order cumulant can be generally defined as :

$$\mathrm{cum}_4(x_1, x_2, x_3^*, x_4^*) = E\{x_1 x_2 x_3^* x_4^*\} - E\{x_1 x_2\}E\{x_3^* x_4^*\} - E\{x_1 x_3^*\}E\{x_2 x_4^*\} - E\{x_1 x_4^*\}E\{x_2 x_3^*\} \tag{1.12}$$

where " $*$ " denotes conjugate operation.

Fourth-order cumulants have the advantage to overcome the colored noise, which is based on these following properties :

(1) The fourth-order cumulant of two statistically independent random processes equals the sum of the cumulants of the individual random processes. Note that, it is not true for higher-order statistics. We denote two independent processes $x(n)$ and $y(n)$, so we can get as follows :

$$\mathrm{cum}_4(x(n) + y(n)) = \mathrm{cum}_4(x(n)) + \mathrm{cum}_4(y(n)) \tag{1.13}$$

(2) The fourth-order cumulant of Gaussian noise is zero. To say, cumulants are blind to any kind of a Gaussian process, whereas correlated not. Consequently, cumulant-based methods boost signal to noise ratio when the measured signals are contaminated by white Gaussian noise.

(3) The fourth-order cumulant of symmetrically distributed signals is not zero, whereas the third-order cumulant has extremely small value, even as zero, for example, Uniform distribution.

Based on the previous discussion, we can get the fourth-order cumulants of the received signals (see Eq. 1.7) as the following :

$$\mathrm{cum}_4(\mathbf{x}(t)) = (\mathbf{a}(\theta_i) \otimes \mathbf{a}^*(\theta_i)) \cdot \mathrm{cum}_4(s_i(t), s_i(t), s_i^*(t), s_i^*(t)) \cdot (\mathbf{a}(\theta_i) \otimes \mathbf{a}^*(\theta_i))^H \tag{1.14}$$

where $'\otimes'$ denotes Kronecker product, and $s_i(t)$ represents the signal sample of i^{th} sources at time t.

A MUSIC-like method based on the fourth-order cumulants of the received signals in [19] was proposed to find the directions of arrival (DOA) of sources, and a method based on nonlinear minimization of a certain cost function was further presented. An blind algorithm based on fourth-order cumulants is proposed in [70] to estimate the steering vectors without *a priori* knowledge of array manifold, which is then used to estimate the directions of arrival. In [20], a fourth-order ESPRIT algorithm is developed based on generalized eigenstructure analysis. A cumulant-based approach combined with an acoustic scattering model in [21] is proposed to estimate the parameters of coherent signal sources in a noisy environment.

1.3 Mathematical optimization methods

1.3.1 Newton optimization

Given a function $f(x)$ and its derivative $f^{'}(x)$, we start with an initial guess x_0, and obtain a better approximation x_1 by

$$x_1 = x_0 - \frac{f(x_0)}{f^{'}(x_0)}. \tag{1.15}$$

Geometrically, x_1 is the intersection point of the tangent line of the graph of f, with the $x-$axis. The process is repeated until a sufficiently accurate value is reached :

$$x_{n+1} = x_n - \frac{f(x_n)}{f'(x_n)} \tag{1.16}$$

We can find a minimum or maximum of a function by Newton's method. Because the derivative is zero at the minimum or maximum point of a function, the iteration of 1.16 can be rewritten as :

$$x_{n+1} = x_n - \frac{f^{'}(x_n)}{f''(x_n)} \tag{1.17}$$

1.3.2 Gradient descent

Gradient descent is a first-order optimization algorithm.

Start a guess of $\mathbf{x}_n$ value, the gradient of function $\nabla F(\mathbf{x}_n)$ at this guess value can be used to tell us which way to move. When one takes steps proportional to the negative of the gradient of each current point at each iteration, a minimum of $F(x)$ is found by following the slope of the function. That can be expressed as by the formulation :

One starts with a guess $\mathbf{x}_0$ for a local minimum of $F(\mathbf{x})$, and considers the sequence $\mathbf{x}_0, \mathbf{x}_1, \cdots, \mathbf{x}_n$, such that $\mathbf{x}_n = \mathbf{x}_{n-1} - \gamma \nabla F(\mathbf{x}_{n-1}), n \geq 0$, where γ is a small enough number.

So we have $F(\mathbf{x}_0) \geq F(\mathbf{x}_1) \geq F(\mathbf{x}_2) \geq \cdots \geq F(\mathbf{x}_n)$, and hopefully the sequence $\mathbf{x}_n$ converges to the desired local minimum. Note that $\mathbf{x}_i$ may be the vectors for multidimensional function. In this case, $\nabla F(x)$ can be computed by $\nabla F(x_1, x_2, \cdots, x_N) = (\frac{\partial F}{x_1}, \frac{\partial F}{x_2}, \cdots, \frac{\partial F}{x_N})$ in N dimensions. The value of step size γ is allowed to change at every step.

Alternatively, if one takes steps proportional to the positive direction of the gradient, one approaches a local maximum of that function. Gradient descent is also known as steepest descent, or the method of steepest descent.

1.3.3 DIRECT method

DIRECT (DIviding RECTangles) algorithm [71, 72], as a modification to Lipschitzian optimization, aims at finding the global minimum of a multivariate function subject to simple bound constraints and a real-valued objective function, which does not need a Lipschitz constant, at the expense of a large and exhaustive search. DIRECT algorithm does not require the knowledge of the criterion to be minimized. DIRECT method attempts a problem which can be expressed as follows :

Let $a, b \in \Re^N$, $\Omega = \{x \in \Re^N : a_i \leq x_i \leq b_i\}$, *and* $f : \Omega \rightarrow \Re$ *be Lipschitz continuous with constant* α. *Find* $x_{opt} \in \Omega$ *such that*

$$f_{opt} = f(x_{opt}) \leq f^* + \epsilon$$

where ϵ *is a given small positive constant.*

When we normalize the search space to be the unit hypercube, the search space of DIRECT method in several dimensions is the n-dimension unit hypercube. In each iteration, we identify the set of potentially optimal rectangles, and select any rectangle. As the algorithm proceeds, this space will be partitioned into hyperrectangles, each with a sampled point at its center, and update the minimum of the function until the iteration limit has been reached. The termination occurred when DIRECT was within 0.01% of the global minimum value. Fig. 1.3 exemplifies three iteration of DIRECT algorithm on Branin's function.

1.4 Conclusion

In chapter 1, we overviewed the basic concept of image segmentation and edge detection in image processing, and presented several existing methods. Then array processing was introduced : we discussed the DOA estimation problem by second-order statistics and higher-order statistics methods, respectively. Later, in this work, we will show how image processing and array processing can be close to each other. At the last, three prominent mathematical optimization methods were presented. They will be applied to different objective functions to optimize our objective in the following chapters.

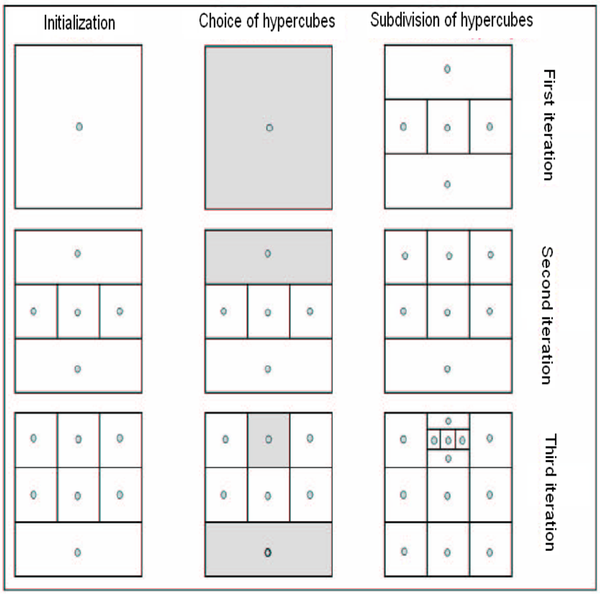

Figure 1.3 — Three iterations of the DIRECT algorithm on Branin's function

CHAPITRE 2

Straight line detection in correlated Gaussian noise environment by higher order cumulants

Multiple line characterization is a most common issue in image processing. It has been demonstrated that a specific formalism turns the contour detection issue of image processing into a source localization issue of array processing [14, 18, 24, 25, 73]. Array processing methods can be applied to signals generated from an image on virtual signals composing an array to estimate straight line orientations. However, the existing methods do not face correlated noise. As a result, in this case, the detection performance of existed methods is degraded. In this chapter, to suppress the correlated Gaussian noise, we propose to improve subspace-based high-resolution methods by computing the fourth-order cumulant slice matrix of the received signals instead of second-order statistics, and estimate contour parameters out of images impaired with correlated Gaussian noise. Simulation results are presented and show that the proposed methods improve line characterization performance compared to second-order statistics.

2.1 Introduction

Extracting the characteristics of lines or object contours from a binary image has been a much-studied problem in the last few decades. This problem is faced for robotic way screening, for the measurement of wafer track width in microelectronics, and generally for the analysis of aerial images.

An extension of the Hough transform is used in order to retrieve the main direction of a set of roughly aligned points. Although this method gives good resolution even in the presence of considerable noise, the restrictions still exist due to the dependence on the choice of the quantization step and the computational cost of the bidimensional search for the maxima.

The line-fitting problem has been transposed to the signal processing framework, and it has been shown that a specific signal generation process yields, when applied to an image containing multiple lines, to signals which follow an array processing model. Then high-resolution methods, such as MUSIC [19, 23, 74] and ESPRIT [20, 53] algorithms, are used. SLIDE (Subspace-based LIne DEtection) algorithm [14, 16, 17] was first proposed to make the analogy between the estimation of straight line orientations and the direction of arrival estimation, which was effectively exploited to estimate line parameters. In [75], they introduced the high resolution method called "Propagator" coming from array processing to estimate straight line orientations and applied MFBLP (Modified Forward-Backward Linear Prediction) method to estimate the offset of straight line. Then this work was extended to estimate distorted curves by optimization algorithms possibly present in the image [76]. However, these methods are based restrictively on second-order statistics and assume that the noise is white. When the noise is correlated, these methods are not efficient.

Because of acquisition conditions, actual noise in some cases of real-world images tends to be spatially correlated. For instance, in medical X-ray imaging, while noise in an X-ray beam is uncorrelated, it is correlated in observed images. This is due to the detectors, where X-ray photons typically evoke multiple light photons that can contribute to different pixels. Non-diagonal coefficients of the covariance matrix of noise realizations are non-zero when noise is correlated, which degrades the performance of the algorithms based on second-order statistics. In [62], fourth-order cumulants to estimate steering vectors are exploited, and then they used these estimated vectors to implement the analysis of frequencies by MFBLP method which distinguishes between coherent sources. The improved MUSIC algorithm was proposed in [68] based on higher-order statistics to detect directions-of-arrival considering possibly coherent sources in array processing, but this technique was applied on a time-dependent signal. They used the whole fourth-order cumulant matrix to implement the eigen-decomposition. As presented in references [62, 68, 77], it has been shown that higher-order statistics, computed in the form of higher-order cumulants, are very efficient in handling correlated Gaussian noise. In other fields of array processing, such as in signal processing for communications, higher-order cumulant-based methods have been widely studied and have shown inherent advantages over second-order statistics-based methods. The reason is mainly based on the fact stated in section 1.2.2.2 : higher-order cumulants (starting from third order) of any Gaussian random variable, and in particular of correlated Gaussian noise, are zero. Thus, the noise parts of the data are canceled out when higher-order cumulants are computed.

The rest of chapter 2 is constructed as follows : we begin by modeling the image data in section 2.2 and formulate the problem by introducing cumulant-based model in section 2.3. In section 2.4, high-resolution algorithms for estimating line's orientation, which are MUSIC-like algorithm and improved TLS-ESPRIT algorithm, are derived from fourth-order cumulants of the signal realizations received by virtual array sensors. After orientation estimation, the extension of the Hough transform is applied to find the line's offset. In section 2.5, numerical simulations are presented to show that cumulant-based methods are efficient when the processed image is impaired by correlated gaussian noise.

2.2 Image model

Let us consider a 2-dimensional binary image $I(x, y)$ (see Fig. 2.1). Here x and y are the indexes of the horizontal and vertical axes, respectively. The pixels of value '1' represent useful information and form the outline of the estimated contour, while the background is composed of '0'-valued pixels. The image consists of N rows and C columns (see Fig. 2.1). It contains a straight line. Each straight line is associated with an offset x_0 (the intersection of the straight line with x-axis) and a parameter θ (the angle between this line and the line of equation $x = x_0$). In order to make an analogy between the image data and signals in array processing, an array of sensors is supposed to be placed aside the image [14]. Each nonzero pixel is assumed to emit an electromagnetic wave, which is narrowband in frequency and only travels along the x-axis in the direction of decreasing x. Each sensor only receives the signal emitted by the source of the corresponding row. If we define an arbitrary propagation constant μ, a signal vector $\mathbf{r}$ of length N is generated out of the components $I(i, l)$ $(i \in 1, \cdots, N; l \in 1, \cdots, C\ )$ of the image matrix. Each component r_i of the signal vector $\mathbf{r}$ is defined as follows :

$$r_i = \sum_{l=1}^{C} I(i, l) e^{-j\mu x_i}, \quad i = 1, \cdots, N, \tag{2.1}$$

where μ is a propagation parameter [14]. If a straight line with parameters x_0, θ is present, the column index of the nonzero-valued pixel at row i is defined by $x_i = x_0 - (i-1)\tan(\theta)$. When there is only one straight line in the image, Eq. (2.1) can be rewritten as :

$$r_i = e^{-j\mu x_0} \cdot e^{j\mu(i-1)tan(\theta)}, \ i = 1, \cdots, N \tag{2.2}$$

The signal generation (see Eq.(2.1)) can be interpreted by a wave propagation in which straight line corresponds to a planar wavefront that propagates along the x-axis and the image background is the propagation medium. The image is supposed to be a frozen snapshot of an underlying wavefront propagation environment, and each pixel on a straight line is assumed to be a secondary source of propagation. Note that when there are horizontal lines, we detect the lines after the rotation of the image.

If there are d straight lines in the image (see Fig. 2.2), the signal received by each sensor is given by :

$$r_i = \sum_{l=1}^{d} e^{-j\mu x_{i_l}} = \sum_{l=1}^{d} e^{-j\mu x_{0_l}} e^{j\mu(i-1)\tan(\theta_l)}, i = 1, \cdots, N. \tag{2.3}$$

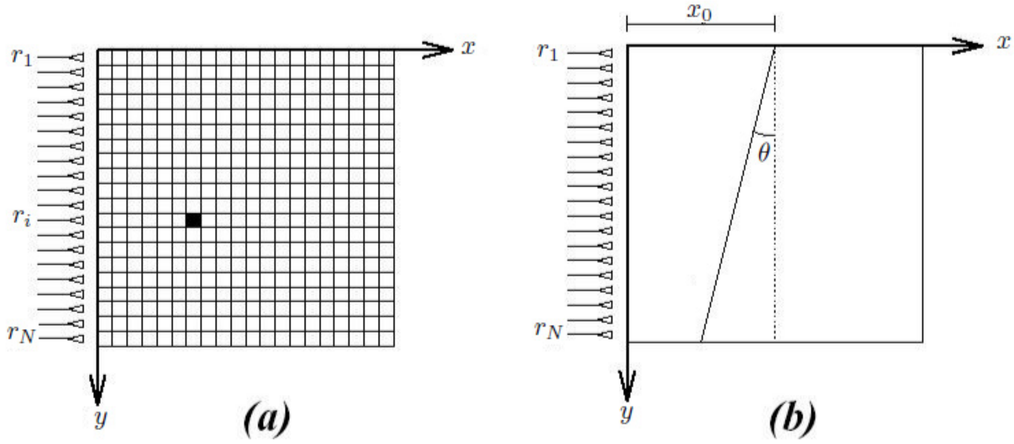

Figure 2.1 — Image data model

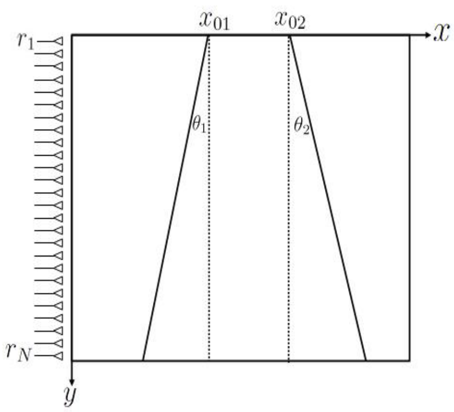

Figure 2.2 — Image containing multiple lines

where x_{0_l} and θ_l are the offset and the orientation of the l-th line. Note that the value of line orientation is positive when the angle between the line and the direction of the x-axis is more than 90°, and it is negative when the angle is less than 90°.

When we consider that the image is impaired by correlated Gaussian noise and denote $a(\theta_l) = e^{j\mu(i-1)\tan(\theta_l)}$ and $s_l = e^{-j\mu x_{0_l}}$, the signals are written in the form of matrix

$$\mathbf{r} = \mathbf{A}(\theta) \cdot \mathbf{s} + \mathbf{n} \tag{2.4}$$

where the received signal vectors $\mathbf{r} = [r_1, r_2, \cdots, r_N]^T$, the steering matrix $\mathbf{A}(\theta) = [\mathbf{a}(\theta_1), \mathbf{a}(\theta_2), \cdots, \mathbf{a}(\theta_d)]$ with l-th column $\mathbf{a}(\theta_l) = [1, e^{j\mu\tan(\theta_l)}, \cdots, e^{j\mu(N-1)\tan(\theta_l)}]^T$, therein $'T'$ denotes transposition operation, the source vector $\mathbf{s} = [s_1, s_2, \cdots, s_d]^T$, $s_k = e^{-j\mu x_{0k}}$ and the noise vector $\mathbf{n} = [n_1, n_2, \cdots, n_N]^T$.

2.3 Problem formulation

Here, we recall the fourth-order cumulant of the complex variables of Eq. (1.11c) in section 1.2.2.2. Quite often the complex random variables are analytical signals, so the last item of the right side of fourth-order cumulant in Eq. (1.12) is identically zero. Note that the definition of the cumulant of a complex random variable is non-unique. In practical terms, continuous signals are often turned into discrete time-series to calculate its fourth-order cumulant. Eq. (1.12) is approximately equivalent to

$$\begin{aligned} &\mathrm{cum}_4(x(t), x(t+\tau_1), x^*(t+\tau_2), x^*(t+\tau_3)) \\ &\approx \tfrac{1}{T}\textstyle\sum_{t=1}^{T} x(t)x(t+\tau_1)x^*(t+\tau_2)x^*(t+\tau_3) \\ &-\tfrac{1}{T^2}\textstyle\sum_{t=1}^{T} x(t)x^*(t+\tau_2)\cdot\sum_{t=1}^{T} x(t+\tau_1)x^*(t+\tau_3) \\ &-\tfrac{1}{T^2}\textstyle\sum_{t=1}^{T} x(t)x^*(t+\tau_3)\cdot\sum_{t=1}^{T} x(t+\tau_1)x^*(t+\tau_3) \\ &-\tfrac{1}{T^2}\textstyle\sum_{t=1}^{T} x(t)x^*(t+\tau_3)\cdot\sum_{t=1}^{T} x(t+\tau_1)x^*(t+\tau_2) \end{aligned} \tag{2.5}$$

Supposing that there is only one source signal s_i and its steering vector is $\mathbf{a}(\theta_i)$, the signals received by the array sensors are defined as the vector Γ_i. For all d signal sources, the received signals at the k-th measurement time are $\Gamma(k) = \sum_{i=1}^{d} \Gamma_i(k) = \sum_{i=1}^{d} \mathbf{a}(\theta_i) \cdot s_i(k)$.

We define the vector $\mathbf{y}_i(k)$ by

$$\mathbf{y}_i(k) = \Gamma_i(k) \otimes \Gamma_i^H(k) = (\mathbf{a}(\theta_i) \otimes \mathbf{a}^*(\theta_i)) \cdot (s_i(k)s_i^*(k)) \tag{2.6}$$

where $'\otimes'$ denotes Kronecker product. Let C_y be a matrix of fourth-order cumulants of $\mathbf{y}_i(k)$ in Eq. (2.6), we get after some calculations,

$$C_y = (a(\theta_i) \otimes a^*(\theta_i)) \cdot \mathrm{cum}_4(s_i(k), s_i(k), s_i^*(k), s_i^*(k)) \cdot (a(\theta_i) \otimes a^*(\theta_i))^H \tag{2.7}$$

Based on the independence property of cumulant and on the fact that the fourth-order cumulants of any Gaussian variable are identically zero [62],[69], we get the following fourth-order cumulant of image data.

$$\begin{aligned} \mathbf{C}_{\mathbf{rr},4} &= \textstyle\sum_{i=1}^{d} C_y \\ &= \textstyle\sum_{i=1}^{d} (\mathbf{a}(\theta_i) \otimes \mathbf{a}^*(\theta_i)) \cdot \mathrm{cum}_4(s_i(k), s_i(k), s_i^*(k), s_i^*(k)) \cdot (\mathbf{a}(\theta_i) \otimes \mathbf{a}^*(\theta_i))^H \end{aligned} \tag{2.8}$$

From the data vector $\mathbf{r} = [r(1), r(2), \cdots, r(N)]^T$, we build K vectors $\mathbf{r}(p)$ of length M as in Eq. (2.9), that is, we collect K snapshots $\{\mathbf{r}(1), \mathbf{r}(2), \cdots, \mathbf{r}(K)\}$. This process, called spatial smoothing, is employed in array processing when we have only a single snapshot across a very large array.

$$\begin{bmatrix} \mathbf{r}(1) & \mathbf{r}(2) & \cdots & \mathbf{r}(K) \end{bmatrix} = \begin{bmatrix} \mathbf{z}_1 \\ \vdots \\ \mathbf{z}_M \end{bmatrix} = \begin{bmatrix} r_1 & r_2 & \cdots & r_{N-M+1} \\ \vdots & \vdots & \ddots & \vdots \\ r_M & r_{M+1} & \cdots & r_N \end{bmatrix} \tag{2.9}$$

where $\{\mathbf{z}_1, \mathbf{z}_2, \cdots, \mathbf{z}_M\}$ are the vectors which will be used further in the following. Some relationships between M, N and K offer $M = N - K + 1$ and $d < M \leq N - d + 1$. For every snapshot in Eq.(2.9),

$$\mathbf{r}(k) = \mathbf{A}(\theta)\mathbf{s}(k) + \mathbf{n}(k), \tag{2.10}$$

where $\mathbf{A}(\theta)$ is now a $M \times d$ matrix with l-th column, $\mathbf{a}(\theta_l) = [1, e^{j\mu \tan(\theta_l)}, \cdots, e^{j\mu(M-1)\tan(\theta_l)}]^T$, and where $s_i(k) = e^{j(k-1)\mu \tan \theta_i} \cdot e^{-j\mu x_{0_i}} (k = 1, \cdots, K)$ is the i-th source signal at k-th snapshot. Now we are ready to apply array processing techniques to our problem. As stated in [14], there is a compromise relationship to be found between M and K. On the one hand, the dimension of M needs to be chosen as large as possible in order to smooth out the eigenvalues corresponding to the noise subspace of the reconstructed cumulant matrix defined in Eq. (2.8). At the same time, in order to approximate the true cumulant matrix for the sample cumulant matrix, a large K has to be chosen.

2.4 Detection algorithms

In this section, we propose to estimate the angles by two high-resolution methods and the offsets by the extended Hough transform method.

2.4.1 Angle estimation

2.4.1.1 MUSIC-Like methods

In order to reduce the computational load, a slice cumulant matrix (for example, the first row of $\mathbf{C}_{\mathbf{rr},4}$), instead of above-mentioned cumulant (see Eq. (2.8)), offers the same properties [62]. Therefore, we have

$$\mathbf{C}'_{\mathbf{rr},4} = \{\mathrm{cum}_4(\mathbf{z}_1, \mathbf{z}_i, \mathbf{z}_1^*, \mathbf{z}_j^*)\}_{j=1,\cdots,M.}^{i=1,\cdots,M;} = \mathbf{A}(\theta) \cdot \Sigma \cdot \mathbf{A}^H(\theta) \tag{2.11}$$

where $\mathbf{z}_i$ is the i-th element in the signals $\mathbf{Z} = [\mathbf{z}_1, \cdots, \mathbf{z}_M]^T$, and $\Sigma = diag(\mathrm{cum}_4(s_1(k), s_1^*(k), s_1(k), s_1^*(k)), \cdots, \mathrm{cum}_4(s_d(k), s_d^*(k), s_d(k), s_d^*(k)))$, the diagonal elements of which are the kurtosis. We notice that there is no noise term in the cumulant slice matrix computed out of the generated signals in Eq. (2.11). Obviously, this reshaped matrix is the Hermitian matrix and its dimension is reduced to $M \times M$ from $M^2 \times M^2$, so the computational load is hugely decreased.

It is easy to get that $\mathbf{C}'_{\mathbf{rr},4}$ has rank d from the definition of matrix $\mathbf{A}(\theta)$ (see Eq. (2.4)), which shows that the columns of $\mathbf{A}(\theta)$ are linearly independent. The MUSIC-like algorithm relies on the singular value decomposition (SVD) of matrix $\mathbf{C}'_{\mathbf{rr},4}$:

$$\mathbf{C}'_{\mathbf{rr},4} = [\mathbf{U}_1, \mathbf{U}_2] \begin{bmatrix} \Lambda & \mathbf{0} \\ \mathbf{0} & \mathbf{0} \end{bmatrix} \begin{bmatrix} \mathbf{U}_1^H \\ \mathbf{U}_2^H \end{bmatrix} \tag{2.12}$$

For independent sources, the columns of $\mathbf{U}_1$ (M $\times$ d) span the signal subspace, the columns of $\mathbf{U}_2$ (M $\times$ (M $-$ d)) span the noise subspace, and $\mathbf{\Lambda} = diag\left(\lambda_1, \lambda_2, \cdots \lambda_{\mathrm{d}}\right)$ where λ_i is the eigenvalue associated with the i-th eigenvector. Hence, $\mathbf{U}_2$ is orthogonal to the steering vector of $\mathbf{a}\left(\theta\right)$. We estimate the orientations of lines by finding the maxima of the pseudo spectrum given by

$$\mathrm{MUSIC}\left(\theta\right) = \frac{1}{\parallel \mathbf{a}^H\left(\theta\right) \cdot \mathbf{U}_2 \parallel^2} \tag{2.13}$$

In conclusion, the practical application of the algorithm involves the following steps :

(1) Estimate the cumulant matrix by Eqs. (2.8), (2.9) and (2.11).

(2) Find the eigen-decomposition of the cumulant matrix by Eq. (2.12) and get the noise subspace $\mathbf{U}_2$. If the number of lines is unknown, the MDL (Minimum Description Length)or AIC (Akaike Information Criterion) criterion [79] are used to estimate by

$$d = \underset{k}{argmin}(\mathrm{MDL}(k)) \text{ or } \underset{k}{argmin}(\mathrm{AIC}(k)), \tag{2.14}$$

where $\mathrm{MDL}(k) = \log\{\frac{\prod_{i=k+1}^{M} \lambda_i^{\frac{1}{M-k}}}{\frac{1}{M-k}\sum_{i=k+1}^{M}\lambda_i}\}^{-(M-k)K} + \frac{k}{2}(2M-k)\log K$

and $\mathrm{AIC}(k) = \log\{\frac{\prod_{i=k+1}^{M} \lambda_i^{\frac{1}{M-k}}}{\frac{1}{M-k}\sum_{i=k+1}^{M}\lambda_i}\}^{-2(M-k)K} + 2k(2M-k)$, where k is a positive integer.

(3) Compute MUSIC(θ) by Eq.(2.13). The orientations of straight lines are estimated through the research of the maxima of MUSIC$\left(\theta\right)$.

2.4.1.2 Improved TLS-ESPRIT method

In this subsection, we define an appropriate matrix for implementing SVD and follow the key steps of TLS-ESPRIT method [53], which is different from the fourth-order cumulant matrix in MUSIC-like algorithm (see Eq. (2.11)) :

$$\mathbf{C}''_{\mathbf{rr},4} = \{\mathrm{cum}_4(\mathbf{z}_i, \mathbf{z}_i, \mathbf{z}_i^*, \mathbf{z}_j^*\}_{j=1,\cdots,M.}^{i=1,\cdots,M;} \tag{2.15}$$

After spatial smoothing procedure is applied to image data as in Eq. (2.9), we obtain M snapshots. In order to follow the key steps of TLS-ESPRIT algorithm, we firstly derive four $(M-1)\times(M-1)$ submatrices from Eq. (2.15) :

$$\mathbf{C}_{11} = \left\{\mathrm{cum}_4(\mathbf{z}_i, \mathbf{z}_i, \mathbf{z}_i^*, \mathbf{z}_j^*)\right\}_{j=1,\cdots,M-1}^{i=1,\cdots,M-1;} \tag{2.16a}$$

$$\mathbf{C}_{12} = \left\{\mathrm{cum}_4(\mathbf{z}_i, \mathbf{z}_i, \mathbf{z}_i^*, \mathbf{z}_j^*)\right\}_{j=2,\cdots,M}^{i=1,\cdots,M-1;} \tag{2.16b}$$

$$\mathbf{C}_{21} = \left\{\mathrm{cum}_4(\mathbf{z}_i, \mathbf{z}_i, \mathbf{z}_i^*, \mathbf{z}_j^*)\right\}_{j=1,\cdots,M-1.}^{i=2,\cdots,M;} \tag{2.16c}$$

$$\mathbf{C}_{22} = \left\{\mathrm{cum}_4(\mathbf{z}_i, \mathbf{z}_i, \mathbf{z}_i^*, \mathbf{z}_j^*)\right\}_{j=2,\cdots,M}^{i=2,\cdots,M;} \tag{2.16d}$$

Then, the following matrix, in place of the covariance matrix, can be used to implement a SVD operation :

$$\mathbf{C} = \begin{bmatrix} \mathbf{C}_{11} & \mathbf{C}_{12} \\ \mathbf{C}_{21} & \mathbf{C}_{22} \end{bmatrix} \tag{2.17}$$

The overall improved TLS-ESPRIT algorithm based on cumulant can be summarized as follows :

(1) form the matrix $\mathbf{C}''_{\mathbf{rr},4}$ by Eqs. (2.9), (2.8) and (2.15) ;

(2) generate four submatrices from Eq. (2.16) and reconstruct the matrix $\mathbf{C}$ by Eq. (2.17) ;

(3) perform SVD operation with $\mathbf{C}$.

$$\mathbf{C} = \mathbf{E}\mathbf{\Lambda}\mathbf{E}^H \tag{2.18}$$

where $\mathbf{\Lambda} = diag(\lambda_1, \cdots, \lambda_{2(M-1)})$ contains the eigenvalues $\lambda_1 \geq \lambda_2 \geq \cdots \geq \lambda_{\mathrm{d}} \geq \cdots \lambda_{2(M-1)}$. The eigenvalues $\lambda_1, \lambda_2, \cdots, \lambda_{\mathrm{d}}$ correspond to the signal subspace. Depending on the available prior knowledge, AIC or MDL criterion are used as in section 2.4.1.1.

(4) let $\mathbf{E}_1$ be the $2(M-1) \times \mathrm{d}$ upper-left matrix of $\mathbf{E}$ and $\mathbf{E}_2$ be $2(M-1) \times \mathrm{d}$ matrix formed by deleting the first row and taking the d first columns of matrix $\mathbf{E}$. We carry out the eigen-decomposition

$$\begin{bmatrix} \mathbf{E}_1^H \\ \mathbf{E}_2^H \end{bmatrix} \begin{bmatrix} \mathbf{E}_1 & \mathbf{E}_2 \end{bmatrix} = \mathbf{F}\Lambda_F\mathbf{F}^H \tag{2.19}$$

$$\mathbf{F} = \begin{bmatrix} \mathbf{F}_{11} & \mathbf{F}_{12} \\ \mathbf{F}_{21} & \mathbf{F}_{22} \end{bmatrix} \tag{2.20}$$

(5) Extract the submatrices $\mathbf{F}_{12}$ and $\mathbf{F}_{22}$, then find the eigenvalues $\{\gamma_k\}$ of $-\mathbf{F}_{12}\mathbf{F}_{22}^{-1}$.

(6) Estimate the orientation of every straight line by $\theta_k = \tan^{-1}(\frac{1}{\mu}\mathrm{Im}(\ln\frac{\gamma_k}{|\gamma_k|})), k = 1, \cdots, \mathrm{d}$.

2.4.2 Offset detection

After we estimate the line orientations, the steering matrix $\mathbf{A}(\theta)$ can be computed, then the maximum likelihood function or other similar methods are used to find the offsets of lines. The well-known method, the "Extension of the Hough Transform" [77], can be used to estimate the offsets of lines, and find the length $\{\rho_k\}$ of the normals from the origin to the lines, where

$$\rho_k = \arg\max_{\rho}\{\sum_{i=1}^{N_p} c(\rho - x_i\cos\theta_k - y_i\sin\theta_k)\} \tag{2.21}$$

and N_p is the number of the edge point in the image. $c(\cdot)$ is the function like

$$c(r) = \begin{cases} \cos(\frac{\pi}{2}\frac{r}{R}) & |r| < R \\ 0 & otherwise. \end{cases} \tag{2.22}$$

2.5 Numerical results

In this section, simulation results are presented and the performance of the proposed algorithms is evaluated.

2.5.1 Correlated Gaussian noise simulation

To evaluate realistically the algorithms, correlated Gaussian noise is simulated by the following steps. First, the 2-dimensional random Gaussian noise matrix is generated, which has the same dimensions as the initial binary image and obeys a Gaussian distribution with mean 0 and variance σ^2. Then, the generated Gaussian noise matrix passes through the spatial Gaussian low pass filter, so that we obtained the expected correlated Gaussian noise by setting the filter's parameter. The impulse response of the filter is expressed as :

$$h(x,y) = \frac{1}{2\pi\sigma_1\sigma_2} e^{-\frac{x^2}{2\sigma_1^2}-\frac{y^2}{2\sigma_2^2}}, \tag{2.23}$$

where σ_1 and σ_2 are vertical and horizontal variance, and determine the correlation strength of noise image. Specially, $\sigma_1 = \sigma_2$ means an isotropic Gaussian low pass filter. In the simulation, the filter function $h(x,y)$ should be discretized to get the filter template, which is center-symmetric. Herein, the correlation length (CL) of correlated Gaussian noise is defined as :

$$CL = \frac{CL_x + CL_y}{2}, \tag{2.24}$$

where CL_x and CL_y are $2\sigma_1$ and $2\sigma_2$.

2.5.2 Numerical simulation

In the simulation, we set the size of processed image as 100×100. As an example in Fig. 2.3, standard variance of white Gaussian noise is 6 and CL of correlated Gaussian noise is 6. For initial image (see Fig. 2.3 (a)), there are two straight lines whose angles are respectively 32° and 20° and offsets are 95 and 55. The estimation results provided by the cumulant-based MUSIC-like algorithm (see Fig. 2.3 (c)) and by the improved TLS-ESPRIT algorithm (see Fig. 2.3 (d)) are more accurate than those provided by second-order based algorithms (see Fig. 2.3 (b)). The orientations of two lines are 32.3° and 20.4° for MUSIC-like algorithm, and 31.8° and 19.9° for improved TLS-ESPRIT algorithm respectively. For the offsets, they are respectively 93.8 and 52.9 for MUSIC-like algorithm, and 92.6 and 54.8 for TLS-ESPRIT

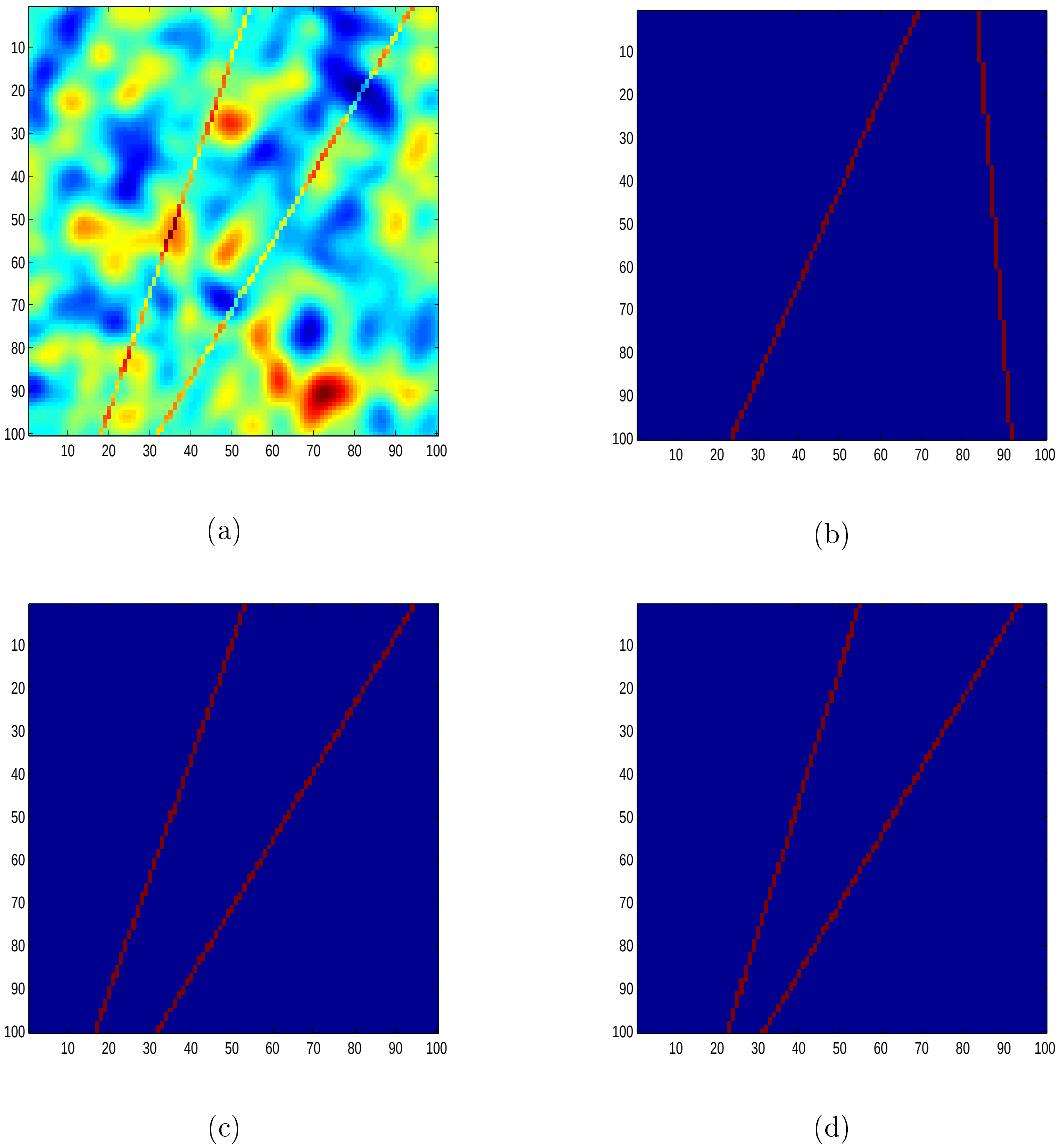

Figure 2.3 — Initial image and estimated results for two lines with 32 and 20 degrees. (a) initial scaled image ; (b) result without cumulant ; (c) MUSIC-like algorithm ; (d) TLS-ESPRIT algorithm.

algorithm. Especially when the images are severely corrupted by correlated Gaussian noise, the cumulant-based algorithms still correctly characterize the lines, while the algorithms using second-order statistics yield a large bias.

The next experiment concerns an image with crossing straight lines in a correlated noise environment. The line offsets are 95 and 25 pixels ; the line angles are $40°$ and $-20°$ (see Fig. 2.4(a)). To generate the correlated Gaussian noise, the standard deviation of the white Gaussian noise is 2, the correlation length of the correlated Gaussian noise is 8.

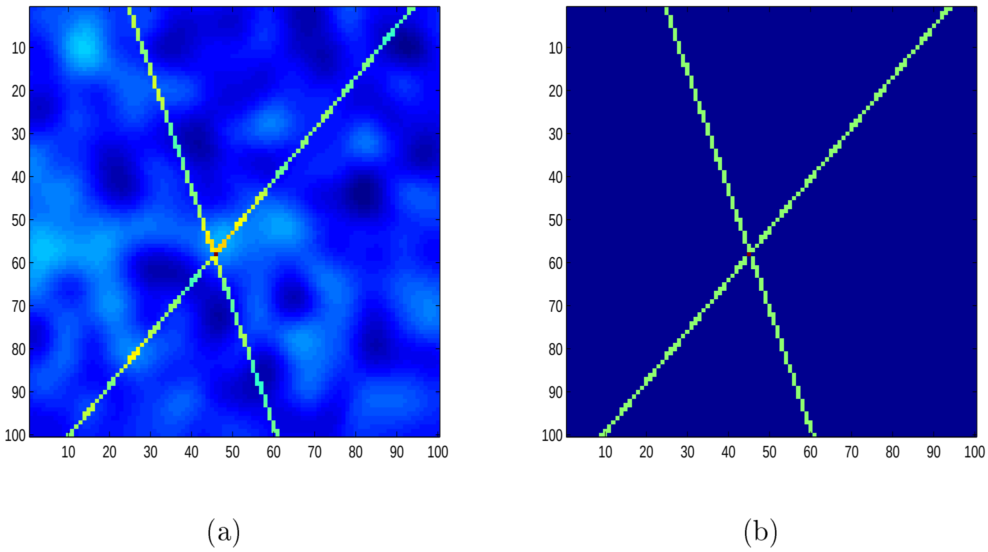

Figure 2.4 — (a) processed image : two cross lines with orientation 40° and −20° and offsets 95 and 25 pixels ; (b) segmentation result by MUSIC-like algorithm .

2.5.2.1 Correlation length of correlated Gaussian noise vs angle detection

We set the standard variance of white Gaussian noise as 10, and let CL be 10, then run 500 trials and analyze the biases of detected angles for MUSIC-like and improved TLS-ESPRIT algorithm .

In Fig. 2.5, the estimated angles using MUSIC-like algorithm are closer to the expected values, and the biases between estimated angles and true values are smaller compared to improved TLS-ESPRIT algorithm for the line with the orientation of 20°. The mean values of the two estimated orientations are respectively 32.2° and 19.9° for MUSIC-like algorithm, while they are 31.9° and 19.7° for improved TLS-ESPRIT.

For K trials, the mean error ME and standard deviation Std are defined like : $ME = \frac{1}{K}\sum_{k=1}^{K}|x_k - \bar{x}|$ and $Std = \sqrt{\frac{1}{K}\sum_{k=1}^{K}(x_k-\bar{x})^2}$, where x_k is each estimated angle and $\bar{x}$ is the mean of all estimated angles. Table 2.1 presents the simulation result with the change of CL. We can see that, the mean error decreases when the correlation length of the correlated noise increases. That is because the correlated noise amplitude decreases when the correlation length increases. In all cases, the performance of cumulant-based algorithms is better comparing the algorithms without the use of cumulant-based algorithms.

2.5.2.2 High resolution performance of the proposed algorithms

The following experiments aim at studying the high resolution capabilities of the proposed algorithm : the high-resolution properties of MUSIC-like and improved TLS-ESPRIT methods

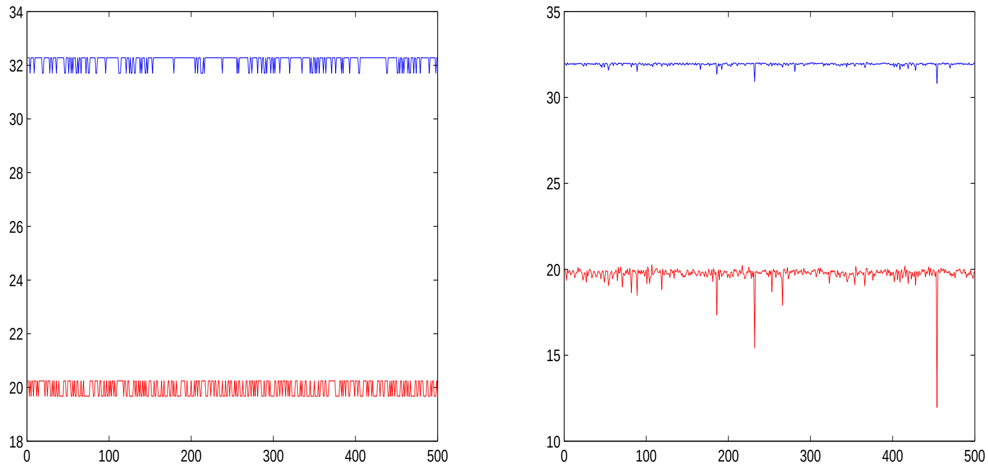

(a) (b)

Figure 2.5 — Estimated two line's angles 32° and 20° for 500 trials. (a) using MUSIC-like algorithm ; (b) using TLS-ESPRIT algorithm.

Tableau 2.1 — Results with increase of CL

		CL=8	12	16
ME(MUSIC-like)	32°	0.2859	0.2831	0.2801
	20°	0.5358	0.2788	0.276
Std(MUSIC-like)	32°	0.2858	0.2616	0.1807
	20°	0.3066	0.2815	0.2766
ME(TLS-ESPRIT)	32°	0.7885	0.3733	0.1782
	20°	1.4014	0.8247	0.3527
Std(TLS-ESPRIT)	32°	1.1963	0.6973	0.2905
	20°	2.427	1.6592	0.9817

which apply in array processing should also apply for the considered image processing issue.

In the first experiment, three lines with 40°, 20° and −20° are considered in the image. The standard variance of the white Gaussian noise is set to 12, and CL is 12. We can get a pseudo spectrum as in Fig. 2.6 (a) for MUSIC-like algorithm. The means of estimated angles for MUSIC-like algorithm are respectively 39.7°, 20.2° and −20.3° if the number of trial is 500, and they are 40.1°, 19.9° and −20.4° for improved TLS-ESPRIT algorithm. In a second experiment, after we change the angles to be 32°, 28° and −20° (see Fig. 2.6 (b)), MUSIC-like algorithm can still evaluate the angles with almost no error. The means of estimated angles are 32.2°, 28.3° and −19.9° for 500 trials. For improved TLS-ESPRIT algorithm, we also get the similar results, their mean values of 500 trials are 32.5°, 28.1° and −19.7°.

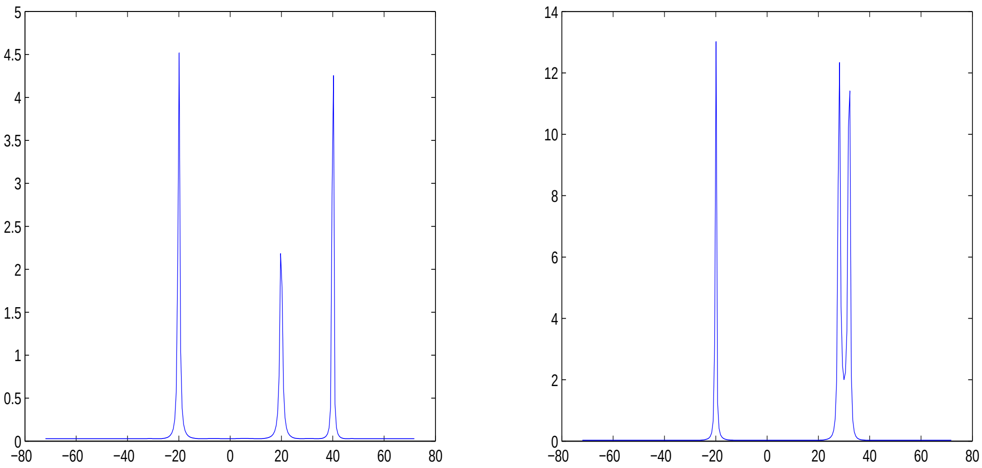

(a) (b)

Figure 2.6 — Pseudo spectrum using MUSIC-like algorithm. (a) three lines with $40°$, $20°$ and $-20°$; (b) three lines with $32°$, $28°$ and $-20°$.

2.5.2.3 Analysis of the computational load of the algorithms

As presented, our algorithms exploit the fourth-order cumulant slice matrix instead of the whole of cumulant matrix. In this experiment, we evaluate the computational load of our algorithms. We run Matlab on a PC (2 Quad CPU @2.83G, 4G memory) and set $M = 36$. For the experiment with detection of three lines with $40°$, $20°$ and $-20°$ as in the previous experiment, when the slice cumulant matrix is used, MUSIC-like algorithm costs 0.37 sec., and the improved TLS-ESPRIT algorithm costs 0.01 sec. If the algorithms based on the whole cumulant matrix are used, computational times are 4972 sec. for MUSIC-like algorithm, and 104.6 sec. for the improved TLS-ESPRIT algorithm respectively, contrary to Hough Transform, 1.43 sec. It is shown that the computational load is considerably decreased when the cumulant slice matrix is used instead of the whole cumulant matrix, especially for MUSIC-like algorithm, because MUSIC-like algorithm reduces the search dimensions for the maxima of the pseudo spectrum.

2.6 Conclusion

In this chapter, the problem of contour detection in images was investigated by setting a link between image data in image processing and array signals in array processing. Considering the circumstance of correlated Gaussian noise, fourth-order cumulant-based MUSIC-like and improved TLS-ESPRIT algorithm for non-Gaussian virtual generated signals from the image were presented to estimate the orientations of lines, while the offsets of lines were estimated by "Extension of the Hough Transform". Numerical simulations show that the proposed cumulant-based algorithms improve the detection performance for the images impaired by correlated Gaussian noise. At the same time, we have shown that exploiting the cumulant slice matrix instead of the whole cumulant matrix evidently accelerates the algorithm in the experiment. These methods can also be applied to detect other contours, such as a distorted linear-like contours and circles, which will be presented in the following chapters.

CHAPITRE 3

Circular-like and star-shaped contour detection

Circular features are commonly sought in various domains such as medical image processing, mechanical parts detection, robotic vision systems. For these applications, the detected images are often affected by white or colored Gaussian noise. In these cases, how to effectively estimate circle or circle-like contour is an interesting problem. Ordinary or total least-squares methods for circle fitting seek to minimize the squared sum of error-of-fit with respect to measures [33, 80]. In [80], circular objects are extracted from an image by a least-squares fitting approach. One of the major limitations of most of least-squares approaches is their sensitivity to outliers. The variants of Hough transform [8, 77, 81] provide an estimate of the circle center coordinates, but their main drawback is that the methods exhibit a huge computational load, although fast versions have been proposed. Array processing methods [14, 18, 22, 56, 76, 82] have been proposed to find some characteristics of linear or circular contours. The formalism proposed by Aghajan [14, 16, 17, 18] detects linear or circular contours. But all of these methods only apply in a white Gaussian noise environment. Moreover, for distorted circular contours, an optimization method is adopted in [22] to retrieve the contour. When the noise level is elevated, the proposed approaches need to be improved.

This chapter is organized as follows : firstly, we overview the problem of circle retrieval, while explaining how to generate a signal from the image, upon a linear antenna. In section 3.2, we present the approach of parameter estimation by linear antenna in white noise environment. In section 3.2.2, we highlight the circular antenna model, and show that a linear phase signal is obtained. Then, we consider the problem of radius estimation in correlated noise environment. In section 3.3, we describe the problem of retrieving a star-shaped contour, and show that an adequate image transformation process permits to reformulate this problem as a damped exponential sinusoidal model, and parameter estimation based on the damped sinusoid characterization method is exploited. Experiments are performed which show that our method offers an improvement in terms of pixel bias and computational load, in particular when strongly concave contours in noisy images are considered. At last, we draw a conclusion of chapter 3.

3.1 Problem formulation

3.1.1 Linear antenna model

We review the principles of signal generation on virtual circular antenna. The generated signals fit classical array processing methods. A two-dimensional binary image $I(l, m)$ is considered to be a square matrix of size $N \times N$ (see Fig. 3.1).

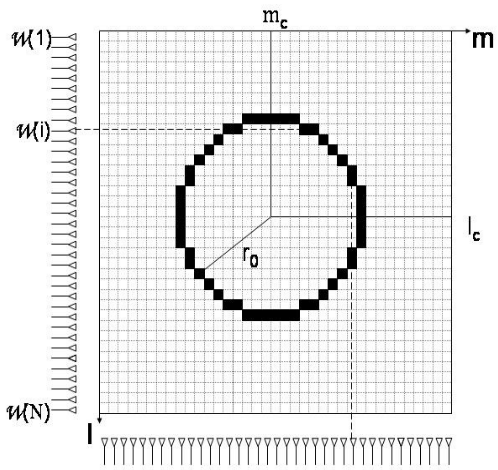

Figure 3.1 — Linear antenna model in an image containing circular contour

An object in the image is made of edge pixels with value 1, over a background of zero-valued pixels. The circle center coordinates are quoted (l_c, m_c) and its radius is r_0. In order to set the link between image data representation and sensor array processing methods, array sensors are supposed to be placed in front of each row and column of the image. Each sensor receives the signals only from its corresponding row or column in the matrix. We adopt the same assumption as in chapter 2 : all the pixels in the image propagate narrow-band electromagnetic waves with zero initial phases, and the waves emanating from pixels in a given row of the image matrix are confined to travel only along that row towards the corresponding sensor. For every row of the image, the signal received by the corresponding sensor is :

$$z_{lin}(l) = \sum_{m=1}^{N} I(l, m) exp(-j\mu m), l = 1, \cdots, N, \tag{3.1}$$

where $I(l, m)$ is the value of pixel (l, m), m is the column index of the pixel, and μ is the propagation coefficient [14]. In the same way, the signal can be generated in every column of the image.

3.1.2 Circular antenna model

From the previous section, we observe that, when there are circles in the image, the generated signals do not exhibit linear phase when signals are generated on a linear antenna. To obtain a linear phase signal from the image, a circular antenna in [22] is proposed to adapt to the processed image : the center of the virtual circular antenna is placed at the center of the circle (see Fig. 3.2(a)). In Fig. 3.2, r denotes the radius of the circle. If a sub-image containing a quarter of circle is extracted, the signal component for a given sensor is generated starting from the top left corner of the sub-image, and ending on the sensor (see Fig. 3.2(b)). In a polar coordinate system, every pixel of the object outline is associated with (ρ, θ). The pixels in every D_i direction contribute to the signal component received by the corresponding sensor i, as follows :

$$z(i) = \sum_{l,m=1;(l,m)\in D_i}^{l,m=N_s} I(l,m)exp(-j\mu\sqrt{l^2+m^2}) \tag{3.2}$$

where N_s is the maximum number of rows and columns in the sub-image, that is, $N_s = \max(N - m_c, N - l_c)$. The minimum number of sensors must be $\sqrt{2}N_s$. For details about the choice of the pixels in each direction D_i and the number of sensors, refer to [22]. In this article, the number of sensors S is chosen as $2N_s$.

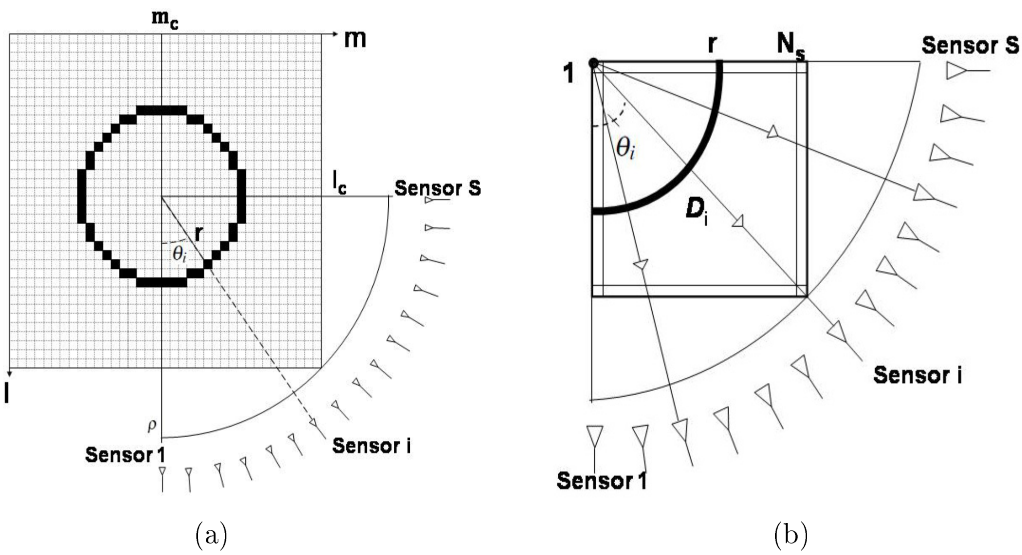

Figure 3.2 — (a) circular antenna model, (b) bottom right quarter of the contour and pixel coordinates in the polar system (ρ, θ) having its origin on the center of the circle

3.2 Parameter estimation

In this section, we propose an approach to estimate the parameters of circle by linear antenna and circular antenna model in white noise environment [83].

3.2.1 Estimation of circle parameters

Usually, an image contains several circles which are possibly not concentric and have different radii (see Fig. 3.3). To apply the proposed method, the center coordinates for each feature are required. To estimate these coordinates, we generate a signal by linear antenna model with constant propagation parameter upon the image left and top sides. The non-zero sections of the signals, as seen at the left and top sides of the image, indicate the presence of features (see Fig. 3.3). Each non-zero section width in the left (respectively the top) side signal gives the height (respectively the width) of the corresponding expected feature. The middle of each non-zero section in the left (respectively the top) side signal yields an approximate value of the center l_c (respectively m_c) coordinate of each feature.

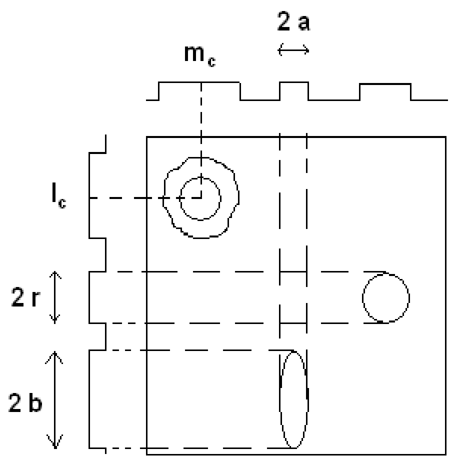

Figure 3.3 — Model for an image containing several nearly circular or elliptic features. r is the circle radius, a and b are the axial parameters of the ellipse.

In this case, an algorithm can be adapted based on signal generation on linear antenna. Signal generation on linear antenna yields a signal with the following characteristics :
The maximum amplitude values of the generated signal correspond to the lines with maximum number of pixels, that is, where the tangent to the circle is either vertical or horizontal. The signal peak values are associated alternatively with one circle and another.

Signal generation on circular antenna yields a signal with the following characteristics :
If the antenna is centered on the same center as a quarter of circle which is present in the image, the signal which is generated on the antenna exhibits linear phase properties [22].

We propose a method that combines linear and circular antenna to retrieve intersecting circles. We exemplify this method with an image containing two circles (see Fig. 3.4). It falls into the following parts :

- Generate a signal on a linear antenna placed at the left and bottom sides of the image ;
- Associate signal peak 1 (P1) with signal peak 3 (P3), signal peak 2 (P2) with signal peak 4 (P4). The peak amplitude values of the generated signal correspond to the lines with maximum number of pixels, that is, where the tangent to the circle is either vertical or horizontal ;
- Diameter 1 is given by the distance P1-P3, diameter 2 is given by the distance P2-P4 ;
- Center 1 is given by the mid point between P1 and P3, center 2 is given by the mid point between P2 and P4 ;
- Associate the circular antenna with a sub-image containing center 1 and P1, perform signal generation. Check the phase linearity of the generated signal ;
- Associate the circular antenna with a sub-image containing center 2 and P4, perform signal generation. Check the linearity of the generated signal.

Fig. 3.4(a) presents, in particular, the squared sub-image to which we associate a circular antenna.

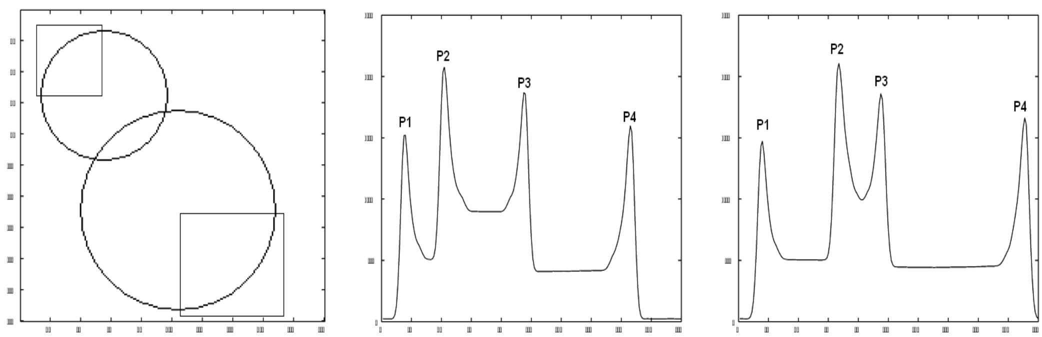

(a) (b) (c)

Figure 3.4 — (a) processed image ; (b) signals generated on the bottom of the image ; (c) signals generated on the left side of the image.

3.2.2 Radius estimation for multiple concentric circles

Most often, there exists more than one circle for one center. We demonstrate how several possibly close radius values can be estimated using a high-resolution method. To estimate the number d of concentric circles, and each radius value, we employ a variable speed propagation scheme [22]. We set $\mu = \alpha(i-1)$, for each sensor indexed by $i = 1, \ldots, S$. From Eq. (3.2), the signal received on each sensor is :

$$z(i) = \sum_{k=1}^{d} exp(-j\alpha(i-1)r_k) + n(i),\ i = 1, \ldots, S \tag{3.3}$$

where $r_k,\ k = 1, \ldots, d$ are the values of the radius of each circle, and $n(i)$ is a noise term due to outliers. All components $z(i)$ compose the observation vector $\mathbf{z}$. TLS-ESPRIT (Total Least Squares-Estimation of Parameters by Rotational Invariance Techniques) algorithm requires the estimation of the covariance matrix of several snapshots. There is no time-dependent signals. So the question arises as how a sample covariance matrix can be formed. This can be done as follows [18] :
From the observation vector we build K sub-vectors of length M with $d < M \leq S - d + 1$: $\mathbf{z}_l = [z(l), \cdots, z(l+M-1)]^T,\ l = 1, \cdots, K$. To maximize the number of snapshots, the first component of a snapshot is the second component of the previous snapshot. This improves the estimation of the covariance matrix that is performed in TLS-ESPRIT algorithm. We obtain then $K = S + 1 - M$ snapshots. Grouping all sub-vectors obtained in matrix form, we get $\mathbf{Z}_K = [\mathbf{z}_1, \cdots, \mathbf{z}_K]$, where

$$\mathbf{z}_l = \mathbf{A}_M\ \mathbf{s} + \mathbf{n}_l, \quad l = 1, \cdots, K. \tag{3.4}$$

$\mathbf{A}_M = [\mathbf{a}(r_1), \cdots, \mathbf{a}(r_d)]$ is a Vandermonde type matrix of size $M \times d$: the i^{th} component of $\mathbf{a}(r_k)$ is $exp(-j\alpha(i-1)r_k)$. $\mathbf{s}$ is a length d vector equal to $[1, 1, \ldots, 1]^T$ -superscript ^{T} denotes transpose- and $\mathbf{n}_l = [n(l), \cdots, n(l+M-1)]^T$.

The signal model of Eq. (4.16) suits TLS-ESPRIT method, a subspace-based method that requires the dimension of the signal subspace, that is, in this problem, the number of concentric circles. MDL criterion estimates the dimension of the signal subspace [18] from the eigenvalues of the covariance matrix.

TLS-ESPRIT is applied on the measurements collected from two overlapping sub-arrays, and falls into two parts : the covariance matrix estimation and the minimization of a total-least-squares criterion. The radius values are obtained as [18] :

$$\hat{r}_k = \frac{-1}{\alpha} Im(\ln(\frac{\lambda_k}{|\lambda_k|})),\ k = 1, \ldots, d \tag{3.5}$$

where $Im(\cdot)$ denotes imaginary part, and $\{\lambda_k,\ k = 1, \ldots, d\}$ are the eigenvalues of a diagonal unitary matrix. It relates the measurements from the first sub-array with the measurements resulting from the second sub-array.

3.2.3 Numerical results

3.2.3.1 Parameter estimation in white noise environment

We first exemplify the proposed method on the image of Fig. 3.5(a), from which we obtain the results of Fig. 3.5, which presents the signal generated on both sides of the image. The signal obtained on the left side exhibits only two peak values, because the radius values are very close to each other. Therefore signal generation on linear antenna provides a rough estimate of each radius, and signal generation on circular antenna refines the estimation of both values. The center coordinates of circles 1 and 2 are estimated as $\{l_{c1},\ m_{c1}\} = \{83,\ 41\}$ and $\{l_{c2},\ m_{c2}\} = \{83,\ 84\}$. Radius 1 is estimated as $r_1 = 24$, radius 2 is estimated as $r_2 = 30$.

The computationally dominant operations while running the algorithm are signal generation on linear and circular antenna. For this image and with the considered parameter values, the computational load required for each step is as follows :

– signal generation on linear antenna : 3.8 10^{-2} sec. ;
– signal generation on circular antenna : 7.8 10^{-1} sec.

So the whole method lasts 8.1 10^{-1} sec. For sake of comparison, generalized Hough transform with prior knowledge of the radius of the expected circles lasts 2.6 sec. for each circle. Then it is 6.4 times longer than the proposed method.

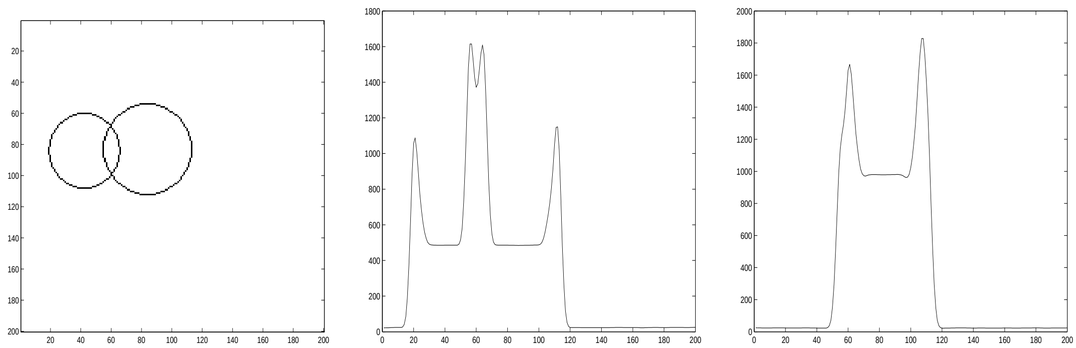

(a) (b) (c)

Figure 3.5 — (a) processed image ; (b) signals generated on the bottom of the image ; (c) signals generated on the left side of the image.

The case presented in Fig. 3.6 illustrates the need for the last two steps of the proposed algorithm. Here was exemplified the ability of the circular antenna to distinguish between ambiguous cases. Indeed the signals generated on linear antenna present the same peak coordinates as the signals generated from the image of Fig. 3.4(a). However, if a subimage is selected, and the center of the circular antenna is placed such as in Fig 3.4(a), the phase of the generated signal is not linear. Therefore, for Fig. 3.6(a), we take as the diameter values the distances P1-P4 and P2-P3. The center coordinates of circles 1 and 2 are estimated as $\{l_{c1},\ m_{c1}\} = \{68,\ 55\}$ and $\{l_{c2},\ m_{c2}\} = \{104,\ 99\}$. The radius of circle 1 is estimated as $r_1 = 87$, the radius of circle 2 is estimated as $r_2 = 27$.

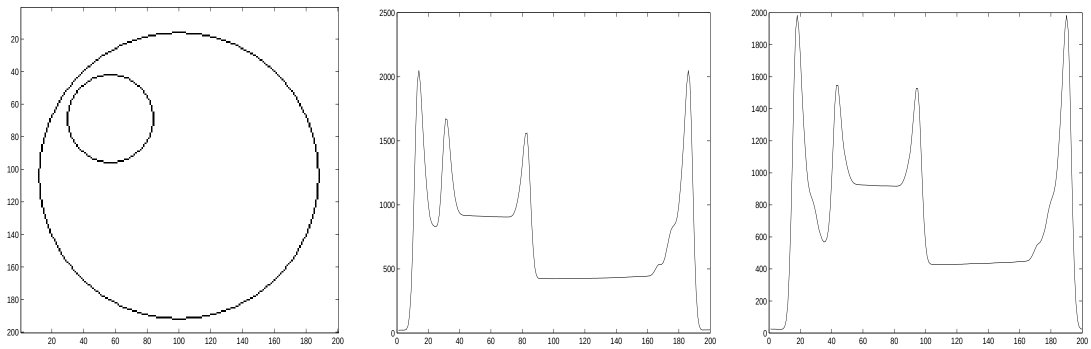

(a) (b) (c)

Figure 3.6 — (a) processed image ; (b) signals generated on the bottom of the image ; (c) signals generated on the left side of the image.

Fig. 3.7 shows the results obtained with a noisy image. The percentage of noisy pixels is 15%, and noise grey level values follow a Gaussian distribution with mean 0.1 and standard deviation 0.005. The presence of noisy pixels induces fluctuations in the generated signals, Figs. 3.7(b) and 3.7(c) show that the peaks that permit to characterize the expected circles are still dominant over the unexpected fluctuations. So the obtained results do not suffer the influence of noise pixels. The center coordinates of circles 1 and 2 are estimated as $\{l_{c1},\ m_{c1}\} = \{131,\ 88\}$ and $\{l_{c2},\ m_{c2}\} = \{53,\ 144\}$. Radius of circle 1 is estimated as $r_1 = 67$, radius of circle 2 is estimated as $r_2 = 40$.

3.2.3.2 Parameter estimation in colored noise environment

For two or more concentric circles with close radii in a correlated noise environment, the previous methods may fail. To face this situation, with the knowledge of the center coordinates, we can exploit the signals of Eq. (3.3), and adapt the high-resolution method proposed in section 2.4.1.2, which integrates higher-order cumulants in a high resolution method.

In the simulation, the dimensions of the processed image are set to 200×200. The propagation parameter is set to $\mu = 5.10^{-3}$ when the constant speed propagation scheme is adopted, and $\alpha = 2.10^{-3}$ for the variable speed propagation scheme. When spatial smoothing

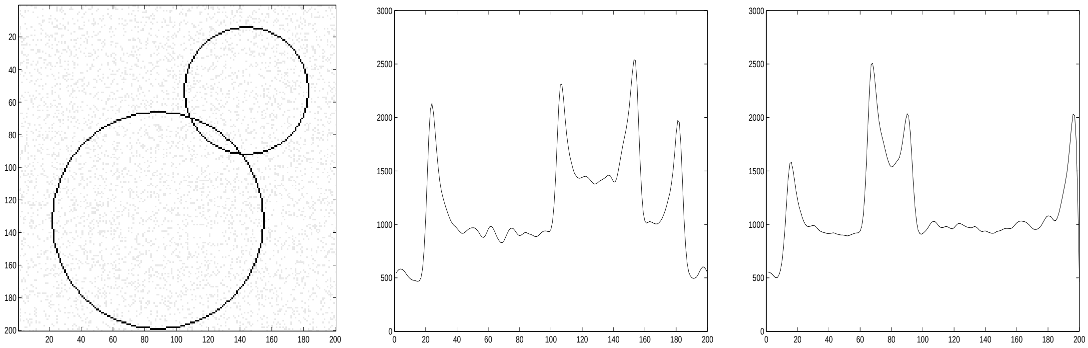

(a) (b) (c)

Figure 3.7 — (a) processed image ; (b) signals generated on the bottom of the image ; (c) signals generated on the left side of the image.

technique is adopted to obtain the sample signal matrix, the length M of each sub-array is 108. Correlated Gaussian noise is simulated as in section 2.5.1. We set σ to 7.5. Besides, to scale the degree of noise correlation, correlation length of generated Gaussian noise is defined as $CL = 2\sigma$.

• Experiment 1 : single circle or ellipse

In the first experiment, we implement the detection of a single circle for the hand-made image including one circle with radius value 50 pixels and center coordinates $(100, 100)$ (see Fig. 3.8(a)). In order to estimate the center coordinates and the radius value, the signals are generated on a linear antenna (see section 3.2.1). Fig. 3.8(b) is the signal generated on the left of the image, and Fig. 3.8(c) is the signal generated on the bottom of the image. We perform 100 trials with a different noise realization for each trial, and analyze the mean value of the radius and coordinates of the center. By detecting the peak values of each signal, the estimated radius value is 49.5 pixels and the estimated center coordinates are $(100.1, 100.5)$. For the ellipse of Fig. 3.8 (2a), we set the center coordinates $(100, 100)$, its semi-major axis 60 pixels, and semi-minor axis 50 pixels. After 100 trials with different correlated noise realization, the mean value of the estimated center is $(99.5, 100.4)$, and the length of two semi-axis are 59.5 and 49.5 pixels respectively.

• Experiment 2 : multiple circles with different radii and different centers

We implement the experiment considering the case of intersecting circle (see Fig. 3.9(1a)). The radius values are respectively 40 and 50 pixels, and the centers of circles are respectively $(70, 80)$ and $(120, 130)$. In this experiment, we still use a linear antenna model to generate the signals and repeat the experiment 100 times, the estimated value of the radius of the two circles are 40.5 and 50.5. The coordinates of two centers are estimated as $(69.8, 79.5)$ and $(119.3, 129.2)$. For intersecting ellipses, similar generated signals are obtained (see Fig. 3.9(2a, 2b, 2c)).

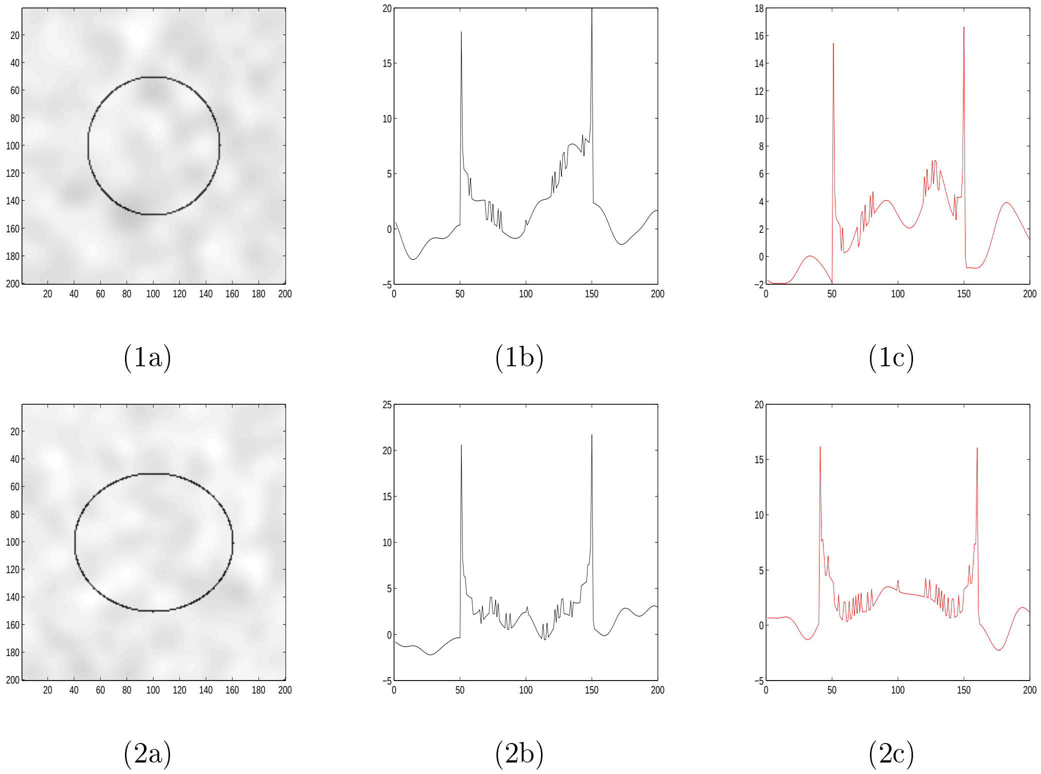

Figure 3.8 — (1a) a single circle ; (1b) signal generated on the left of detected image (1a) ; (1c) signal generated on the bottom of detected image (1a) ; (2a) a single ellipse ; (2b) signal generated on the left of detected image (2a) ; (2c) signal generated on the bottom detected image (2a)

• Experiment 3 : multiple concentric circles with close radii

As mentioned above, when there are multiple concentric circles with close radius values, using linear antenna model to generate the signal leads to close peak positions, and this sometimes causes errors of estimation of radius value and center coordinates (see Fig. 3.10). Therefore, we implement the following experiments to estimate the radius of multiple concentric circles by high-resolution methods.

In this simulation, we make a comparison between the improved TLS-ESPRIT algorithm and GHT method. Since GHT method needs the prior knowledge of center coordinates to provide the estimation of the radii, we create an image which contains two concentric circles with center coordinates $(100, 100)$ and radius values 45 and 50 pixels. Then we perform 100 trials with different correlated noise realizations.

When the proposed method is applied, MDL criterion is used to estimate the number of circles. The estimated radius values when the proposed method is used are respectively 44.5 and 51 pixels, and with Hough transform method 45 and 50 pixels (see Fig. 3.11). In the same experimental environment (Intel 2 Quad CPU, 2.83GHz, with 4G memory), the

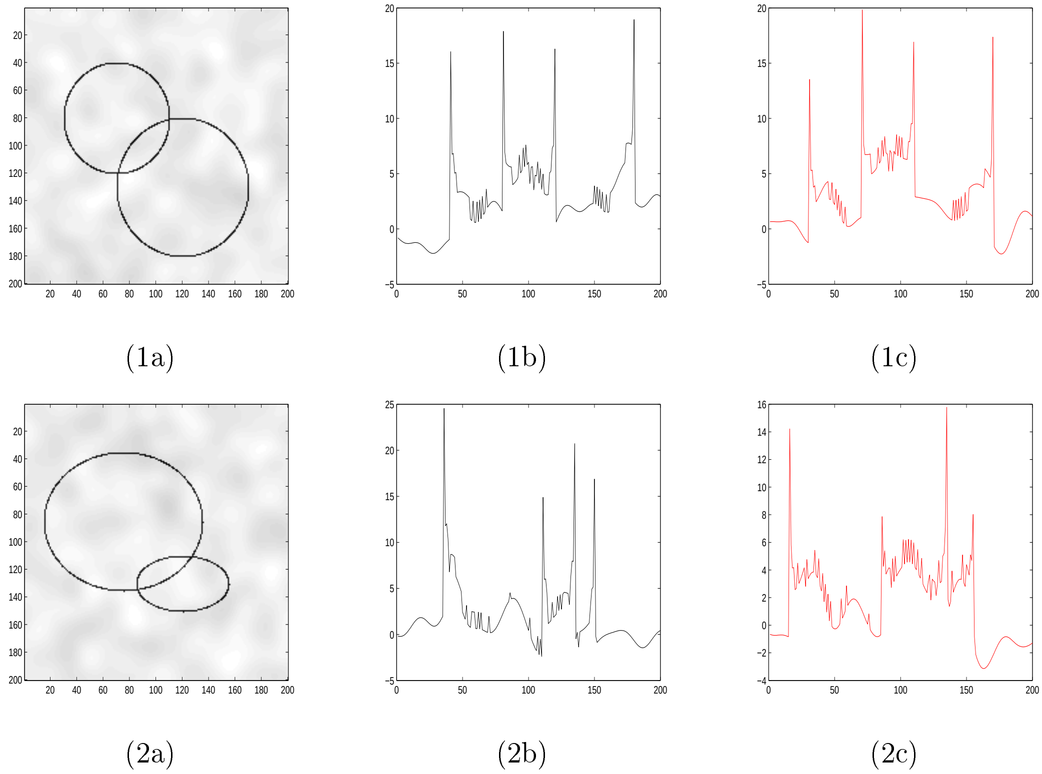

Figure 3.9 — (1a) two intersecting circles, (2a) two intersecting ellipses; (1b, 2b) signal generated on the left side of the image; (1c, 2c) signal generated on the bottom side of image

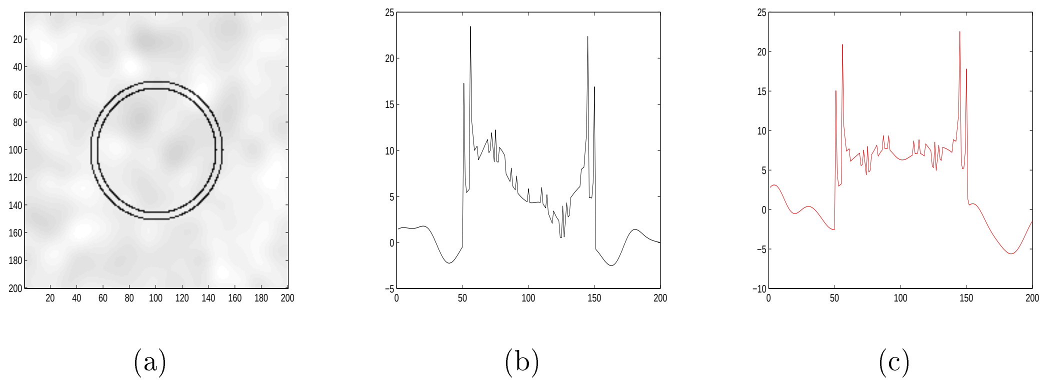

Figure 3.10 — (a) two concentric circles; (b) signal generated on the left side of the image; (c) signal generated on the bottom side of the image

computational time is only 0.13 sec. for TLS-ESPRIT algorithm, while it is 0.27 sec. for GHT method when the step of ρ is 0.05 pixel and the step of θ is quantized to the number of sensors used in circular antenna model.

In this experiment, the effect of correlation length of correlated noise is analyzed. In theory, with the increase of correlation length of correlated noise, the percentage of noise pixels is

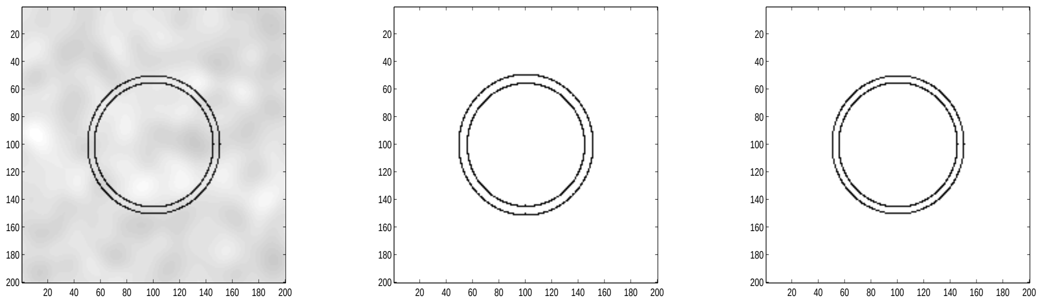

(a) (b) (c)

Figure 3.11 — (a) processed image with two concentric circles ; (b) result obtained by the proposed method ; (c) result obtained by GHT ;

Tableau 3.1 — Mean errors(ME) vias correlation length (CL)

	CL	14	16	18	20
ME	$\rho = 50$	4.84	2.96	2.74	2.71
	$\rho = 43$	5.63	3.25	2.68	2.81
	CL	22	24	26	28
ME	$\rho = 50$	2.25	1.93	1.20	1.19
	$\rho = 43$	2.32	1.65	1.57	1.31
	CL	30	32	34	36
ME	$\rho = 50$	0.95	1.08	0.93	0.46
	$\rho = 43$	1.29	1.04	0.86	0.78

less, but the degree of correlated noise increases. The mean error on radius estimation, here, defined as $ME = (1/T)\sum_{i=1}^{T} |\rho(i) - \rho|$, where $T = 100$ is the number of trials and $\rho(i)$ is the estimated radius for each trial. Table. I shows that the mean error decreases when the correlation length of the correlated noise increases. That is because there is less correlated noise in the image as the correlation length increases when the amplitude of the white Gaussian noise passing the filter keeps constant.

3.3 Detection of highly concave contours in noisy environment by a damped sinusoid characterization method

In this section, we discuss the problem of recovering a star-shaped contour with the assumption that the contour coordinates can be decomposed into damped sinusoids.

First, we exploit array signals generated from the image, and propose to characterize circle contours in white and colored noise environment. Especially, for the concentric closed circles in the image with color noise, we introduce higher-order statistical high-resolution method to estimate their radius.

Secondly, we detect star-shaped contours which may exhibit strong concavity. For this, we detect blindly the center of gravity of the contour [22], and choose an adequate system of polar coordinates which permits to consider the contour as star-shaped. Getting inspired from an existing signal generation method [22], we transform the content of the data composed of a 2-D image into a 1-D signal. The obtained signal contains the information of the contour radial coordinates. Contrary to what has been done in previous works, the contour is no longer supposed to be linear, circular, or polygonal. We assume that the polar coordinates of a closed circular-like contour edge is the sum of several damped sinusoidal components. In this way, the problem of edge characterization is transformed into the estimation of the amplitude, frequency, and damping factor of each sinusoidal component. In this way, we are able to characterize entirely the contour coordinates with a parametric estimation method of multiple damped sinusoids [50]. The advantage of using a parametric method is that the computational load is independent from the parameter values. In particular, we may retrieve very concave contours if the frequency and the amplitude values are sufficiently elevated.

Thirdly, we take into account the requirements of the frequency estimation method about the algebraic structure of the signal generated out of the image : the generated signal must be refined to fit the model required for the damped frequency estimation. For this, we rearrange the data as a Hankel matrix form, and we refine the signal by solving a so-called Structured Total Least Norm (STLN) problem [84], to get a processed matrix which is rank deficient. This process is necessary only in the case of high noise, where it slightly decreases the bias between expected and estimated contours.

3.3.1 Problem overview

Based on the simplification of Eq. (3.2), where the propagation parameter is not considered, the signal component for a given sensor i is generated by the pixels in every D_i direction as follows :

$$z_i = \sum_{l=1}^{N_s} \sum_{\substack{m=1 \\ (l,m)\in D_i}}^{N_s} I_{l,m} \sqrt{l^2+m^2}, \; i = 1, \cdots, S \tag{3.6}$$

where N_s is the maximum number of rows and columns in the sub-image. The signal components form the signal vector $\mathbf{z} = [z_1, z_2, \ldots, z_S]^T$.

The considered signal generation process requires the knowledge of the center coordinates (l_c, m_c). To estimate them, a linear array of sensor is placed along the left (or bottom) side of the image [18, 56], and the following signal generation schemes can be adopted : $z_l^{left} = \sum_{m=1}^{N} I_{l,m}, \; l = 1, \cdots, N$ and $z_m^{bottom} = \sum_{l=1}^{N} I_{l,m}, \; m = 1, \cdots, N$. These signal components form the vectors $\mathbf{z}^{left} = \left[z_1^{left}, \ldots, z_N^{left}\right]^T$ and $\mathbf{z}^{bottom} = \left[z_1^{bottom}, \ldots, z_N^{bottom}\right]^T$. By detecting the dominant components in signals $\mathbf{z}^{left}$ and $\mathbf{z}^{bottom}$, we can compute the center coordinates, with a method similar to [22]. There exist some other methods, such as the extension of the Hough transform [8], and the least squares method [85] to find the center coordinates of a circle.

When a single one-pixel wide circular contour with radius r is present, the signal components read :

$$z_i = r, \quad i = 1, \ldots, S \tag{3.7}$$

The radius value can be estimated as :

$$r = \bar{z}, \tag{3.8}$$

where $\bar{z}$ is defined as : $\bar{z} = \frac{1}{S}\sum_{i=1}^{S} z_i$.

We now consider the more general case of any star-shaped contour in a noisy environment. The contour radial coordinates are contained in the vector $\rho = [\rho_1, \rho_2, \ldots, \rho_Q]^T$, where $Q = 4S - 1$. To retrieve all contour coordinates, we need as many sensors as contour coordinates. Therefore, we associate the image with a circular antenna which surrounds the whole image and is compound of Q sensors. The number of sensors that permits a perfect characterization of a contour is such that $Q \geq 2\sqrt{2} * N$. An example of contour and this antenna are represented on Fig. 3.12.

When any one-pixel wide star-shaped contour is present, the signal components read :

$$z_i = \rho_i + n_i, \quad i = 1, \ldots, Q \tag{3.9}$$

where n_i is a noise term originated by the noise pixels. Note that the signal generation process is simplified compared to the one proposed in [22] : no propagation constant is used, and signal components are directly related to the contour coordinates. This simplification is permitted because a single contour is expected.

For the star-shaped, we express the radial coordinates of the edge pixels as :

$$\rho_i = r + x_i, \; i = 1, \cdots, Q, \tag{3.10}$$

where x_i is the oscillation of the i^{th} pixel around the circle of radius r (see Fig. 3.12). Therefore, the generated signal of Eq. (3.9) now can be reformulated as :

$$z_i = r + x_i + n_i, \quad i = 1, \ldots, Q \tag{3.11}$$

To characterize entirely the expected contour, it is necessary to retrieve, from the signal components $z_i, \; i = 1, \ldots, Q$, the parameters r and $x_i, \; i = 1, \ldots, Q$. Existing methods such as Gradient descent [22], or least squares [80] could be adapted for this purpose. Snakes methods such as GVF [10] can retrieve closed contours in a noisy environment. However, least

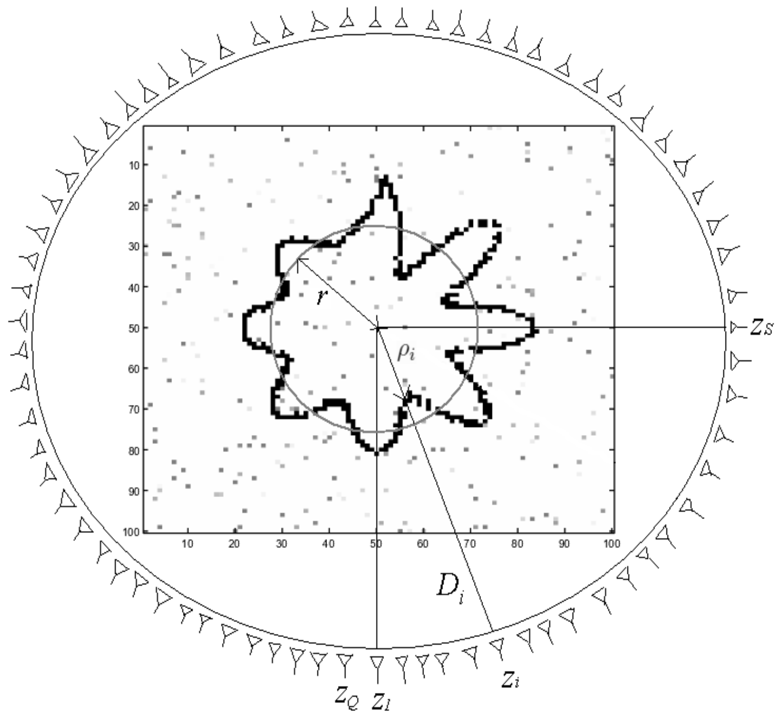

Figure 3.12 — Star-shaped contour with coordinates ρ_i, $i = 1, \ldots, Q$, fitting circle with radius r, array of Q sensors, example of direction for signal generation D_i, generated signal components z_i, $i = 1, \ldots, Q$

squares are sensitive to noise, and the two other methods exhibit drawbacks which will be demonstrated in the result section. That is why we formulate the problem in a different, novel way.

3.3.2 Problem formulation

From the signals $\mathbf{z} = [z_1, z_2, \cdots, z_Q]^T$ of Eq. (3.11), we wish to retrieve the radius value r, and the oscillations x_i, $i = 1, \cdots, Q$, in particular from contours presenting a strong concavity. Without loss of generality, we define r as the mean value of the components z_i, $i = 1, \ldots, Q$. r is estimated as :

$$r = \bar{z} \tag{3.12}$$

Then, we can compute :

$$x_i = z_i - r, \ i = 1, \ldots, Q \tag{3.13}$$

The values x_i, $i = 1, \cdots, Q$ are exactly the edge oscillation values in the case where the image is not impaired with noise. If the image is impaired with uniformly distributed noise, the computation of Eq. (3.13) provides signal components x_i, $i = 1, \ldots, Q$, which are impaired by random noise, due to the influence of random noise pixels on the signal generation process. Therefore, we seek for a method which retrieves the oscillations of possibly strongly concave contours, and which is robust to noise. For this, we propose in the next subsection a model for edge oscillations $x_i,\ i = 1, \cdots, Q$. We will further adapt an advanced damped frequency retrieval method to characterize the edge oscillations, in accordance with the proposed model.

3.3.3 Damped sinusoidal model for edge oscillations

For the edge oscillations of a star-shaped contour, the pixel coordinates in a polar representation are supposed to follow a generalized version of the sinusoidal model, that is, K damped sinusoidal components, each of which has respective amplitude, frequency and damping factor. So we model the edge oscillations as follows [86] :

$$x_i = \sum_{k=1}^{2K} a_k e^{j\phi_k} e^{(-d_k + j\omega_k)(i-1)} = \sum_{k=1}^{2K} c_k w_k^{(i-1)}, \quad i = 1, \ldots, Q \tag{3.14}$$

where $j = \sqrt{-1}$. In Eq. (3.14), x_i represents the oscillation magnitude for $i = 1, \ldots, Q$, a_k is amplitude of the k-th sinusoidal component, d_k its damping factor, ω_k its angular frequency, and ϕ_k its initial phase. Note that damping factor d_k may be negative. In this case, the amplitude of k-th component grows with index i. $c_k = a_k e^{j\phi_k}$ is the complex-valued amplitude of k-th component, and $w_k = e^{(-d_k + j\omega_k)}$.

The observed signal segment $\mathbf{x} = [x_1, x_2, \ldots, x_Q]^T$ is entirely characterized by the parameters a_k, d_k, ω_k, ϕ_k, $k = 1, \ldots, 2K$. The number K of sinusoidal components can be estimated by MDL criterion [79].

3.3.4 Parameter estimation

In this section, we determine the parameters cited above by applying a variant of the parameter estimator in [48]. Firstly, we rearrange the signal segment $\mathbf{x}$ in a Hankel matrix with $L \times M$ as follows :

$$\mathbf{X} = \begin{bmatrix} x_1 & x_2 & \ldots & x_M \\ x_2 & x_3 & \ldots & x_{M+1} \\ \vdots & \vdots & & \vdots \\ x_L & x_{L+1} & \ldots & x_Q \end{bmatrix} \tag{3.15}$$

where L, K, and Q are related by : $L \geq 2K$, $M \geq 2K$ and $Q = L + 2K - 1$.

Then, by implementing the Vandermonde Decomposition (VD) for Hankel data matrix of Eq. (3.15) with rank of $2K$, $\mathbf{X}$ can be written as :

$$\mathbf{X} \overset{\mathrm{VD}}{=} \mathbf{S}\mathbf{C}\mathbf{T}^T,$$

where $(\cdot)^T$ denotes matrix transposition, $\mathbf{C} = diag(c_1, c_2, \ldots, c_{2K})$,

$$\mathbf{S} = \begin{bmatrix} 1 & 1 & \dots & 1 \\ w_1^1 & w_2^1 & \dots & w_{2K}^1 \\ \vdots & \vdots & & \vdots \\ w_1^{L-1} & w_2^{L-1} & \dots & w_{2K}^{L-1} \end{bmatrix},$$

$$\mathbf{T} = \begin{bmatrix} 1 & 1 & \dots & 1 \\ w_1^1 & w_2^1 & \dots & w_{2K}^1 \\ \vdots & \vdots & & \vdots \\ w_1^{M-1} & w_2^{M-1} & \dots & w_{2K}^{M-1} \end{bmatrix}.$$

According to the shift-invariant property in column space,

$$\mathbf{S}^L = \mathbf{S}^F \mathbf{Z}, \tag{3.16}$$

where $\mathbf{S}^L$ is a matrix containing all but the first row of $\mathbf{S}$, and $\mathbf{S}^F$ is a matrix containing all but the last row of $\mathbf{S}$. $\mathbf{Z}$ is a diagonal matrix whose nonzero terms depend on the expected parameters. By performing SVD, $\mathbf{X}$ can be decomposed as :

$$\mathbf{X} \stackrel{\text{SVD}}{=} \begin{bmatrix} \mathbf{U}_1 & \mathbf{U}_2 \end{bmatrix} \begin{bmatrix} \mathbf{\Sigma}_1 & \mathbf{0} \\ \mathbf{0} & \mathbf{\Sigma}_2 \end{bmatrix} \begin{bmatrix} \mathbf{V}_1^H \\ \mathbf{V}_2^H \end{bmatrix} \tag{3.17}$$

where $(\cdot)^H$ is the Hermitian transposition, $\mathbf{\Sigma}_1$ contains the largest $2K$ singular values of $\mathbf{X}$ and $\mathbf{\Sigma}_2$ the $L-2K$ singular values of $\mathbf{X}$. The matrices $\mathbf{U}_1$ and $\mathbf{V}_1^H$ contain the first $2K$ left and right singular vectors, and their dimension is $L \times 2K$ and $M \times 2K$, respectively. Because the rank of $\mathbf{X}$ is $2K$, all values of $\mathbf{\Sigma}_2$ are null. Therefore, we can express $\mathbf{X}$ as :

$$\mathbf{X} = \mathbf{U}_1 \mathbf{\Sigma}_1 \mathbf{V}_1^H, \tag{3.18}$$

and we get the following equation from Eq. (3.16) by orthogonal basis transformation :

$$\mathbf{U}_1^F \mathbf{Z}^u = \mathbf{U}_1^L \tag{3.19}$$

where $\mathbf{U}_1^F$ contains all but the last row of matrix $\mathbf{U}_1$, $\mathbf{U}_1^L$ contains all but the first row of matrix $\mathbf{U}_1$, and $\mathbf{Z}^u$ is a similarity transform of $\mathbf{Z}$. The damping factors d_k and frequencies ω_k ($k = 1, \dots, 2K$) of the exponential sinusoidal model (see Eq. (3.14)) are estimated from the eigenvalues of $\mathbf{Z}^u$. Then we substitute these estimated d_k and ω_k in Eq. (3.14) and compute the least squares solution of the N linear equations. Finally, the amplitude a_k and phase ϕ_k of each component are determined from the magnitude and angle of c_k in Eq. (3.14). According to these estimated parameters, we can reconstruct the contour with oscillations. The pixel coordinates in the contour are given as :

$$\rho_i = r + \tilde{x}_i, \quad i = 1, \cdots, Q$$

where $\tilde{x}_i$ is initial estimation of x_i, $i = 1, \cdots, Q$. To get closer to real-world conditions, we consider that the image is degraded by two sources of impairment : identically distributed white noise is added to the image, and/or the edge pixels are displaced randomly. The signal model of Eq. (3.14) becomes then :

$$x_i' = x_i + n_i$$

So in the next section, we show how the signal can be refined to optimize the contour estimation.

3.3.5 Signal refinement

We get the initial estimation $\tilde{\mathbf{x}}$ from the previous section, which is the approximation of the original pixel oscillations. This estimation can be expressed as :

$$\tilde{\mathbf{x}} = \mathbf{x} + \triangle\mathbf{x} \tag{3.20}$$

where $\triangle\mathbf{x} = [\triangle x_1, \triangle x_2, \ldots, \triangle x_Q]^T$ is the perturbation vector contained in the initial estimation. Now, our aim is to minimize the norm of $\triangle\mathbf{x}$, *e.g.* $\|\triangle\mathbf{x}\|_2$, so that the final approximation is as close as possible to the original signals, while keeping $\tilde{\mathbf{x}}$ as a sum of $2K$ complex exponential sinusoids.

We rearrange the signal vector $\tilde{\mathbf{x}}$ in a Hankel matrix as :

$$\tilde{\mathbf{X}} = \begin{bmatrix} \tilde{\mathbf{X}}_L & \tilde{\mathbf{X}}_R \end{bmatrix} \tag{3.21}$$

where

$$\tilde{\mathbf{X}}_L = \begin{bmatrix} x_1 & x_2 & \ldots & x_{2K-1} \\ x_2 & x_3 & \ldots & x_{2K} \\ \vdots & \vdots & \vdots & \vdots \\ x_J & x_{J+1} & \ldots & x_{Q-1} \end{bmatrix}, \tilde{\mathbf{X}}_R = \begin{bmatrix} x_{2K} \\ x_{2K+1} \\ \vdots \\ x_Q \end{bmatrix}$$

and the number J of rows of Hankel matrix $\tilde{\mathbf{X}}$ should be greater than the number of signal components $2K$ while $J + 2K - 1 = Q$.

Then $\tilde{\mathbf{X}}$ can be represented by the form similar to Eq. (3.20),

$$\tilde{\mathbf{X}} = \begin{bmatrix} \mathbf{X}_L + \triangle\mathbf{X}_L & \mathbf{X}_R + \triangle\mathbf{X}_R \end{bmatrix} = \begin{bmatrix} \mathbf{X}_L & \mathbf{X}_R \end{bmatrix} + \begin{bmatrix} \triangle\mathbf{X}_L & \triangle\mathbf{X}_R \end{bmatrix}$$

where $\begin{bmatrix} \mathbf{X}_L & \mathbf{X}_R \end{bmatrix}$ is a Hankel data matrix as the one in Eq. (3.15) and $\begin{bmatrix} \triangle\mathbf{X}_L & \triangle\mathbf{X}_R \end{bmatrix}$ is a perturbation matrix, also with Hankel form.

Thus, we seek for the minimum norm of $\begin{bmatrix} \triangle\mathbf{X}_L & \triangle\mathbf{X}_R \end{bmatrix}$ so that the approximation is the closest to the initial estimation, while the matrix $\tilde{\mathbf{X}}$ is the rank-deficient, and matrices $\begin{bmatrix} \mathbf{X}_L & \mathbf{X}_R \end{bmatrix}$ and $\begin{bmatrix} \triangle\mathbf{X}_L & \triangle\mathbf{X}_R \end{bmatrix}$ have Hankel structure. This problem can be solved as the structured Total Least Norm problem by the iterative algorithm STLNB [84].

3.3.6 Experimental results

In this section, we apply the proposed method to test images and evaluate its performance. At the same time, we compare it with other methods, such as Hough transform [8] dedicated to circular-like contours, GVF (Gradient Vector Flow) method [10], and gradient optimization method following a specific signal generation scheme [22].

3.3.6.1 Parameter setup

In the simulations, the size of processed images is 100×100 pixels. We start by creating test images with a circular-like contour, where the contour center of gravity is set to be $(50, 50)$. According to the statement in section 3.3.1, an adequate number of sensors for the circular antenna is $Q = 1600$. This elevated number of sensors is required because we seek for strongly concave contours. For the comparative methods Gradient and GVF, the parameters which best fit the expected contours and which are used in the experiments (unless specified) are the following : Gradient method [22] is run with step $\beta = 0.05$, and 150 iterations. GVF method is run as follows [10] : for the computation of the edge map : 100 iterations ; $\mu_{GVF} = 0.09$ (regularization coefficient) ; for the snakes deformation : 100 initialization points and 400 iterations ; $\alpha_{GVF} = 0.02$ (tension) ; $\beta_{GVF} = 0.03$ (rigidity) ; $\gamma_{GVF} = 1$ (regularization coefficient) ; $\kappa_{GVF} = 0.8$ (gradient strength coefficient). We define vectors $\mathbf{x}^{'} = \left[x_1^{'}, \ldots, x_Q^{'}\right]^T$ and $\mathbf{x}^{''} = \left[x_1^{''}, \ldots, x_Q^{''}\right]^T$ as the first and second derivatives of edge curve vector $\mathbf{x}$, where $x_i^{'}$ and $x_i^{''}$ $(i = 1, \ldots, Q)$ are the first and second derivative of edge curve vector $\mathbf{x}$ at the i^{th} pixel. We use the finite differences to approximate the derivatives :
$x_1^{'} = 0$, and $\forall\ i = 2, \cdots, Q$ $x_i^{'} = x_i - x_{i-1}$, and
$x_1^{''} = 0$, $\forall\ i = 2, \cdots, Q-1$ $x_i^{''} = x_{i+1} - 2x_i + x_{i-1}$, and $x_Q^{''} = x_{Q-1}^{''}$.
We define the curvature of contour at each pixel location as follows :

$$\kappa_i = \frac{|x_i^{''}|}{(1+x_i^{'2})^{3/2}},\ i = 1, \cdots, Q,$$

The mean value of all κ_i $(i = 1, \cdots, Q)$ is computed by :

$$\overline{\kappa} = \frac{1}{Q}\sum_{i=1}^{Q} \kappa_i.$$

When the mean value $\overline{\kappa}$ is large, the contour is considered to be strongly concave.

The efficiency of the proposed method is measured by the mean error $ME_{\mathbf{x}}$ over the coordinates of the pixels of the contour. For the four quarters of an image, the coordinates of the pixels of the contour are contained in the vector $\mathbf{x} = [x_1, \cdots, x_Q]^T$ defined in Eq. (3.14), and their estimates are contained in vector $\hat{\mathbf{x}} = [\hat{x}_1, \cdots, \hat{x}_Q]^T$. The mean error value of the estimation for each trial is defined as :

$$ME_{\mathbf{x}} = \frac{1}{Q}\sum_{i=1}^{Q} |\hat{x}_i - x_i|,$$

where $|\cdot|$ means absolute value. So for J trials, the mean error on pixel position is given by :

$$ME = \frac{1}{J}\sum_{j=1}^{j=J} ME_{\mathbf{x}_j},$$

where $ME_{\mathbf{x}_j}$ is the mean error value corresponding to the j^{th} trial.

To evaluate the robustness of the methods, the root mean squared error ($RMSE$) of pixel bias is also used and defined as follows :

$$RMSE = \sqrt{\frac{1}{J}\sum_{j=1}^{j=J}|ME_{\mathbf{x}_j} - ME|^2}.$$

3.3.6.2 Results

- Experiment 1 : circular-like contour

In this experiment, we construct a nearly circular star-shaped contour, and add Gaussian white noise in images with mean value 0 and standard deviation 1, to compare our method with the Hough transform, Gradient and GVF methods. From Figs. 3.13 (b)-(d), where the result contour is plotted in gray, it can be seen that all four methods detect the contour with a rather low bias : values of mean error $ME_{\mathbf{x}}$ are 1.65, 1.71, 3.24 and 1.85 pixels respectively. The number of iterations is 60 for Gradient method and 200 for GVF method.

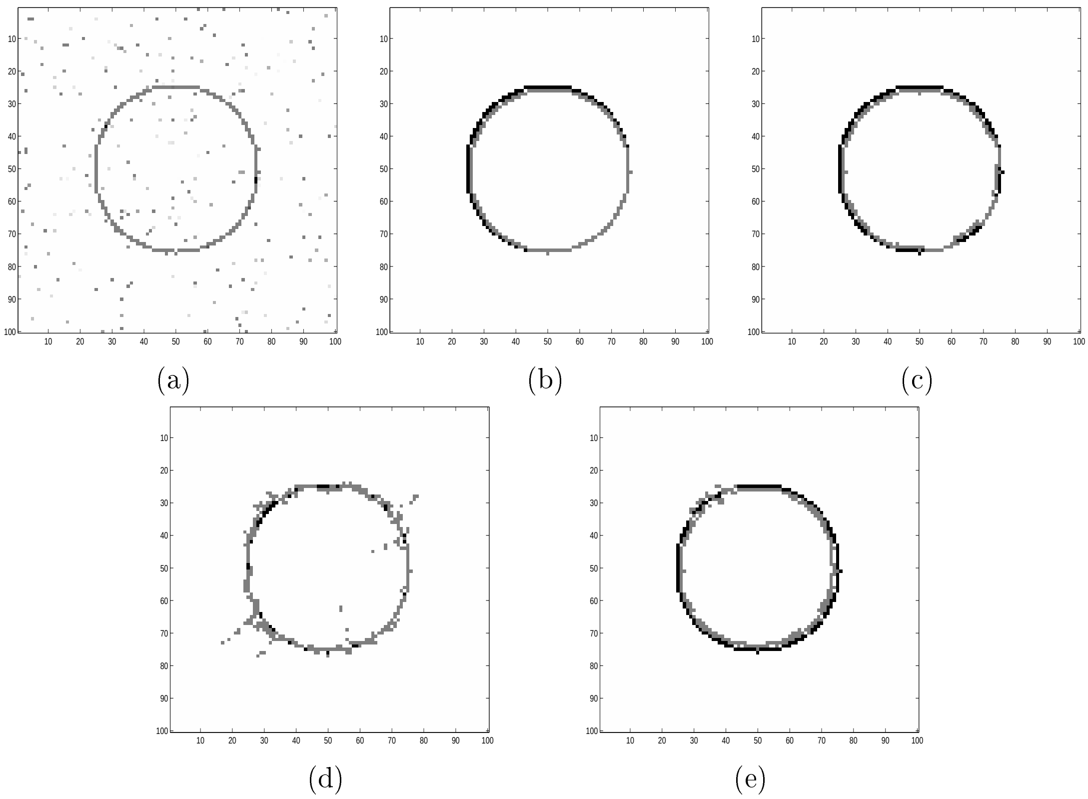

Figure 3.13 — (a) processed image ; (b) superposition expected contour and result obtained by Hough method : $ME_{\mathbf{x}} = 1.62$; (c) superposition expected contour and result obtained by the proposed method : $ME_{\mathbf{x}} = 1.67$; (d) superposition expected contour and result obtained by Gradient method : $ME_{\mathbf{x}} = 3.64$; (e) superposition expected contour and result obtained by GVF method : $ME_{\mathbf{x}} = 1.71$.

- Experiment 2 : contour with four lobes

In the experiment, the initial center radius of 25 is estimated and is used to furthermore determine the contour edge by the parameter estimation and signal refinement procedures (see Fig. 3.14(b)). For this processed contour, it can be seen that from Fig. 3.14(c), (d) and (e), the proposed method performs better than Gradient method and GVF method, where the numbers of iterations are 60 and 400, respectively. Because of the influence of noise pixels on the optimization criteria, Gradient method detects some pixels which are not exactly in the boundary of contour.

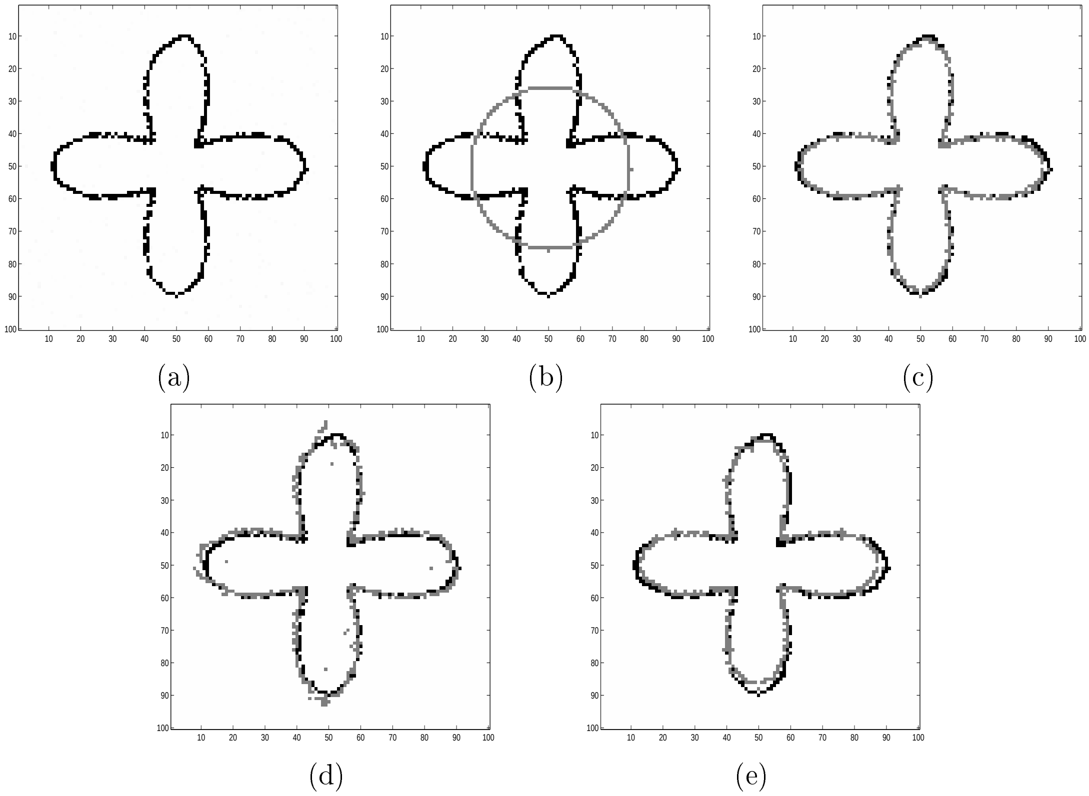

Figure 3.14 — (a) processed image ; (b) initialization of the processed image ; (c) superposition processed and result obtained by our proposed method ; (d) superposition processed and result obtained by Gradient method ; (e) superposition processed and result obtained by GVF method.

• Experiment 3 : case of small/large edge oscillations

In some cases, due to the acquisition conditions or the image quantization, the continuous form of contour edge is not perfect. It is therefore very interesting to evaluate the robustness of the proposed method to pixel location errors. We produce test images by initially creating a star-shaped contour (see Fig. 3.15 (a)) ; and then adding pixel displacement by modifying the actual pixel radial coordinates with a Gaussian random variable with mean value 0 and standard deviation 1 (see Fig. 3.15(b)). We assume there exists equally distributed random noise in the image, with mean value 0 and standard deviation 10^{-2}. Referring to Figs. 3.15

(d)-(i), when the proposed method is applied, the mean error is $ME_{\mathbf{x}} = 1.61$ when small random displacements are added ; and $ME_{\mathbf{x}} = 1.86$ when larger random displacements are added. When Gradient method is applied, the mean error value is increased dramatically from $ME_{\mathbf{x}} = 1.78$ to $ME_{\mathbf{x}} = 2.25$. When GVF is applied, the mean error value is increased from $ME_{\mathbf{x}} = 1.90$ to $ME_{\mathbf{x}} = 2.42$. So, Figs. 3.15 (d)-(i) show that the proposed method is not sensitive to the random pixel displacements, contrary to Gradient method and GVF method. This is due to the fact that the proposed method processes the signal generated from the image as a whole, providing parameters of interest, whereas Gradient method and GVF are local methods, which may focus on random pixels.

- Experiment 4 : Sensitivity to background noise and strong contour concavity

We now consider a contour with stronger concavity. Fig. 3.16(a) shows the noisy processed image. The noise mean value and standard deviation are 0 and 10^{-2} (see Fig. 3.16(b)). The initial estimated radius obtained from Eq. (3.12) is 30 (see Fig. 3.16(c)). Figs. 3.16 (d) and (g) show the results obtained by the proposed method, which match well the expected contour, though the contour concavity is strong and the noise level is elevated. From the least to the most noisy image, the mean pixel bias changes just from 1.61 to 1.86. From Figs. 3.16 (e), (f), (h) and (i), we get that Gradient method and GVF method (run with 100 and 500 iterations respectively) do not converge very well to the expected contour. After increasing the noise level, the mean error values increase from $ME_{\mathbf{x}} = 1.80$ to $ME_{\mathbf{x}} = 4.02$ when Gradient is run, and from $ME_{\mathbf{x}} = 3.17$ to $ME_{\mathbf{x}} = 3.21$ when GVF is run. This proves that our method performs better than Gradient method and GVF method for a strongly concave contour with either low or high level noise, and that Gradient method is very sensitive to the noise level, whereas GVF method does not cope with a contour with strong concavity. Note that, considering the computational load and the accuracy of estimation for Gradient method and GVF method, we may choose different iteration times for different levels of concavity. We choose the number of iterations so that the accuracy of the result is not significantly improved when the number of iterations is increased.

The values of mean error with different levels of noise and contour concavity are presented in Table 3.2, where the first case corresponds to the curvature 0, that means, the contour is a circle as in Fig. 3.13, and the last case corresponds to the strongly concave contour as in Fig. 3.16. Each experiment is repeated 50 times with a different noise realization. It shows that :

- the proposed method is insensitive to both noise level and contour concavity ;
- the GVF method is sensitive to contour concavity ;
- the Gradient method is sensitive to noise.

At the same time, we see that when noise variance is reduced, the accuracy of estimation for all methods is improved.

With different levels of noise and contour concavity, the values of RMSE are shown in

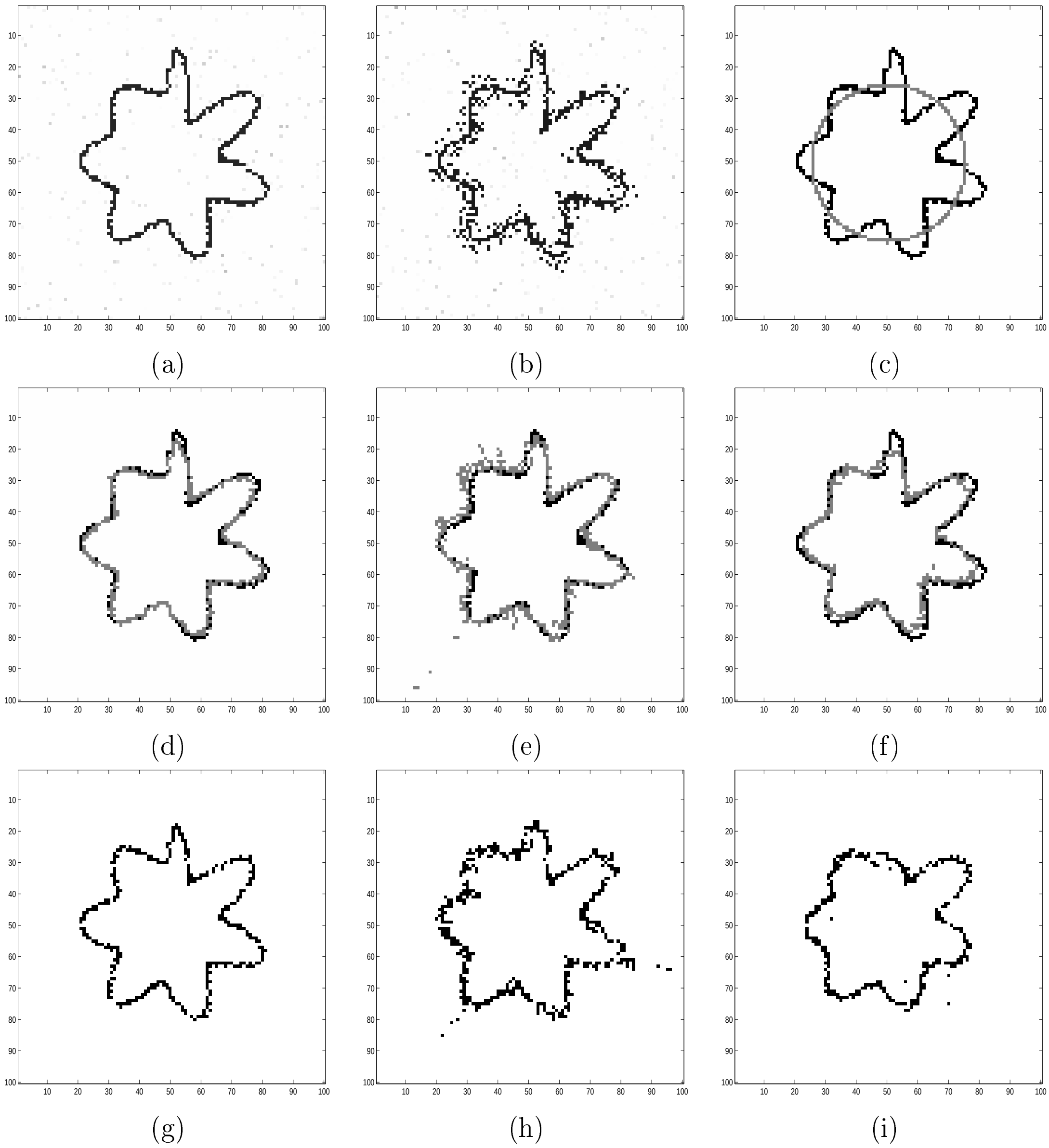

Figure 3.15 — (a) processed image : $\overline{\kappa} = 2.7\ 10^{-3}$, with small edge perturbation and noise $(0, 10^{-2})$; (b) processed image, with large edge perturbation and noise $(0, 10^{-2})$; (c) initialization of the methods for both processed images ; (d-f) superposition processed and result obtained on 'a' by the proposed method ($ME_{\mathbf{x}} = 1.58$), Gradient method ($ME_{\mathbf{x}} = 1.78$), and GVF method ($ME_{\mathbf{x}} = 1.90$) ; (g-i) result obtained on 'b' by the proposed method ($ME_{\mathbf{x}} = 1.86$), Gradient method ($ME_{\mathbf{x}} = 2.25$), and GVF method ($ME_{\mathbf{x}} = 2.42$).

Table. 3.3. It can be seen that the proposed method always yields small RMSE value, which means that the proposed method is robust to the contour concavity and the noise level. As seen from Tables. 3.2 and 3.3, the proposed method has the best performance in both accuracy and robustness, followed by GVF method and Gradient method.

To evaluate the computational load of proposed method, each method is run 50 times

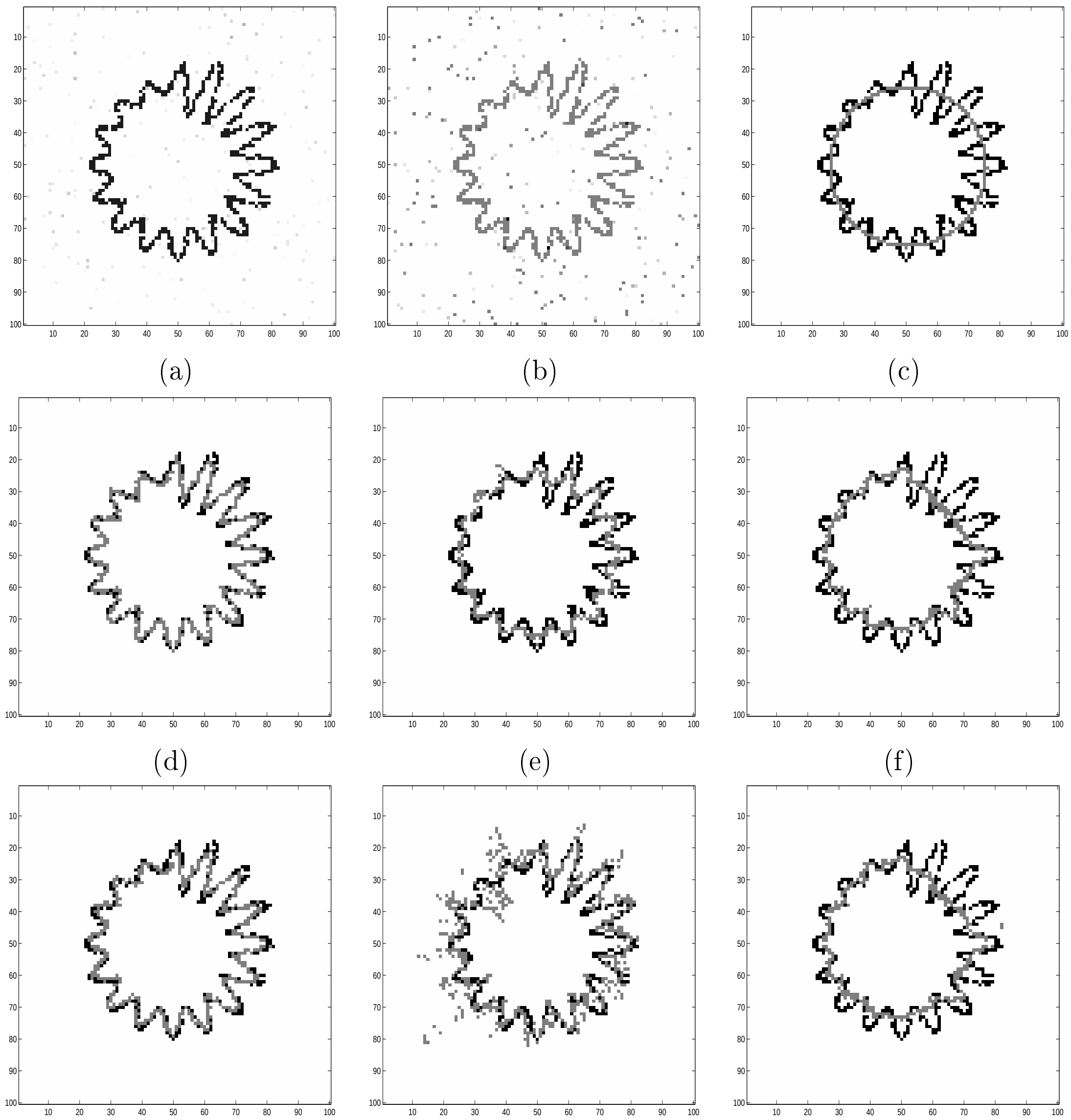

(a) (b) (c)

(d) (e) (f)

(g) (h) (i)

Figure 3.16 — (a) processed image with contour concavity $\overline{\kappa} = 1.17\ 10^{-2}$ and noise parameters $(0, 10^{-2})$; (b) processed image with same contour and noise parameters $(0, 1)$; (c) superposition expected contour and initialization circle for both processed images; (d-f) superposition expected contour and result obtained from 'a' by the proposed method ($ME_{\mathbf{x}} = 1.61$), Gradient method ($ME_{\mathbf{x}} = 1.80$), and GVF ($ME_{\mathbf{x}} = 3.17$); (g-i) superposition expected contour and result obtained from 'b' by the proposed method ($ME_{\mathbf{x}} = 1.96$), Gradient method ($ME_{\mathbf{x}} = 4.15$), and GVF ($ME_{\mathbf{x}} = 3.29$).

on a PC with 2 Quad CPU 2.83GHz and 4Gb memory. Whatever the concavity strength and the noise parameters, the average elapsed time is 1.098 *sec.* to detect the parameters of the damped exponential sinusoid model, and it needs 60.91 *sec.* to refine the signals when the noise level is elevated. When the noise level is very low, it is not necessary to adopt the

Tableau 3.2 — ME values (in pixel) obtained with the proposed method (value with refinement/without refinement) (A), Gradient method (B) and GVF method (C), versus concavity and noise percentage.

concavity $\overline{\kappa}$ \ noise	$(0,10^{-3})$			$(10^{-2},10^{-2})$		
	(A)	(B)	(C)	(A)	(B)	(C)
0	1.49/1.50	1.52	1.70	1.53/1.55	1.76	1.70
$2.2\ 10^{-3}$	1.53/1.54	1.55	1.79	1.54/1.55	1.81	1.78
$2.7\ 10^{-3}$	1.57/1.58	1.59	1.91	1.59/1.60	1.79	1.92
$1.17\ 10^{-2}$	1.58/1.60	1.66	3.29	1.63/1.65	1.84	3.30
concavity $\overline{\kappa}$ \ noise	$(0,10^{-1})$			$(0,1)$		
	(A)	(B)	(C)	(A)	(B)	(C)
0	1.60/1.72	2.21	1.70	1.67/1.91	3.64	1.71
$2.2\ 10^{-3}$	1.68/1.74	2.27	1.79	1.69/1.98	3.87	1.80
$2.7\ 10^{-3}$	1.75/1.78	2.46	1.92	1.78/2.00	3.93	1.93
$1.17\ 10^{-2}$	1.89/1.97	2.83	3.27	1.96/2.35	4.15	3.29

Tableau 3.3 — $RMSE$ values (in pixel) obtained with the proposed method (A), Gradient method (B) and GVF method (C), versus concavity and noise percentage.

concavity $\overline{\kappa}$ \ noise	$(0,10^{-3})$			$(10^{-2},10^{-2})$		
	(A)	(B)	(C)	(A)	(B)	(C)
0	0.12	0.68	0.19	0.16	0.99	0.20
$2.2\ 10^{-3}$	0.13	0.69	0.21	0.15	0.97	0.24
$2.7\ 10^{-3}$	0.17	0.76	0.30	0.19	1.03	0.32
$1.17\ 10^{-2}$	0.20	0.75	0.45	0.21	1.15	0.49
concavity $\overline{\kappa}$ \ noise	$(0,10^{-1})$			$(0,1)$		
	(A)	(B)	(C)	(A)	(B)	(C)
0	0.24	1.32	0.19	0.30	1.44	0.21
$2.2\ 10^{-3}$	0.27	1.40	0.29	0.34	1.37	0.28
$2.7\ 10^{-3}$	0.31	1.55	0.33	0.45	1.59	0.33
$1.17\ 10^{-2}$	0.52	1.83	0.48	0.59	2.25	0.51

refinement of the signals : with noise parameters $(0,10^{-3})$ and $(10^{-2},10^{-2})$, the improvement is around 1 %. When the noise level is higher, that is, with noise parameters $(0,10^{-1})$ and

(0,1), the improvement is around 4 % and 16 % respectively. The accuracy of the estimation depends essentially on the adequate signal generation and the damped frequency estimation method. Depending on the application, one may want to refine the signals at the expense of a higher computational load.

Concerning Gradient algorithm : as soon as the noise variance is higher than 10^{-2}, Gradient method does not provide satisfying results (see for instance Fig. 3.16(h)) ; then we provide the computational load when noise parameters are $(0{,}10^{-3})$: for concavity 2.2 10^{-3}, Gradient method needs 0.11 *sec.* for 150 iterations. For concavity 1.17 10^{-2}, Gradient method needs 0.22 *sec.* for 300 iterations. So Gradient is faster than the proposed methods, but breaks down as soon as the noise is slightly elevated, which is a drawback for any real-world application. GVF does not provide satisfying results for concavity values which are higher than 2.5 10^{-3}. For concavity 2.2 10^{-3}, and noise parameters $(0{,}10^{-3})$, Gradient method requires 1.989 *sec.* for 400 iterations, while GVF method lasts 2.020 *sec.* to characterize the contour edge.

When the refinement step is not needed, our method presents the following advantage : we do not need to specify any *a priori* known number of iterations. Contrary to the two comparative methods, the proposed method works in both harsh conditions : strong concavity and high noise level. Moreover, it exhibits the same computational load whatever the experimental conditions : concavity and noise level. In the considered conditions, this computational load is two times lower than for GVF.

3.4 Conclusion

In this chapter, we have proposed to detect a circular-like contour by exploiting a linear antenna model and circular antenna model, which fit signals generated out of the processed image : an adequate transformation of the image content provides a one-dimensional signal. We have formulated the detection problem and performed the parameter estimation of radius and center coordinates in white noise environment and in colored noise environment, incorporating the high-resolution methods. For strongly concave contours, we have exploited a damped sinusoid model, and then a frequency estimation method was used to retrieve the polar coordinates of the contour pixels. Furthermore, we additionally refined the generated signals by STLNB optimization method so that they better fit the proposed model, in order to improve the estimation when the noise level is high.

CHAPITRE 4

Blurred contour detection

In this chapter, contours with blurred characteristics are studied in digital image processing. Most of the existing techniques try to detect blurred contours by fuzzy techniques. We propose to model the blurred contours by generating signals by a virtual antenna associated with the image, and provide a new viewpoint to detect blurred contour. Especially, the blurred contour with exponential distribution can be presented by three parameters. Array processing methods are adopted to estimate these parameters, and optimization method is also considered when the spread parameter is estimated.

4.1 Introduction

Blurred contours also occur very often in images, owing to object movements, light transmission environment, illumination changes, defocus, etc. Light has been recently shed on the characterization of contours, regions or objects which are not simply defined by a one-pixel wide contour [5, 31]. Several methods have been proposed in the image processing community to solve this problem. They fall into two major categories : those which perform region-based segmentation [5, 87, 88], and those which perform contour-based segmentation [11, 31, 89, 90, 91]. Firstly, region-based segmentation can produce the regions that are as large as possible, but allow some flexibility for variation within the region. Also, a fuzzy paradigm was adopted in the frame of mathematical morphology to characterize the repartition of objects in an image by "fuzzy" relationships [87, 88]. In this paradigm, one could localize an object at left or at the right-hand side of another object.

Secondly, contour-based segmentation methods consider blurred contours as contours which are not necessarily defined by gradient. In particular a recent model for active contours based on techniques of curve evolution, which was adapted from the level set paradigm [38], was proposed to segment contours "without edges" [31]. In [90], the authors present a novel fast model for active contours to detect objects in an image, based on techniques of curve evolution. The proposed model can detect objects whose boundaries are not necessarily defined by gradient. In [11], an enhanced, region-aided, geometric active contour that is more tolerant toward blurred contours and noise is introduced. In [91], an algorithm is proposed which is based on the traditional and generalized Hough transforms [8, 92]. The authors use their new algorithm to roughly estimate the actual locations of boundaries of an internal organ and determine a region of interest around the organ. The methods presented in [11, 91] combine the region-based and the contour-based approaches.

Within the contour-based methods, an original one consists in transferring high resolution methods of array processing to image segmentation as presented in Chapter 2 and Chapter 3. Recent advances permitted to handle correlated noise [93]. These methods can estimate exactly the different parameters which characterize the contour. However, an important limitation of these methods [18, 22] is that they are restricted to one-pixel wide contours. Also, the image model on which they are based is only binary, *i.e.* pixels are supposed to have value 1 or 0. As blur occurs very often in photographies, it is more realistic to consider contours which are no longer one-pixel wide. The contour model which is introduced in this chapter is more general. A contour is characterized by its mean position, along a straight line or a circle. Additionally, a contour includes a spread parameter, which describes the evolution of the gray levels aside the contour mean position. Therefore the parameters of interest in this study are the following : orientation, offset, and spread in the case where linear-like blurred contours are expected ; center coordinates, radius, and spread in the case where circular-like blurred contours are expected.

Hence the main contribution of the chapter is twofold. We aim at characterizing blindly a blurred contour by a limited number of parameters. Firstly, we show that the signal generated out of an image containing a blurred contour fits an array processing model, which permits to adapt subspace-based high-resolution methods of array processing such as MUSIC [74] to retrieve the contour mean position. Secondly, we propose a criterion to be optimized in order to get an estimate of the spread parameter. This permits to characterize entirely the image content by a few parameters. The proposed method essentially remains in the category of the contour-based methods. But, through the spread parameter computation, it also characterizes the gray level variations in the region aside the contour main position.

Compared to previous works based on array processing methods [18, 22, 56], the advantage of the proposed method is that it is no longer restricted to one-pixel wide contours, and that the image model is no longer binary. Concerning other contour detection methods : Hough transform exhibits a computational load which depends on the number of noise pixels [8, 92], and does not characterize the contour blur. On the contrary, the computational load of the proposed method does not depend on the number of noise pixels. Level set methods [38] require delicate adjustments of many parameters, which are typically determined empirically. On the contrary, the methods proposed in this chapter rely on a few parameters which are easy to tune and robust to changes in movement, illumination, etc.

The proposed model permits, for instance, to characterize gray level variations such as those encountered at the frontier between homogeneous regions. This is a partial surface effect which is well-known in medical imaging, but also airborne or satellite imaging. The segmentation of blurred contours is indeed often associated with medical applications, such as the segmentation of the heart [94], the Human vision system [95, 96], or protein spots in 2DGE (two-dimensional gradient electrophoresis) images [97].

The assumed contour models, either linear or circular, are general enough to correspond to various applications, as different as trajectory characterization, retina analysis (namely glaucoma detection), and fire front characterization.

The remainder of chapter 4 is organized as follows. In section 4.2, we present the problem of characterization of blurred linear contour by introducing a specific signal generation scheme, and we propose subspace-based methods which fit the derived signal models to estimate either main orientation and offset of linear-like contours. In section 4.3, we state the problem of blurred triangular contour retrieval and the characteristics of the images, and propose to adapt subspace-based methods of array processing which are originally dedicated to multiple incoherently distributed sources, to retrieve the orientation and spread parameters of blurred contours. In section 4.4, we consider blurred circular contours, and apply subspace-based methods to estimate its radius. Then we estimate the spread parameter by an optimization strategy. We present the results obtained by the proposed methods, and compare them with a level set type method which is adapted to blurred contours [31]. At last, we draw the conclusion of the chapter.

4.2 Blurred linear contour detection

4.2.1 Problem statement

In this section, we provide the models that we adopt for the processed image, for contours which are present in the image, in particular their gray level distribution [98]. Let $I(l, m)$ be an $N \times N$ recorded image (see Fig. 4.1(a). We assume that $I(l, m)$ is composed of either several blurred contours, and an additive uniformly distributed noise. A linear-like contour is supposed to have main orientation θ and center offset x_0. The pixels whose coordinates are defined by these two parameters constitute the central position of the contour.

In this case the gray level values of the pixels decrease gradually aside the central position of the contour. The variation of the gray level values is described by an exponential function, for example, a Gaussian evolution depends on a spread parameter σ : $g(x) = \frac{1}{\sqrt{2\pi}\sigma} exp(-\frac{x^2}{2\sigma^2}) = Gexp(-\frac{x^2}{2\sigma^2})$, where G is the maximum gray level value. The contour is supposed to have width $2X_f$ (see Fig. 4.1(b)). If we define a gaussian attenuation threshold of the pixel grey level value as δ_T, the relationship among X_f, σ, and δ_T is $\delta_T = \frac{1}{\sqrt{2\pi}\sigma} exp(-\frac{X_f^2}{2\sigma^2})$.

We expect that such a contour model, in particular the exponential distribution of the

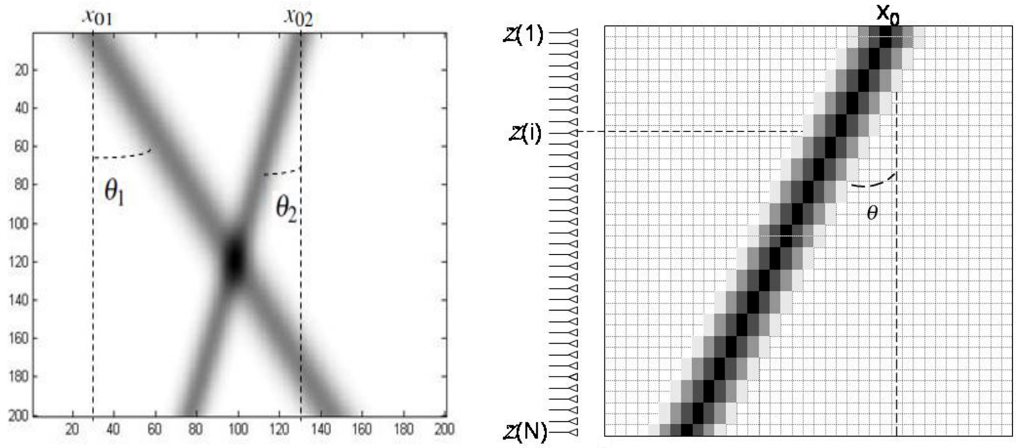

(a) (b)

Figure 4.1 — (a) blurred contours characterized by the main orientations θ_k and offsets x_{0k} in the image ; (b) linear antenna model in an image containing a blurred line

gray level values in both cases, facilitates the transfer of array processing methods to the considered parameter estimation issue. To retrieve linear-like contours, the array sensors are supposed to be placed in front of each row of the image. Fig. 4.1(b) represents the linear arrays associated with an image containing a blurred linear contour. Each sensor is related to one signal component calculated by weighted summation of the gray level values of pixels at specific positions.

In the case where linear-like contours are expected, we adopt the signal generation scheme as in the previous two chapters. Pixels along one row yield one signal component. The row indexed by i yields the signal component $z(i)$:

$$z(i) = \sum_{m=1}^{N} I(i,m)\ e^{-j\mu m},\ \ i = 1, \ldots, N, \tag{4.1}$$

where $j = \sqrt{-1}$, and μ is an *a priori* set propagation parameter. The signal components form the following signal vector : $\mathbf{z} = [z(1), z(2), \ldots, z(N)]^T$. Further, the propagation parameter is adapted so that, in each case, the signal vector fits an array processing model.

4.2.2 Signal model

Firstly, we assume that the image contains only one blurred contour of width $2X_f$, main orientation θ, offset x_0, and spread parameter σ. The signal generated on the i^{th} sensor is then expressed as :

$$\begin{aligned} z(i) = \quad & G\ \textstyle\sum_{x=1}^{X_f} e^{-j\mu(x_0+x-(i-1)tan(\theta))} e^{-\frac{x^2}{2\sigma^2}} + G\ \textstyle\sum_{x=1}^{X_f} e^{-j\mu(x_0-x-(i-1)tan(\theta))} e^{-\frac{x^2}{2\sigma^2}} \\ & + G\ e^{-j\mu(x_0-(i-1)tan(\theta))} \end{aligned} \tag{4.2}$$

That is :

$$\begin{aligned} z(i) = & \quad G \ \sum_{x=-X_f}^{X_f} e^{-j\mu(x_0+x-(i-1)tan(\theta))} e^{-\frac{x^2}{2\sigma^2}} \\ = & \quad G \ e^{-j\mu x_0} e^{j\mu(i-1)tan(\theta)} \sum_{x=-X_f}^{X_f} e^{-j\mu x} e^{-\frac{x^2}{2\sigma^2}} \end{aligned} \tag{4.3}$$

where X_f is the half-width of the contour.

Let's consider the following expression :

$$\sum_{x=-X_f}^{X_f} e^{-j\mu x} e^{-\frac{x^2}{2\sigma^2}} \tag{4.4}$$

We set : $f(x) = e^{-j\mu x} e^{-\frac{x^2}{2\sigma^2}}$. Eq. (4.4) can be written :

$$\sum_{x=-X_f}^{X_f} f(x) = \sum_{x=1}^{2X_f+1} f(x-(X_f+1)) = \frac{\varphi-\phi}{n} \sum_{x=1}^{n} f(\phi + x\frac{\varphi-\phi}{n}) \tag{4.5}$$

with : $\phi = -(X_f+1),\ n = 2X_f+1,\ \varphi = X_f$.

We set : $S_n = \frac{\varphi-\phi}{n} \sum_{x=1}^{n} f(\phi + x\frac{\varphi-\phi}{n})$. S_n is a Riemann summation, such that $\underset{n\to+\infty}{lim} S_n = \int_\phi^\varphi f(x)dx$.

So if we consider that X_f is large enough, we get the following approximation :

$$\sum_{x=-X_f}^{X_f} f(x) = \int_{-X_f-1}^{X_f} f(x)dx \tag{4.6}$$

Moreover, we notice that, if σ is small enough, $|f(x)|$ decreases rapidly and is negligible for $|x| > X_f$. Therefore we can adopt the following approximation :

$$\int_{-X_f-1}^{X_f} f(x)dx \approx \int_{-\infty}^{\infty} f(x)dx \tag{4.7}$$

So, from Eqs. (4.6) and (4.7), we get :

$$\sum_{x=-X_f}^{X_f} e^{-j\mu x} e^{-\frac{x^2}{2\sigma^2}} \approx \int_{-\infty}^{\infty} e^{-j\mu x} e^{-\frac{x^2}{2\sigma^2}} dx \tag{4.8}$$

A general formula provides the equality :

$$\int_{x=-\infty}^{+\infty} e^{-ax^2+jbx} dx = \sqrt{\frac{\pi}{a}} e^{-\frac{b^2}{4a}}. \tag{4.9}$$

which yields :

$$\sum_{x=-X_f}^{X_f} e^{-j\mu x} e^{-\frac{x^2}{2\sigma^2}} \approx \sqrt{2\pi}\sigma e^{-\frac{\mu^2\sigma^2}{2}} \tag{4.10}$$

It is easy to express Eq. (4.3) by

$$z(i) = \sqrt{2\pi}G\ e^{-j\mu x_0}\ e^{j\mu(i-1)tan(\theta)}\sigma\ e^{-\frac{\mu^2\sigma^2}{2}} \tag{4.11}$$

Eq. (4.11) is the signal in the i-th row in the case where there exists only one blurred contour in the image.

Secondly, we consider the case where the image contains :

- d blurred contours, with orientations θ_k, offsets x_{0k}, and spread parameters σ_k $(k = 1, \ldots, d)$;
- identically distributed noise pixels.

The expression of the signal received by the i^{th} sensor becomes :

$$z(i) = \sqrt{2\pi}G\ \sum_{k=1}^{d} e^{-j\mu x_{0k}} e^{j\mu(i-1)tan(\theta_k)}\sigma_k e^{-\frac{\mu^2{\sigma_k}^2}{2}} + n(i) \tag{4.12}$$

where $n(i)$ is a noise term originated by the noise pixels during the signal generation process. The expression of the signal components in Eq. (4.12) permits to adopt the notations coming from array processing. We define :

1. the source amplitude associated with the k-th contour as :
   $$s(k) = G\ e^{-j\mu x_{0k}} \sum_{x=-X_f}^{X_f} e^{-j\mu x} e^{-\frac{x^2}{2{\sigma_k}^2}},\ k = 1, \cdots, d.$$
   When the continuous approximation holds, the source amplitude components are expressed as :
   $$s(k) = \sqrt{2\pi}Ge^{-j\mu x_{0k}}\sigma_k e^{-\frac{\mu^2{\sigma_k}^2}{2}}, k = 1, \cdots, d \tag{4.13}$$
2. the steering vector associated with the k-th contour as :
   $$\mathbf{c}(\theta_k) = [c_1(\theta_k), c_2(\theta_k), \cdots, c_i(\theta_k), \cdots, c_N(\theta_k)]^T,\ \text{with}\ c_i(\theta_k) = e^{j\mu(i-1)\tan(\theta_k)}.$$
3. the noise vector $\mathbf{n} = [n(1), n(2), \ldots, n(N)]^T$.

These notations permit to express the signal generated out of the image in a matrix form :

$$\mathbf{z} = \mathbf{C}(\theta)\mathbf{s} + \mathbf{n} \tag{4.14}$$

where $\mathbf{z} = [z(1), z(2), \ldots, z(N)]^T$, $\mathbf{C}(\theta) = [\mathbf{c}(\theta_1), \mathbf{c}(\theta_2), \cdots, \mathbf{c}(\theta_d)]$, $\mathbf{s} = [s(1), s(2), \cdots, s(d)]^T$.

Eq. (4.14) shows that, by adopting the signal generation scheme of Eq. (4.1) and the proposed model for blurred contours, we can make an analogy between the signals generated out of the image and an array processing signal model. Therefore, we expect that array processing methods can yield the parameters of the expected contours.

4.2.3 Subspace based methods of array processing for orientation and offset estimation

4.2.3.1 Estimation of the blurred contour main orientation

An array processing method can be applied to the generated signal provided in Eq. (4.14), to characterize the contours in the image by retrieving their parameters. We split the array (of length N) into smaller overlaying sub-arrays (of length M) by spatial smoothing technique. There exist a constraint on M, and a relationship between N, M and the number of snapshot $P: d < M \leq N - d + 1$; and $M = N - P + 1$. From the observation vector $\mathbf{z}$ we obtain P overlapping sub-vectors. By grouping all sub-vectors obtained in matrix form, we get :

$$\mathbf{Z}_P = [\mathbf{z}_1, \cdots, \mathbf{z}_P] \tag{4.15}$$

where

$$\mathbf{z}_p = \mathbf{C}_M(\theta)\mathbf{s}_p + \mathbf{n}_p,\ p = 1, \cdots, P. \tag{4.16}$$

Each column of $\mathbf{C}_M(\theta)$ is a vector of length M expressed as :
$\mathbf{c}(\theta_k) = [c_1(\theta_k), \cdots, c_i(\theta_k), \cdots, c_M(\theta_k)]^T$, with $c_i(\theta_k) = e^{j\mu(i-1)tan(\theta_k)}$, and $\mathbf{s}_p = [s_p(1), \cdots, s_p(k), \cdots s_p(d)]^T$, where $s_p(k) = \sqrt{2\pi}G\sigma_k e^{-j\mu x_{0k}} e^{\frac{-\mu^2\sigma_k^2}{2}} e^{j(p-1)\mu tan(\theta_k)}$, $p = 1, 2, \cdots, P$.

The covariance matrix of all sub-vectors of Eq. (4.15) is defined by :

$$\mathbf{R}_{zz} = \frac{1}{P}\sum_{p=1}^{P} \mathbf{z}_p \mathbf{z}_p{}^H \tag{4.17}$$

where $(\cdot)^H$ denotes Hermitian transpose. We operate the singular value decomposition (SVD) of $\mathbf{R}_{zz}$.

$$\mathbf{R}_{zz} = [\mathbf{U}_1 \quad \mathbf{U}_2]\ \mathbf{\Lambda}\ \mathbf{V} \tag{4.18}$$

For independent sources, the columns of matrix $\mathbf{U}_1\,(\mathrm{M} \times \mathrm{d})$ span the signal subspace, the columns of matrix $\mathbf{U}_2\,(\mathrm{M} \times (\mathrm{M} - \mathrm{d}))$ span the noise subspace, and $\mathbf{\Lambda} = diag\,(\lambda_1, \lambda_2, \cdots \lambda_d)$ where λ_i is the eigenvalue associated with the i^{th} eigenvector. Hence, $\mathbf{U}_2$ is orthogonal to the steering vectors $\mathbf{c}\,(\theta_k)\,,\ k = 1, \ldots, d$. We estimate the θ_k parameters $(k = 1, \ldots, d)$ through the maxima of the pseudo spectrum [74] given by

$$\mathrm{MUSIC}\,(\theta_k) = \frac{1}{\parallel \mathbf{c}^H\,(\theta) \cdot \mathbf{U}_2 \parallel^2} \tag{4.19}$$

where $\mathbf{c}^H\,(\theta)$ is a model for the signal subspace vectors.

4.2.3.2 Estimation of the blurred contour offset

Once the orientation values are known, the offset values can be estimated by variable speed generation scheme [76] and TLS-ESPRIT algorithm [18]. Variable speed propagation scheme consists in setting $\mu = \alpha(i-1)$. Eq. (4.12) becomes :

$$z(i) = \sqrt{2\pi}G \sum_{k=1}^{d} e^{-j\alpha(i-1)x_{0k}} e^{j\alpha(i-1)^2 tan(\theta_k)} \sigma_k e^{-\frac{(\alpha(i-1))^2 {\sigma_k}^2}{2}} + n(i) \tag{4.20}$$

We can consider for instance the first orientation $\theta = \theta_1$.

As θ_1 value has been estimated, we can divide $z(i)$ by the term $e^{j\alpha(i-1)^2 tan(\theta_1)}$, and obtain :

$$w(i) = z(i)/e^{j\alpha(i-1)^2 tan(\theta_1)} = \sqrt{2\pi}G\ e^{-j\alpha(i-1)x_{01}} \sigma_1 e^{-\frac{(\alpha(i-1))^2 {\sigma_1}^2}{2}} + n'(i) \tag{4.21}$$

where $n'(i)$ is a noise term resulting from the influence of noisy pixels and all but the first contour.

At this point, the value of σ_1 is not known and we propose an approximation which permits to get momentarily a gross estimate of x_{01} without the prior knowledge of σ_1. If the propagation parameter α is chosen such that $\alpha(i-1) << 1,\ \forall\ i = 1, \dots, N$, we can adopt the following approximation :

$$w(i) \approx \tilde{w}(i) = \sqrt{2\pi}G\ e^{-j\alpha(i-1)x_{01}} \sigma_1 + n^{'}(i) \tag{4.22}$$

The signal $\tilde{\boldsymbol{\omega}} = [\tilde{w}(1), \tilde{w}(2), \dots, \tilde{w}(N)]$ fits the model required by the frequency estimation TLS-ESPRIT method [18] which retrieves the first offset value x_{01} from eq. (4.22).

The division process of Eq. (4.21) and the adaptation of TLS-ESPRIT method are repeated for each value $k = 1, \dots, d$. At this point a gross estimate of the offset values is available, which will be used to estimate the spread parameter values.

4.2.4 DIRECT method for spread parameter estimation of the blurred contours

In this subsection we propose a least-square criterion which involves the signal generated out of the image and the signal model of Eq. (4.14). This criterion depends on the parameters of all contours. We adapt DIRECT optimization method to retrieve the spread parameter values by minimizing this criterion.

4.2.4.1 Least-squares criterion derivation

The contour orientations estimated by MUSIC algorithm are used to compute the steering matrix $\mathbf{C}(\theta)$ (see Eq. (4.14)). The source vector $\mathbf{s}$ depends not only on the offset parameters x_{0k} $(k = 1, \dots, d)$, but also on the spread parameters σ_k $(k = 1, \dots, d)$. Therefore we propose to retrieve the components of the source vector $\mathbf{s}$, through the following criterion minimization :

$$\hat{\mathbf{s}} = \underset{\mathbf{s}}{argmin} ||\mathbf{Z} - \mathbf{C}\mathbf{s}||^2 \tag{4.23}$$

It is easy to show that the density function of the measurement noise is Gaussian if the outliers are identically distributed over the image [18]. Therefore, the above least-squares problem provides the maximum likelihood estimate for the source vector. The relationship between the source vector components and the spread parameter values is given by (see Eq. (4.13)) :

$$s(k) = f(\sigma_k) = \sqrt{2\pi} G \sigma_k e^{-j\mu x_{0k}} e^{-\frac{\mu^2 \sigma_k{}^2}{2}} \tag{4.24}$$

We denote by $\boldsymbol{\sigma} = [\sigma_1, \ldots, \sigma_d]^T$ the vector containing all spread parameter values, and by $\mathbf{f}(\sigma) = [f(\sigma_1), \ldots, f(\sigma_d)]^T = [s(1), \ldots, s(d)]^T$ the source vector. We denote by $\hat{\boldsymbol{\sigma}} = [\hat{\sigma_1}, \ldots, \hat{\sigma_d}]^T$ the vector containing the estimates of all spread parameter values. From Eqs. (4.23) and (4.24), we get :

$$\hat{\boldsymbol{\sigma}} = \underset{\boldsymbol{\sigma}}{argmin} ||\mathbf{Z} - \mathbf{C}\mathbf{f}(\boldsymbol{\sigma})||^2 \tag{4.25}$$

which can be expressed as :

$$\hat{\boldsymbol{\sigma}} = \underset{\boldsymbol{\sigma}}{argmin} (J(\boldsymbol{\sigma})) \tag{4.26}$$

where J denotes the criterion to be minimized. To solve Eq. (4.26) and minimize criterion J, we adopt a recurrence loop to modify recursively the vector $\hat{\boldsymbol{\sigma}}$. The series vectors are obtained from the relation $\forall q \in \mathbb{N}$:

$$\hat{\boldsymbol{\sigma}}^q \rightarrow \mathbf{f}(\hat{\boldsymbol{\sigma}}^q) \rightarrow J(\hat{\boldsymbol{\sigma}}^q) \tag{4.27}$$

When q tends to infinity, the criterion J tends to zero and $\hat{\sigma}_k^q = \sigma_k, \ \forall \ k = 1, \ldots, d$. To carry out this recurrence loop, we adopt the global DIRECT (DIviding RECTangles) optimization method [71]. DIRECT method is initialized by $\hat{\boldsymbol{\sigma}}^0$, and a research space which is an acceptable interval for each value. Vector $\hat{\boldsymbol{\sigma}}^0$ and the research space are *a priori* fixed by the user. The main property of DIRECT is that it is able to obtain the global minimum of a function. DIRECT normalizes the research space in a hypercube and evaluates the solution which is located at the center of this hypercube. Then, some solutions are evaluated and the hypercube is divided into smaller cubes, supporting the zones where the evaluations are small. When the required number of iterations $q = It$ is reached, DIRECT provides the estimated vector of spread parameters $\hat{\boldsymbol{\sigma}}^{It} = [\sigma_1, \sigma_2, \ldots, \sigma_d]$.

4.2.5 Refined estimation of the offset values

The knowledge of all spread values σ_k, $k = 1, \ldots, d$ permits to avoid the approximation made in section 4.2.3, which led to signal components $\tilde{w}(i)$ out of signal components $w(i)$ (see Eq. (4.22)). Starting from the expression of $w(i)$ in Eq. (4.21), we derive the signal $\omega(i)$, $i = 1, \ldots, d$:

$$\omega(i) = w(i)/(\sqrt{2\pi}\sigma_1 e^{-\frac{(\alpha(i-1))^2 {\sigma_1}^2}{2}}) = G\ e^{-j\alpha(i-1)x_{01}} + n'(i) \tag{4.28}$$

where $n'(i)$ is a noise term resulting from the influence of all but the first contour. The signal components $\omega(i)$ fit TLS-ESPRIT method, which is applied d times to retrieve the exact offset values $x_{0k},\ k = 1, \ldots, d$.

4.2.6 Summary of the proposed algorithm

An outline of the proposed blurred contour estimation method is given as follows :

- find out the mean position of the pixels of the contour :
  - choose μ as a constant value, and estimate the orientations θ_k $(k = 1, \ldots, d)$ by MUSIC method ;
  - choose μ as a variable value $\mu = \alpha(i-1)$, and estimate the offsets x_{0k} $(k = 1, \ldots, d)$ by TLS-ESPRIT method ;
- estimate the spread parameters σ_k $(k = 1, \ldots, d)$ through the minimization of a least-squares criterion by DIRECT optimization method ;
- obtain a refined estimation of x_{0k} $(k = 1, \ldots, d)$, with the knowledge of the previously estimated σ_k values.

4.2.7 Experimental results

4.2.7.1 Hand-made images

In all numerical experiments, we consider images of size $N \times N$ where $N = 200$. At the same time, all experiments are performed on a computer equipped with 2.83GHz 2 Quad CPU and 4Go memory. As concerns parameter μ, [18] provides a study that gives the maximum value of an estimated orientation. Adequate parameters are $\mu = 10^{-1}$, to estimate the orientation parameters with MUSIC method, and $\mu = 10^{-3}$, to estimate the spread parameters with DIRECT method. The value of α is set as 2.5 10^{-3}.

• Example 1 : σ is small enough

In the following example, the orientations of two blurred lines are 30° and −28° respectively, the two offsets of the blurred contours are 130 and 50, and the spread parameters σ equal to 1.

From Fig. 4.2, we can see that the estimation is exactly the same as the initial image. MUSIC algorithm can estimate the orientations of the blurred contours during the mean time 0.049 *sec*, which are 30° and −28°. When TLS-ESPRIT algorithm is used to estimate the offsets of lines, there are only little bias, respectively, 131 and 51, and the algorithm lasts 0.178 *sec*. For the estimation of the spread parameter σ, the optimization method is applied.

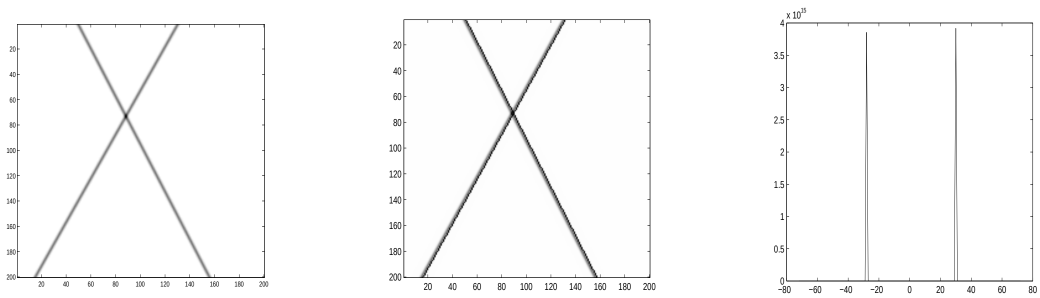

(a) (b) (c)

Figure 4.2 — (a) processed image with two blurred linear contour ; (b) superposition of the initial image and the estimation for the image with two blurred contours ; (c) pseudo spectrum when MUSIC algorithm is exploited

When the number of iterations increases, the values of the estimated σ is closer to the expected values. Considering the computational load and the accuracy of the estimation, the iteration number is chosen to be 15. When we operate 100 trials, the mean error of the estimation σ is less than 2% and the mean computation time is 0.056 *sec.*

• Example 2 : the spread parameters of two blurred contours have both large values.

Fig. 4.3 exemplifies the case where the spread parameters are 8 and 8 respectively, the center offsets of two blurred contours are $x_{01} = 150$ and $x_{02} = 40$, and the main orientation of two contours are $\theta_1 = 10°$ and $\theta_2 = -10°$. The proposed method is compared with Chan and Vese's level set method [31], which is meant to delimitate blurred contours.

Orientation values are estimated as 10° and −10°. For this, signal generation and MUSIC algorithm last 0.069 *sec.* Offset values are estimated as 150 and 40. For this, TLS-ESPRIT algorithm lasts 0.17 *sec.* The spread parameters are estimated as 8.01 and 7.98 by 15 iterations of DIRECT in 0.053 sec. From Fig. 4.3(d), we can see that Chan and Vese method provides a boundary for the two expected contours. Namely, the method converges, and the active contour stops inside the blurred boundaries of the object. However, we denote that the proposed method characterizes the whole contour including gray level variation, whereas the levelset method considers local properties to stop the evolution of the active contour.

• Example 3 : concurrence between blurred contour and high-contrast contour in the image.

In the following experiment, we try to detect the image including blurred contour and high-contrast, one-pixel wide contour. The main orientation of the blurred line is 10°, its offset is 150, and the spread parameter σ is 8. For the high-contrast straight line, its orientation and offset are −10° and 40.

From Fig. 4.4, the estimated orientation of blurred contour is 10°. The offset is estimated

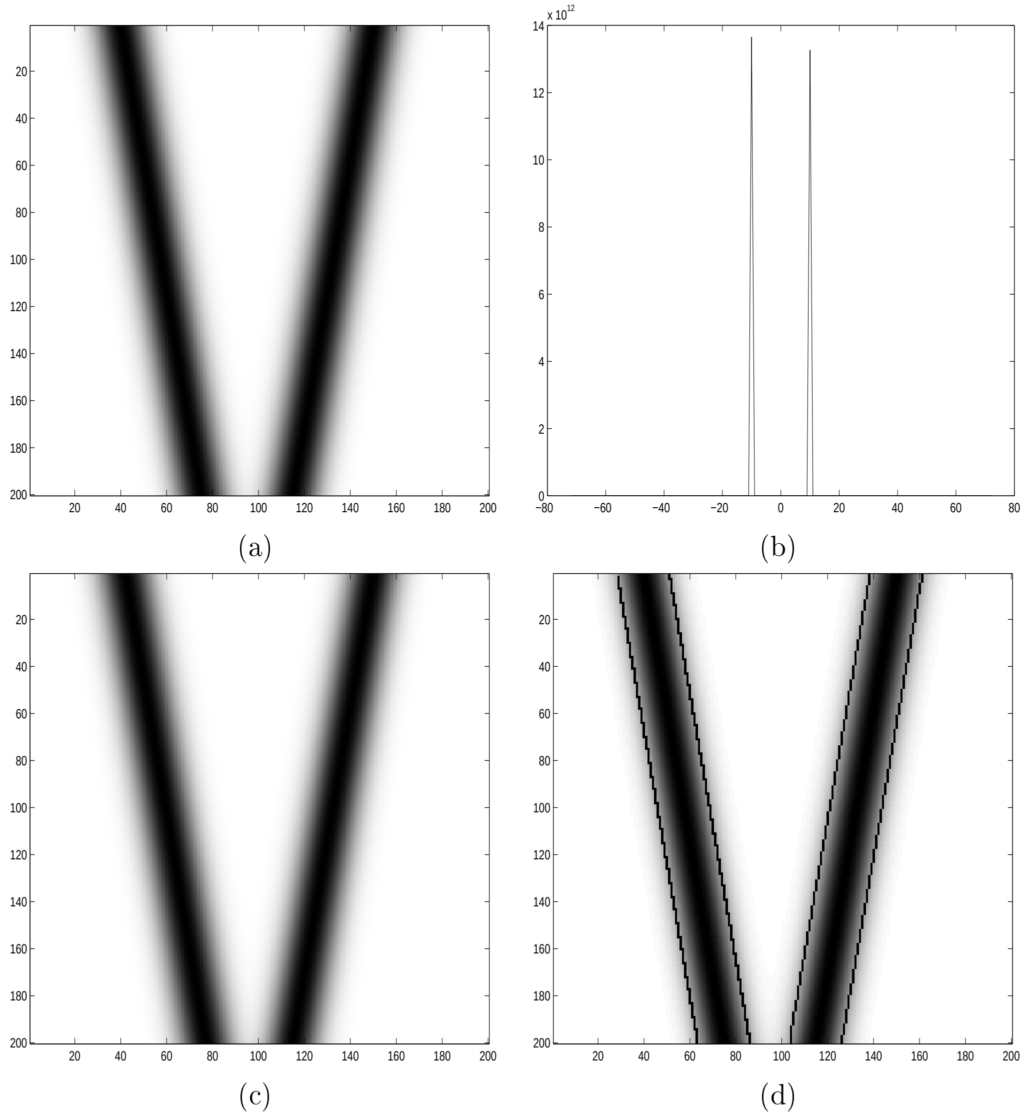

Figure 4.3 — (a) processed image with two blurred linear contours ; (b) pseudo spectrum when MUSIC algorithm is exploited ; (c) estimation by the proposed method ; (d) superposition of the initial image and Chan and vese result

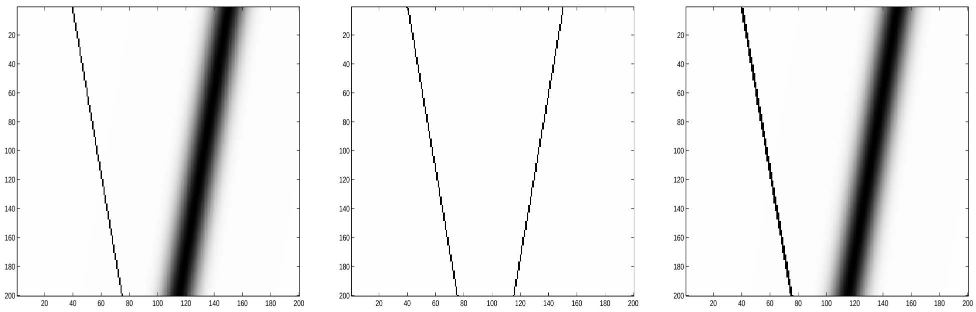

(a) (b) (c)

Figure 4.4 — (a) processed image ; (b) contour center pixels ;(c) superposition of the initial image and the center pixel estimation

as 149.6 pixels. The estimated spread parameter is 8. The detection of high-contrast line contour is characterized by the estimated orientation $-10°$ and offset 40.3. The estimated spread parameter is found to be 0.01. So the bias on the estimated parameters is always 1% or less.

4.2.7.2 Real-world images

We consider the estimation of the cinematic parameters of multiple objects in an image. In [73], a technique is proposed for estimating the parameters of two-dimensional (2-D) uniform motion of multiple moving objects in a scene, based on long-sequence image processing and the application of a multi-line fitting algorithm.

A specific formalism and a line detection algorithm yields the cinematic parameters of the objects [73]. However the proposed method does not take into account the variation along time of the cinematic parameters of the objects. Fig. 4.5 shows the first and last images among a set of 100 images representing two helicopters moving on a fixed background with a supposedly uniform speed. Estimated cinematic parameters [73] are $v_{1x} = 1.1$ pixels/frame and $v_{1y} = -0.2$ pixels/frame ; $v_{2x} = -1.5$ pixels/frame and $v_{2y} = 0.9$ pixels/frame. This estimation would be valid for a punctual object and a constant speed. The trajectory is not a straight line because of the size of the object and the slight speed variations.

We propose to measure the imprecision due to the size of the object and the speed variation. Fig. 4.6 is the bottom right image of Fig. 4.5. By estimating the spread parameter σ for the two contours, we deduce the accuracy of the estimation of the cinematic parameters. In this case the estimated spread parameters are $\sigma_1 = 10$ and $\sigma_2 = 15$, which yields a maximum bias on the trajectory slopes and thereby on the speeds of $\Delta v_{1y} = \sigma_1/N = 5\%$ and $\Delta v_{2y} = \sigma_2/N = 7.5\%$.

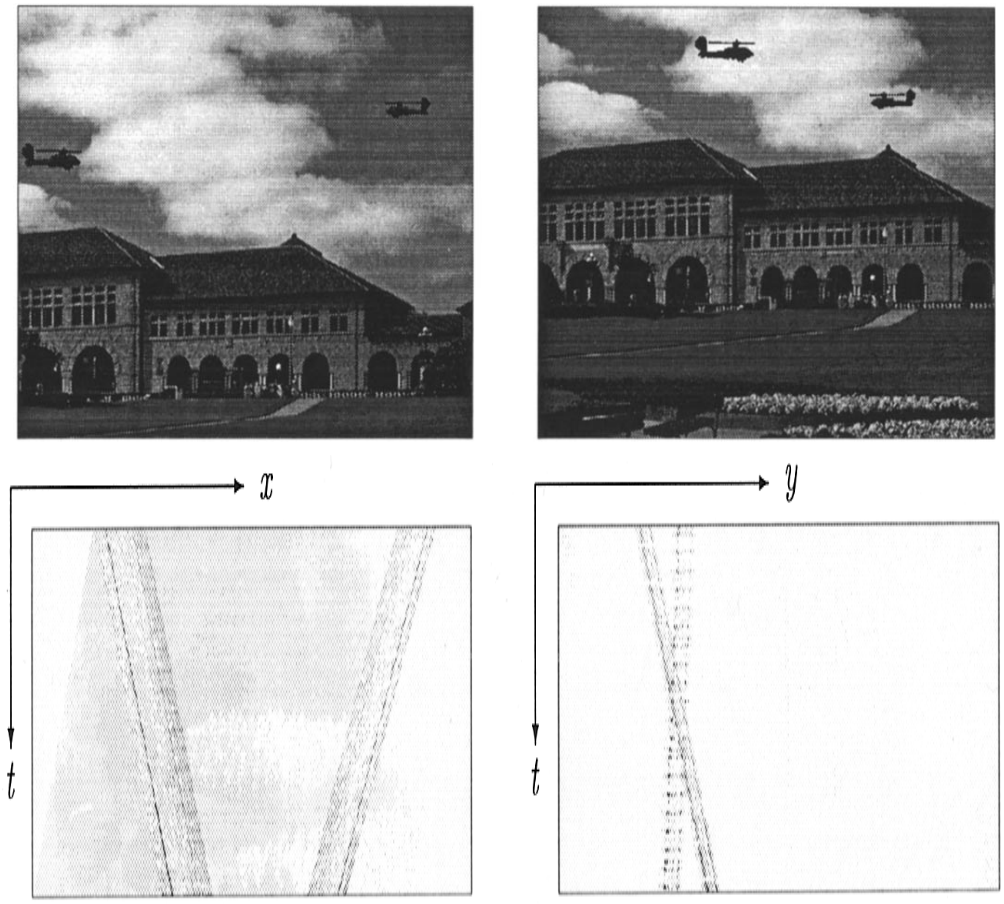

Figure 4.5 — Motion estimation : image sequence and trajectories [73]

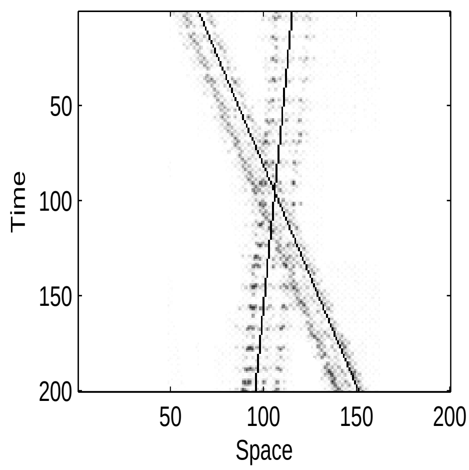

Figure 4.6 — Trajectory characterization

4.3 Blurred triangular contour detection

4.3.1 Image model

In this section, we consider an image model which is composed of a blurred triangular contour (see Fig. 4.7) [99]. The blurred triangular contour is supposed to have main orientation θ and center offset x_0. The pixel values are supposed to be small enough to be neglected at a distance θ_f on each side of the main orientation of the contour. The gray level evolution of the blurred contour around its main orientation in every row can be, in a general manner, described by a Gaussian evolution depending on a spread parameter σ. If we define the gaussian attenuation threshold of the pixel as δ_T, the relationship among θ_f, σ, and δ_T is :

$$\delta_T = \frac{1}{\sqrt{2\pi}\sigma} e^{-\frac{\theta_f^2}{2\sigma^2}}.$$

Below this threshold value, the pixel values are supposed to be negligible.

We adopt the signal generation scheme proposed as in the section 4.2, and yield an array processing signal model handled by subspace-based methods.

4.3.2 Array processing signal model

Firstly, we assume that the image contains only one blurred contour of main orientation θ, angle spread $2\theta_f$, offset x_0, and standard variance σ for the Gaussian distribution of the pixel values. On the i^{th} sensor we get :

$$z(i) = \sum_{\breve{\theta}=-\theta_f}^{\theta_f} e^{-j\mu(x_0-(i-1)tan(\theta+\breve{\theta}))} \cdot \frac{1}{\sqrt{2\pi}\sigma} e^{-\frac{\breve{\theta}^2}{2\sigma^2}} \quad (4.29)$$

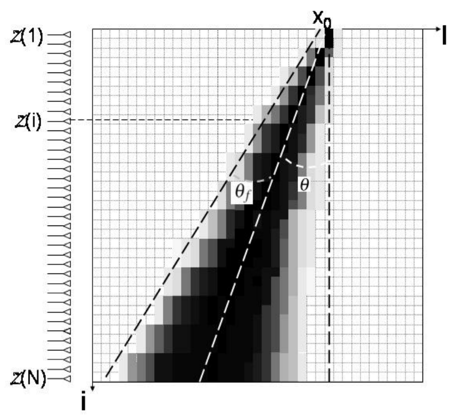

Figure 4.7 — Linear antenna model in an image containing a blurred contour

For small values of $\breve{\theta}$, we get the following approximation with a Taylor series expansion :

$$\tan(\theta + \breve{\theta}) \simeq \tan\theta + \frac{1}{\cos^2\theta}\breve{\theta} \tag{4.30}$$

Combining Eqs. (4.29) and (4.30) yields :

$$z(i) = \frac{1}{\sqrt{2\pi}\sigma} e^{-j\mu x_0} e^{j\mu(i-1)\tan\theta} \sum_{\breve{\theta}=-\theta_f}^{\theta_f} e^{\frac{j\mu(i-1)\breve{\theta}}{\cos^2\theta}} \cdot e^{-\frac{\breve{\theta}^2}{2\sigma^2}} \tag{4.31}$$

When σ is small enough (note that it is coherent with the fact that θ_f is small enough), we can turn the considered discrete calculation into a continuous case calculation :

$$z(i) \simeq \frac{1}{\sqrt{2\pi}\sigma} e^{-j\mu x_0} e^{j\mu(i-1)\tan\theta} \int_{\breve{\theta}=-\infty}^{\breve{\theta}=+\infty} e^{-\frac{\breve{\theta}^2}{2\sigma^2}+\frac{j\mu(i-1)\breve{\theta}}{\cos^2\theta}} d\breve{\theta} \tag{4.32}$$

According to the general formula of Eq. (4.9), it is easy to express Eq. (4.32) by :

$$z(i) = e^{-j\mu x_0} \cdot e^{j\mu(i-1)tan(\theta)} \cdot e^{-\frac{\mu^2\sigma^2(i-1)^2}{2\cos^4\theta}} \tag{4.33}$$

Eq. (4.33) is the signal generated on the i^{th} sensor in the case where there exists only one blurred contour in the image.

Secondly, we consider the case where the image contains :

- d blurred contours, with orientations θ_k, offsets x_{0k}, and standard variance σ_k ($k = 1, \ldots, d$) ;
- identically distributed noise pixels.

The expression of the signal received by the i^{th} sensor becomes :

$$z(i) = \sum_{k=1}^{d} e^{-j\mu x_{0k}} \cdot e^{j\mu(i-1)tan\theta_k} \cdot e^{-\frac{\mu^2\sigma_k^2(i-1)^2}{2\cos^4\theta_k}} + n(i) \tag{4.34}$$

where $n(i)$ is a noise term originated by the noise pixels during the signal generation process. The expression of the signal components in Eq. (4.34) permits to adopt the notations coming from array processing. We define :

1. When the continuous approximation holds, the source amplitude components are expressed as :

$$s(k) = e^{-j\mu x_{0k}}, k = 1, \cdots, d \tag{4.35}$$

2. the steering vector associated with the k-th contour as : $\mathbf{c}(\eta_k) = [c_1(\eta_k), c_2(\eta_k), \cdots, c_i(\eta_k), \cdots, c_N(\eta_k)]^T$, where $\eta_k = [\theta_k, \sigma_k]^T$, with $c_i(\eta_k) = e^{j\mu(i-1)\tan\theta_k} \cdot e^{-\frac{\mu^2\sigma_k^2(i-1)^2}{2\cos^4\theta_k}}$.
3. the noise vector $\mathbf{n} = [n(1), n(2), \ldots, n(N)]^T$.

These notations permit to express the signal generated out of the image in a matrix form :

$$\mathbf{z} = \mathbf{C}(\eta)\mathbf{s} + \mathbf{n} \tag{4.36}$$

where $\mathbf{z} = [z(1), z(2), \ldots, z(N)]^T$, $\mathbf{s} = [s(1), s(2), \cdots, s(d)]^T$, $\mathbf{C}(\eta) = [\mathbf{c}(\eta_1), \mathbf{c}(\eta_2), \cdots, \mathbf{c}(\eta_d)]$.

Equation (4.36) shows that, by adopting the signal generation scheme of Eq. (4.1) and the proposed model for blurred triangle contours, we can make an analogy between the signals generated out of the image and an array processing signal model. Therefore, we predict that array processing methods can yield the parameters of the expected contours.

4.3.3 Subspace based methods of array processing for orientation and spread parameter estimation

4.3.3.1 Main orientation and spread estimation : DSPE

In this subsection, we propose to adapt a method coming from array processing and originally dedicated to distributed source characterization [64, 65]. An array processing method can be applied to the generated signal provided in Eq. (4.36), to characterize the contours in the image by retrieving their parameters. Subspace-based parameter estimation methods such as MUSIC [74] assume that several realizations of a signal are available. Before we apply these method, we still adopt spatial smoothing technique to obtain multiple signal snapshots as in the section 4.2.3. Eq. (4.36) is rewritten as $\mathbf{z}_t = \mathbf{C}(\eta)\mathbf{s}_t + \mathbf{N}_t,\ t = 1, 2, \cdots, T$, where each steering vector $\mathbf{c}(\eta_k)$ of length M is defined as : $\mathbf{c}(\eta_k) = [c_1(\eta_k), c_2(\eta_k), \cdots, c_i(\eta_k), \cdots, c_M(\eta_k)]^T$, with $c_i(\eta_k) = e^{j\mu(i-1)\tan\theta_k} \cdot e^{-\frac{\mu^2\sigma_k^2(i-1)^2}{2\cos^4\theta_k}}$, and $\mathbf{s}_t = [s_1(t), s_2(t), \cdots, s_d(t)]^T$ where $s_k(t) = e^{-j\mu x_{0k}} e^{-\frac{\mu^2\sigma_k^2(t-1)^2}{2cos^4\theta_k}} e^{j(t-1)\mu tan\theta_k}$.

The covariance matrix of $\mathbf{z}(t)$ is defined by : $\mathbf{R}_{zz} = \frac{1}{T}\sum_{t=1}^{T} \mathbf{z}_t {\mathbf{z}_t}^H$ where $(\cdot)^H$ denotes Hermitian transpose. We perform eigenvalue decomposition of $\mathbf{R}_{zz}$,

$$\mathbf{R}_{zz} = [\mathbf{U}_1 \quad \mathbf{U}_2]\ \mathbf{\Lambda}\ \mathbf{U}$$

In the literature, we can find two types of distributed sources, namely, decorrelated, also called incoherently distributed (ID), and coherently distributed (CD) sources [66]. An interesting property of the spatial smoothing technique is that it decorrelates the sources [18]. Therefore, in our study, we can consider that all sources are decorrelated. As we are ensured to have decorrelated sources thanks to the spatial smoothing process, the columns of matrix $\mathbf{U}_1$ (M $\times$ d) span the signal subspace, the columns of matrix $\mathbf{U}_2$ (M $\times$ (M $-$ d)) span the noise subspace, and $\mathbf{\Lambda} = diag\,(\lambda_1, \lambda_2, \cdots \lambda_d)$ where λ_i is the eigenvalue associated with the i^{th} eigenvector. Hence, $\mathbf{U}_2$ is orthogonal to the steering vectors $\mathbf{c}\,(\theta_k)\,,\ k = 1, \ldots, d$. We estimate the η_k parameters $(k = 1, \ldots, d)$ through the bidimensional search procedure of the maxima of the pseudo spectrum given by the DSPE (Distributed Signal Parameter Estimator) method [64, 66] :

$$\mathrm{DSPE}\,(\eta_k) = \frac{\parallel \mathbf{c}\,(\boldsymbol{\eta}_k) \parallel^2}{\parallel \mathbf{c}^H\,(\boldsymbol{\eta}_k) \cdot \mathbf{U}_2 \parallel^2} \tag{4.37}$$

where $\mathbf{c}\,(\boldsymbol{\eta}_k)$ is a model for the signal subspace vectors. Thus, DSPE method provides the orientation and spread values, through the relationship : $\boldsymbol{\eta}_k = [\theta_k, \sigma_k]^T,\ \forall\ k = 1, \ldots, d$. In the next subsection, we illustrate the performance of the proposed method for the estimation of the orientation and spread parameter values in several application cases.

4.3.3.2 Offset estimation : variable speed generation scheme

To estimate all offset values, we adopt a variable speed generation scheme [18], and a specific "dechirping" procedure : we set the propagation parameter as a value which depends on the row index. Parameter μ becomes $\alpha(i-1)$. Then, for each η_k estimated at subsection 4.3.3.1, we apply a specific signal transformation with the knowledge of θ_k and σ_k. For all $k = 1, \ldots, d$ successively, we get :

$$w(i) = z(i)/(e^{j\alpha(i-1)^2 tan\theta_k} \cdot e^{-\frac{\alpha^2\sigma_k^2(i-1)^4}{2\cos^4\theta_k}}) \tag{4.38}$$

For instance, when $k = 1$, we aim at estimating the first offset value x_{01} :

$$w(i) = e^{-j\alpha(i-1)x_{01}} + n'(i) \tag{4.39}$$

where $n'(i)$ is a noise term resulting from the transformation of the original noise term by the dechirping procedure.

Equation (4.39) shows that any subspace-based method such as TLS-ESPRIT [18, 22] can be applied to retrieve the offset value x_{01}. The same process is applied for all $k = 1, \ldots, d$. At this point, we estimated all offset values x_{0k}, $k = 1, \ldots, d$.

4.3.4 Results

In this section, we illustrate the propose method on hand-made and real-world images. All experiments are performed on a computer equipped by 2.83GHz 2 Quad CPU and 4G memory. Images have size 200×200 pixels. Adequate parameter values found experimentally, which are used for signal generation, are $\mu = 2.3\ 10^{-2}$ and $\alpha = 2.5\ 10^{-3}$, the size of the sub-arrays used for the spatial smoothing procedure is $M = 4$.

4.3.4.1 Hand-made images

We propose a statistical study which characterizes the performance of the proposed method. The proposed method is run for several triplets of values $(\theta\,; \sigma\,; x_0)$. The results obtained are provided in Table 4.1, which provides the estimated values ($\hat{\theta}$; $\hat{\sigma}$; $\hat{x}_0$), and the bias (E_θ ; E_σ ; $E_{x_{0k}}$) defined by : $E_\theta = |\hat{\theta} - \theta|$, $E_\sigma = |\hat{\sigma} - \sigma|$, and $E_{x_0} = |\hat{x}_0 - x_0|$. These results show that the proposed method always provides a very accurate estimation of the orientation θ, and that the best estimation results for σ are obtained for values between 1.5 and 2.4. The bias on the estimated offset values x_0 is always equal to or less than 1 pixel. Note that the case $\sigma = 0$ was considered, and leads to an estimate $\hat{\sigma} = 0.36$. The result contour appears then as a 1-pixel wide contour. As an illustration of the proposed algorithm, Figs. 4.8(a,d)

Tableau 4.1 — Estimated values $\hat{\theta}$; $\hat{\sigma}$; $\hat{x}_0$ and mean error values E_θ ; E_σ ; E_{x_0} in (° ;pixels ;pixels) obtained with the proposed method, versus contour characteristics (θ ; σ ; x_0).

(θ ; σ ; x_0)	($\hat{\theta}$; $\hat{\sigma}$; $\hat{x}_0$)	(E_θ ; E_σ ; E_{x_0})
(10 ; 0 ; 50)	(11.7 ; 0.36 ; 49)	(1.7 ; 0.36 ; 1)
(9 ; 0.5 ; 48)	(8.6 ; 0.74 ; 49)	(0.4 ; 0.24 ; 1)
(11 ; 1 ; 51)	(10.9 ; 1.47 ; 50.5)	(0.1 ; 0.47 ; 0.5)
(10 ; 1.2 ; 80)	(10.9 ; 1.3 ; 80)	(0.0 ; 0.1 ; 0)
(10 ; 1.5 ; 50)	(9.9 ; 1.76 ; 49.5)	(0.1 ; 0.26 ; 0.5)
(12 ; 1.7 ; 45)	(11.9 ; 1.87 ; 45)	(0.1 ; 0.17 ; 0)
(5 ; 1.9 ; 60)	(4.9 ; 1.92 ; 60)	(0.1 ; 0.02 ; 0)
(13 ; 2 ; 39)	(13.0 ; 1.94 ; 39)	(0.0 ; 0.06 ; 0)
(-12 ; 2.2 ; 53)	(-12.0 ; 2.10 ; 53)	(0.0 ; 0.10 ; 0)
(-10 ; 2.4 ; 36)	(-9.9 ; 2.41 ; 36)	(0.1 ; 0.01 ; 0)
(10 ; 3 ; 50)	(9.9 ; 2.19 ; 50)	(0.1 ; 0.81 ; 0)

provide the processed image, containing one or two fuzzy contour(s) whose characteristics are to be estimated.

Figs. 4.8(b,e) provide the result image, containing the contour drawn from the estimated contour parameters. Figs. 4.8(c,f) provide the difference image. The difference images are not entirely white, which is due to the slight bias on the estimation of σ. This bias may be due to approximations of Eqs. (4.30) and (4.32) : the adequation between signal model and generated signal cannot be strictly fulfilled. The whole computational time need to estimate the orientation and spread values is 2.30 sec. In comparison, the computational load which is needed to generate the signal is negligible, and the time needed for the offset estimation step is 0.9 sec.

4.3.4.2 Real-world images

Figs. 4.9 illustrates the proposed algorithm on a real-world image. Our goal is to study the beam which is produced by a space instrument.

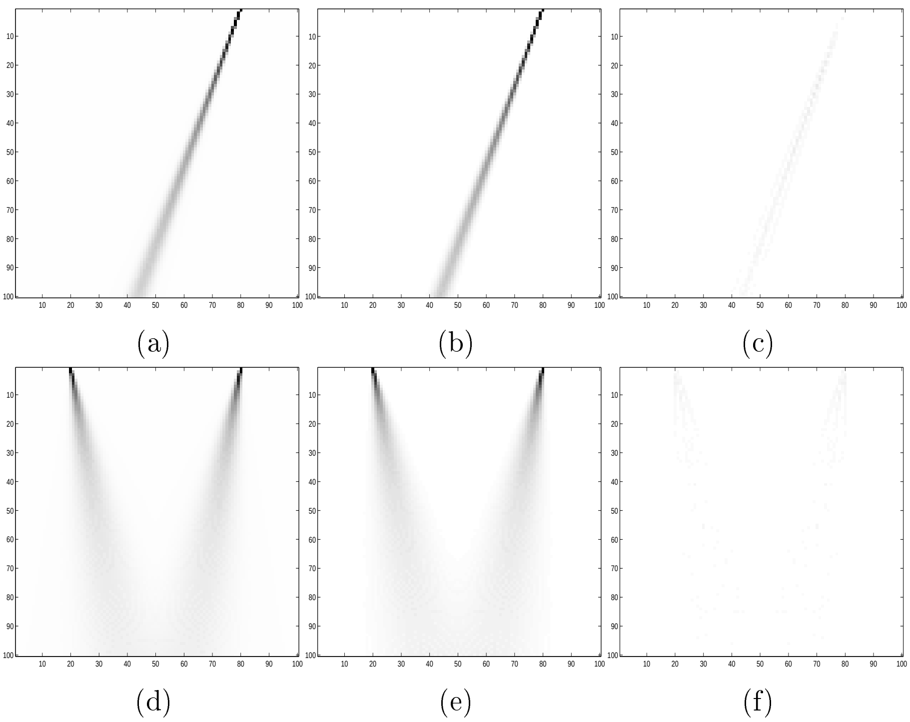

Figure 4.8 — Estimation of (θ ; σ ; x_0) : (a) processed (20° ; 1.2 ; 80) ; (b) result (20° ; 1.01 ; 80) ; (c) difference processed - result ; (d) processed (10° ; 5.1 ; 80) and (−10° ; 5.1 ; 20) ; (e) result (10° ; 5.01 ; 80) and (−10° ; 5.01 ; 20) ; (f) difference processed - result

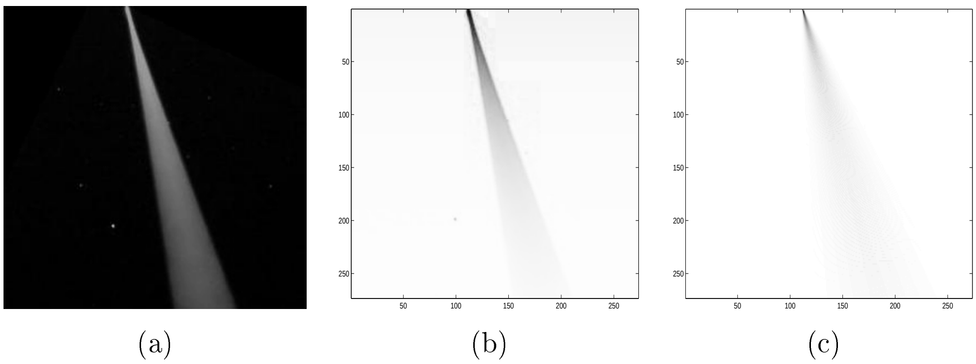

Figure 4.9 — Light beam characterization : (a) original real-world image ; (b) processed ; (c) result (−19° ; 6.01 ; 112)

We seek for the main orientation and spreading of the light beam. Fig. 4.9 focuses on the part of interest of the image (see Fig. 4.9(b)), and provides the image simulated with the estimated parameters (see Fig. 4.9(c)). The estimated parameters are $\hat{\theta} = -19°$; $\hat{\sigma} = 6.01$ pixels ; $\hat{x}_0 = 112$ pixels.

We notice that the visual aspect of Fig. 4.9(c) is very close to the aspect of Fig. 4.9(b), which means that the contour characteristics were accurately estimated.

These experiments show that there exists an interval $\sigma = [1.5, \ldots, 3]$ where the approximations of Eqs. (4.30) and (4.32) are both valid : the expected parameters are retrieved with a small bias. Moreover, the proposed method handles the case of 1-pixel wide contours.

4.4 Blurred circular contour detection

In this section, we provide the model that we adopt for the image including blurred circular contour [100]. Let consider $I(l,m)$ be an $N \times N$ recorded image, which contains a blurred circular contour and an additive uniformly distributed noise. The gray level values of blurred contour follow a Gaussian distribution, that is,

$$I(l,m) = Ge^{-\frac{(\sqrt{(l-l_c)^2+(m-m_c)^2}-r_0)^2}{2\sigma^2}} \tag{4.40}$$

The maximum gray value is $I_{\max} = G$. A circular-like contour is supposed to have center coordinates (m_c, l_c). The pixels with value G compound a circle with center coordinates (m_c, l_c) and radius r_0. The gray level values of the pixels decrease gradually aside the set of pixels with value G. The blurred circular-like contour has width $2r_f$ aside the set of maximum-valued pixels.

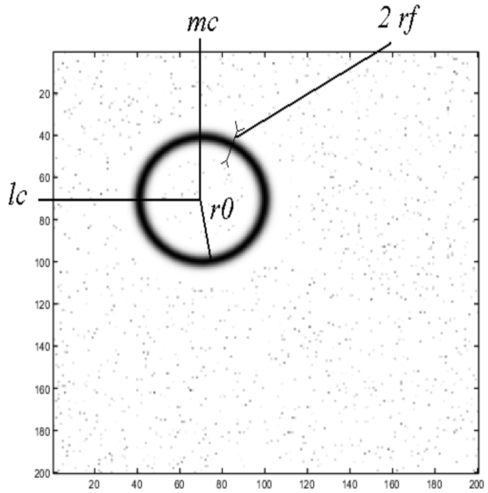

Figure 4.10 — Blurred circular contour characterized by center coordinates (m_c, l_c), radius r_0, and width $2r_f$.

We restrict the type of contour which can be retrieved, which permits to characterize the contours by only three parameters : center coordinates (m_c, l_c), radius r_0 and spread parameter σ. To set the link between image data representation and sensors array processing methods, we adopt the model as in Fig. (3.2). For more detail, see the section 3.2.2.

4.4.1 Signal model

Let's consider a 1-pixel wide contour, that is, $I(l,m) = 1$ if $\sqrt{l^2 + m^2} = r_0$ and $I(l,m) = 0$ otherwise. According to signal generation model by circular antenna, and referring to Eq. (3.2),

$$z(i) = \sum_{l,m=1;(l,m)\in D_i}^{l,m=N_s} I(l,m)exp(-j\mu\sqrt{l^2+m^2}),$$

we get $z(i) = exp(-j\mu r_0)\ \forall\ i$. As μ has a fixed constant value, this "constant speed" generation scheme yields signal components of same values. To fit the signal model of frequency retrieval methods, we adopt, instead of the fixed parameter μ, a propagation parameter whose value depends on the sensor index. That is, we choose $\mu = \alpha(i-1)$, where α is a constant. The propagation parameter is therefore variable, hence the denomination of the "variable speed" generation scheme which provides, $\forall\ i$:

$$z(i) = \sum_{\substack{l=1\\(l,m)\in D_i}}^{N_s} \sum_{m=1}^{N_s} I(l,m)exp(-j\alpha(i-1)\sqrt{l^2+m^2}) \tag{4.41}$$

To simplify the expression in Eq. (4.40), we denote by $\triangle r$ the shift between a pixel and the contour mean position. The gray level variation of a blurred circular contour can then be expressed as follows :

$$g(\triangle r) = \frac{1}{\sqrt{2\pi}\sigma}exp(-\frac{\triangle r^2}{2\sigma^2}) = G\ exp(-\frac{\triangle r^2}{2\sigma^2}) \tag{4.42}$$

Referring to Eqs. (4.41) and (4.42), the generated signal components are formulated as :

$$\begin{aligned} z(i) &= \textstyle\sum_{\triangle r=-r_f}^{r_f} exp(-j\alpha(i-1)(r_0+\triangle r))g(\triangle r) \\ &= G\textstyle\sum_{\triangle r=-r_f}^{r_f} exp(-j\alpha(i-1)(r_0+\triangle r))exp(-\frac{\triangle r^2}{2\sigma^2}) \\ &= Gexp(-j\alpha(i-1)r_0)\textstyle\sum_{\triangle r=-r_f}^{r_f} exp(-j\alpha(i-1)\triangle r)exp(-\frac{\triangle r^2}{2\sigma^2}) \end{aligned} \tag{4.43}$$

If σ is small enough compared with the number of pixels along the direction D_i of signal generation, we can turn the considered discrete calculation into a continuous case calculation :

$$z(i) = Gexp(-j\alpha(i-1)r_0)\int exp(-j\alpha(i-1)\triangle r)exp(-\frac{\triangle r^2}{2\sigma^2})d(\triangle r) \tag{4.44}$$

Using the general formula of Eq. (4.9), Eq. (4.44) is rewritten as :

$$z(i) = exp(-j\alpha(i-1)r_0)exp(-\frac{\sigma^2\alpha^2(i-1)^2}{2}). \tag{4.45}$$

We notice that, contrary to Eq. (4.11), Eq. (4.45) contains a quadratic term, which is the modulus of each signal term. If we account for noise and consider the signal terms $z^{'}(i)$ such that :

$$z^{'}(i) = \frac{z(i)}{|z(i)|} = exp(-j\alpha(i-1)r_0) + n(i) \tag{4.46}$$

we get the following expression :

$$\mathbf{z}' = \mathbf{c}(r_0) + \mathbf{n} \tag{4.47}$$

with $\mathbf{c}(r_0) = [1, exp(-j\alpha r_0), \ldots, exp(-j\alpha(S-1)r_0)]^T$ and $\mathbf{n} = [n(1), \ldots, n(S-1)]^T$ is the noise vector.

4.4.1.1 Estimation of prior information needed for contour characterization

The proposed method is entirely blind. We propose to distinguish the contours with two linear antennas, placed aside the image on the left or the top side. A threshold value is applied to the generated signals to reduce the noise influence.

When the signals received on both antennas exhibit first and last components which are zero-valued in the case with no noise in image, one or several circles are present. Their center coordinate l_c (resp. m_c) are given by the middle point of the non-zero sections of the signal generated on the left (resp. bottom) array. The details refer to the section 3.2.1.

4.4.2 Estimation of the radius

At this point the center coordinates (m_c, l_c) are known. From Eq. (4.47), we notice that the problem of radius estimation is similar to the retrieval of harmonics in several signal processing fields such as radar, sonar, communication. The resulting signal appears as a single sinusoid with unitary amplitude and frequency :

$$f = -\alpha r_0 / 2\pi \tag{4.48}$$

MFBLP method (Modified Forward-Backward Linear Prediction) is adequate for frequency retrieval from coherent signals, in particular signals with unitary amplitude. We adapt it to estimate the radius, which was initially introduced in spectral estimation techniques.

Considering one blurred circle, and adopting MFBLP method to the signal vector $\mathbf{z}'$ (see Eq. (4.47)), the specific steps are as follows :

1) For a N-data vector $\mathbf{z}'$, form matrix $\mathbf{Q}$ of size $2*(N-L) \times L$, where $1 \leq L \leq N-1$. The j^{th} column $\mathbf{q}_j$ of $\mathbf{Q}$ is defined by $\mathbf{q_j} = \left[z'(L-j+1), ..., z'(N-j), z'^*(j+1), ..., z'^*(N-L+j)\right]^T$.

Then build a length $2*(N-L)$ vector : $\mathbf{h} = \left[z'(L+1), ..., z'(N), z'^*(1), ..., z'^*(N-L)\right]^T$, and calculate the singular value decomposition of $\mathbf{Q}$: $\mathbf{Q} = \mathbf{U}\Lambda\mathbf{V}^H$.

2) Form a matrix Σ, setting to 0 the $L-1$ smallest singular values contained in Λ.

3) Form vector $\mathbf{g}$ from the following matrix computation : $\mathbf{g} = [g_1, g_2, ..., g_L]^T = -\mathbf{V} * \Sigma^\sharp * \mathbf{U}^H * \mathbf{h}$, where $\Sigma^\sharp$ is the pseudo-inverse of Σ.

4) Determine the roots of polynomial function H, where $H(\gamma) = 1 + g_1\gamma^{-1} + g_2\gamma^{-2} + ... + g_L\gamma^{-L}$.

5) One zero of H is located on the unit circle. The complex argument of this zero is the frequency value; according to equation (4.48) this frequency value is proportional to the radius, the proportionality coefficient being $-\alpha$.

If one wishes to reduce the computational load of the radius estimation step, and on condition that still one circle is solely expected, the Fourier transform with adequate frequency can be adapted to retrieve the radius value.

4.4.3 Optimization strategy for spread parameter estimation of the blurred contours

In this subsection, we propose least-square criteria which involve the signals generated out of the image and the signal model of Eq. (4.45) for circular contours. The proposed optimization strategy should provide the spread parameter σ for the blurred circular contour.

We start from the signal $\mathbf{z} = [z(1), z(2), \ldots, z(S)]^T$ whose components $z(i)$ are defined in Eq. (4.45). The value of r_0 is known at this point, and can be used to obtain the signal components $z^{''}(i)$ defined as follows : $z^{''}(i) = z(i)/exp(-j\alpha(i-1)r_0)$. Let's then denote by $\mathbf{z}^{''}_{model}$ the signal whose components are defined by $z^{''}_{model}(i) = exp(-\frac{\sigma^2\alpha^2(i-1)^2}{2})$, and let's denote by $\mathbf{z}^{''}_{image}$ the signal whose components are defined by :
$z^{''}_{image}(i) = z(i)/exp(-j\alpha(i-1)r_0)$ and obtained from the signal components $z(i)$ generated out of the image. With these notations, the spread parameter σ can be estimated as follows :

$$\hat{\sigma} = \underset{\sigma}{argmin} ||\mathbf{z}^{''}_{image} - \mathbf{z}^{''}_{model}||^2 \tag{4.49}$$

which can be expressed as :

$$\hat{\sigma} = \underset{\sigma}{argmin}(J_{circle}(\sigma)) \tag{4.50}$$

where J_{circle} denotes the criterion to be minimized.

Contrary to the case of linear blurred contours described in subsection 4.2.4, the global optimization method DIRECT [71] is not adequate to minimize the criterion J_{circle} presented in Eq. (4.50). We adapt the Newton algorithm, and expect that Newton algorithm retrieves efficiently the single unknown parameter σ, through the following loop : $\forall\ q \in \mathbb{N}$,

$$\hat{\sigma}^q \rightarrow \mathbf{z}^{''}_{model\ estimated\ for\ \hat{\sigma}^q} \rightarrow J_{circle}(\hat{\sigma}^q) \tag{4.51}$$

Newton algorithm performs as follows :

$$\forall\ q \in \mathbb{N} : \quad \sigma^{q+1} = \sigma^q - \lambda\overline{\nabla(J_{circle}(\sigma^q))} \tag{4.52}$$

where λ is the step for the descent and $\bar{\cdot}$ denotes mean value. The gradient is obtained through the derivative of $\mathbf{z}^{''}_{model}$ as a function of σ.

4.4.4 Summary of the proposed algorithm

An outline of the proposed blurred contour estimation method is given as follows :

- find out the mean position of the pixels of the contour :
  - Find the center coordinates (l_c, m_c) by linear antenna [22] : perform constant speed generation scheme with an array placed on the left (resp. bottom) side of the image and retrieve l_c (resp. m_c) as the middle of the non-zero section ;
  - choose μ as a variable value $\mu = \alpha(i-1)$, and estimate the radius r_0 by determining the roots of the polynomial function H ;
- estimate the spread parameters σ_k $(k = 1, \ldots, d)$ by Newton method (see Eq. (4.50)) ;

4.4.5 Results

This subsection presents results obtained on hand-made and real-world images. All experiments are performed on a computer equipped with 2.83GHz 2 Quad CPU and 4G memory. Unless specified, we consider images of size $N \times N$ where $N = 200$. We also compared the proposed method with Chan and Vese method [31]. The parameters which are adequate when running this method are as follows : the level is 0.7, the number of iterations is 50, and weighting terms for the energy are $\mu = 0.03 * 255^2$, $v = 0$, $\lambda_1 = \lambda_2 = 1$. In the considered experiments, the number of sensor S is chosen adequately, that is, larger than $\sqrt{2}N_s$. The center coordinates can be estimated using the method proposed in [22] which is based on linear antenna. Aside, the gray level values are considered as negligible.

4.4.5.1 Discussion about the approximation which yields an integral from a discrete summation

In this subsection, we discuss the approximation which yields Eq. (4.45) from Eq. (4.43) in subsection 4.4.1. This is done with a view to giving an interval for the parameters of the problem where this approximation is valid. This permits to justify the experimental conditions chosen in the following subsections of this section. For a given propagation parameter α, the parameters of interest in Eq. (4.45) are the half number of pixels r_f on which the summation is performed, and the spread parameter σ. We expect that the higher r_f and the smaller σ, the smaller the difference between the right second term of Eq. (4.43) and the right second item of Eq. (4.45).

We choose as maximum r_f the value $r_f = 78$, which is coherent with the size chosen for most of the images. This value is attained as soon as the sub-image containing the expected quarter of circle has size 55×55, which is less than N. Viewing the size of the images, we fix the maximum value of σ to $\sigma = 8$.

In subsection 4.4.1, a variable speed propagation scheme is chosen to fit the signal model of a frequency retrieval method. We set $\mu = \alpha(i-1)$, $\forall\ i = 1, \ldots, S$. For $\alpha = 2\ 10^{-3}$ and $S = 500$, the extreme values of μ are then 0 and 1. Therefore, for the propagation parameter $\mu = 1$, for 100 values of r_f equi-spaced between 42 and 78, and for 100 values of σ equi-spaced between 1 and 8, the relative error is computed as follows :

$$Er = \frac{|\mathcal{L} - \mathcal{R}|}{min(\mathcal{L}, \mathcal{R})} \tag{4.53}$$

where $\mathcal{L} = \sum_{r=-r_f}^{r_f} e^{-j\mu r} e^{-\frac{r^2}{2\sigma^2}}$ and $\mathcal{R} = \sqrt{2\pi}\sigma e^{-\frac{\mu^2\sigma^2}{2}}$, which are from Eq. (4.43) and Eq. (4.45).

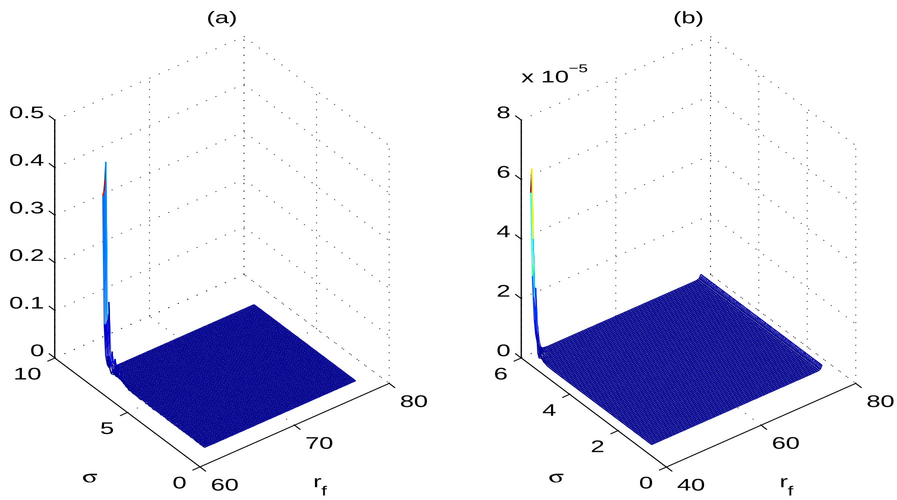

Figure 4.11 — Relative error values Er for : (a) $\sigma \in [1:8]$ and $r_f \in [62:78]$; (b) $\sigma \in [1:6]$ and $r_f \in [42:78]$

We notice that, in the conditions of Fig. 4.11(b), which are the strongest ones but still coherent with the size of the processed images, the relative error is always less than 5%. Significant values are the following :

r_f	65	78	52	70	42
σ	8	7	6	4	2
Er	$1.4\ 10^{-2}$	$1.1\ 10^{-6}$	$6.2\ 10^{-10}$	$2.6\ 10^{-14}$	$1.4\ 10^{-16}$

From these significant values, we confirm that the relative error is always less than 1.5% as soon as r_f is larger than or equal to 65 for values of σ which are up to 8. We notice also that, even for a rather large value of σ (7), the relative error is only $1.1\ 10^{-6}$ when $r_f = 78$. As a conclusion to the study presented in this subsection, we assess that the approximation of Eq. (4.10) is valid in the considered experimental conditions.

4.4.5.2 Hand-made image

– Hand-made image containing one blurred contour

We present a result obtained from an image of size 200 $\times$ 200 pixels (see Fig. 4.12). The number of sensors S is chosen as 200. The experimental conditions and expected values for the blurred circular contour are as follows : the center coordinates are (m_c, l_c)= (100, 100) ; the radius is $r_0 = 60$ pixels ; the spread value is σ= 4. The parameters used while running the proposed methods are as follows : signal generation : α=4 10^{-3} ; Gradient method : 50 iterations, λ=5.

The proposed methods yield the following estimated parameters out of the generated signals : the estimated radius value is 62.6 pixels, and the estimated spread value is σ= 4.34. The required computational times are as follows : our method requires 3.9 10^{-2} sec. to estimate the center coordinates, 1.61 10^{-1} sec. to estimate the radius and 1.17 sec to estimate the spread parameter ; Chan and Vese level-set requires 7.21 sec. to retrieve the contours.

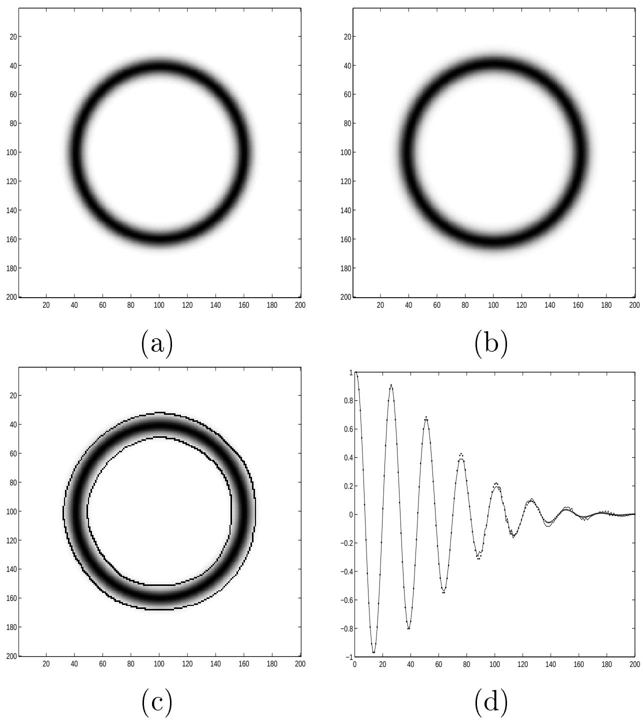

Figure 4.12 — Hand-made image : (a) initial image ; (b) result ;(c) results by Chan and vese method ;(d) comparison between signal generated from image and theoretical signal

When the center coordinates are not at the center of image, we can still get the similar results (see Fig. (4.13)). The expected blurred circular contour is characterized by the following parameters : the center coordinates are (m_c, l_c)= (120, 95) ; the radius is $r_0 = 45$ pixels ; the spread value is σ= 4. After 200 iterations to estimate the spread parameter, where $\lambda = 0.5$, the estimated radius value obtained by MFBLP method is 44.6 pixels, and the estimated sigma is 4.01. To estimate the radius value, the required computational times as follows : 3.35 10^{-2} sec. to estimated the center position, 1.41 sec. to estimate the radius value with MFBLP, and 7.7 10^{-3} to estimate sigma by Newton optimization.

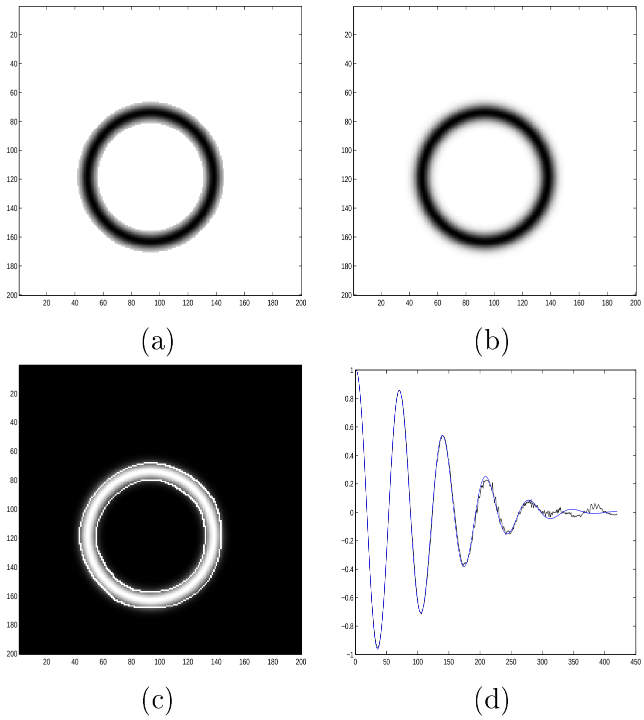

Figure 4.13 — Hand-made image : (a) initial image ; (b) result ;(c) results by Chan and vese method ;(d) comparison between signal generated from image and theoretical signal

– Hand-made image containing three blurred contours and noise

The processed image (see Fig. 4.14) contains three blurred circles with following parameters :

	center	radius	spread
(1)	$\{40; 170\}$	8	2
(2)	$\{160; 95\}$	10	3
(3)	$\{90; 30\}$	12	4

The image is impaired on 5% of the pixels with a Gaussian identically distributed noise with mean 0.4 and standard deviation 0.02. The proposed methods are run to get first the center coordinates, and then the center radius and the spread of each contour. The estimated parameters are as follows :

	center	radius	spread
(1)	$\{41; 170\}$	8.2	2.7
(2)	$\{161; 95\}$	9.0	3.9
(3)	$\{91; 30\}$	12.3	4.7

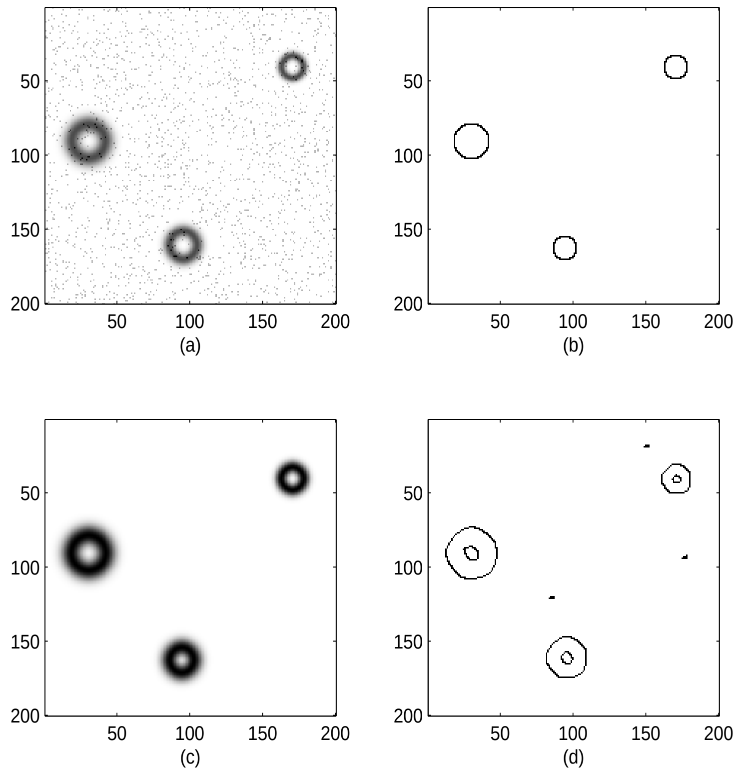

Figure 4.14 — (a) Processed image ; (b) Center circle ; (c) Final result obtained with the proposed methods ; (d) Result obtained by Chan and Vese

All but the second radius values and spread values are just slightly overestimated, and Fig. 4.14(b) and (c) exhibit satisfactory visual results. Fig. 4.14(d) shows that Chan and Vese method provides the inner and outer frontiers of the blurred contours, but also unexpected pixels due to the convergence of noise pixels. On the contrary, the proposed method provides only the expected contours. The computational loads required by the proposed methods and comparative Chan and Vese method are as follows : for each circle, center estimation requires $4.25\ 10^{-2}$ sec. TLS-ESPRIT method to estimate the radius requires $8.8\ 10^{-3}$ sec. To estimate the spread parameter σ, Newton algorithm requires $4.8\ 10^{-3}$ sec. In this case, the ALS loop is not run because there is only one circle, and so one spread value to retrieve for each center.

For the image as a whole, Chan and Vese method requires 2.64 sec. Other experiments have shown that the method breaks down for noise mean value higher than 0.4 when the same standard deviation of 0.02 is used.

– Hand-made image containing a one pixel-wide contour and a blurred contour

The processed image (see Fig. 4.15) contains a sharp one pixel-wide contour and one blurred circle. The characteristic parameters of these circles are as follows : the radius values are $r_{01} = 20$ and $r_{02} = 30$, the center coordinates are $\{l_{c1}, m_{c1}\} = \{48, 135\}$ and $\{l_{c2}, m_{c2}\} = \{156, 47\}$, and the spread parameters are $\sigma_1 = 0$ and $\sigma_2 = 4$.

The one pixel-wide circle is detected as follows : we perform a test on the mean value of the derivative of $|\mathbf{z}|$, where $\mathbf{z}$ is the signal whose components are defined in Eq. (4.45), and $|\cdot|$ denotes absolute value. Indeed, when $\sigma = 0$, $|\mathbf{z}|$ is constant for all components of $\mathbf{z}$.

The estimated values are as follows : $\hat{r}_{01} = 21.4$ and $\hat{r}_{02} = 32.5$, the center coordinates are $\{\hat{l}_{c1}, \hat{m}_{c1}\} = \{48, 136\}$ and $\{\hat{l}_{c2}, \hat{m}_{c2}\} = \{156, 47\}$, and the spread parameters are $\hat{\sigma}_1 = 0$ and $\hat{\sigma}_2 = 4.20$.

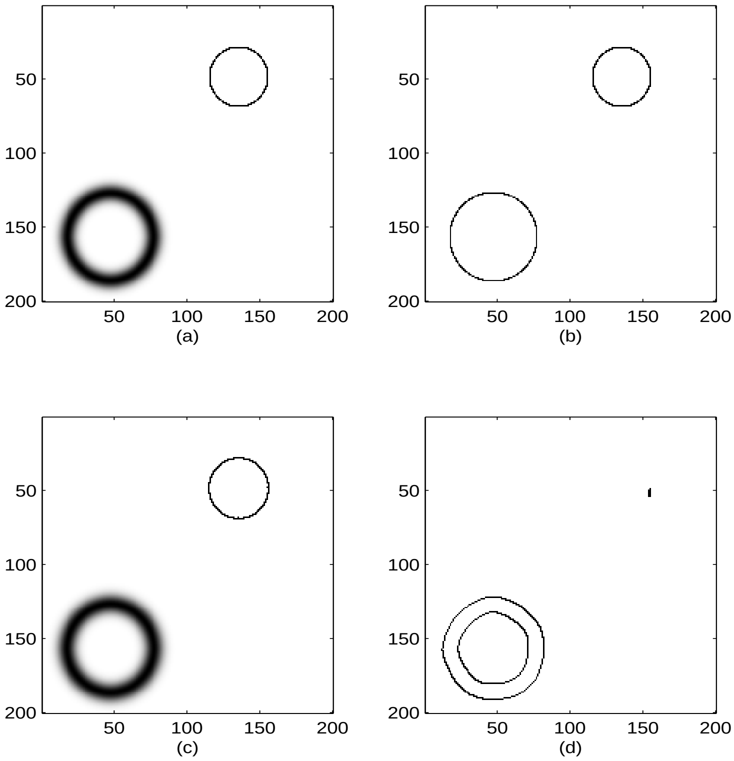

Figure 4.15 — (a) Processed image ; (b) Center circle ; (c) Final result obtained with the proposed methods ; (d) Result obtained by Chan and Vese

We notice that in this case and with the parameters used in this section, Chan and Vese method does not retrieve both blurred and sharp contours.

4.4.5.3 Real-world images

We consider images of size 200 $\times$ 200. The parameters which are adequate to such an image are α=1 10^{-3} ; 50 iterations and λ=5 for Gradient method.

– Example 1 : retina

We consider in the following two images of retina. These retina images come from the database which is also exploited in [96]. We aim at characterizing the optic nerve head to detect a glaucoma. The optic nerve head is divided into two regions : the center which appears as a white region, and the neuroretinal rim which is a disk compounding a darker region. In the case of a healthy retina, the rim is wide tending slowly to be white towards the center. In the case of a non-healthy retina exhibiting a glaucoma, the neuroretinal rim is narrower, tending rapidly to be white towards the center. The same parameters are chosen for both images in the proposed method and in Chan and Vese method. A retina image such as in Fig. 4.16(a) is preprocessed to get the Cb channel from the YCbCr representation (see Figs. 4.16(b)). This reduces the influence of the blood vessels. Soft threshold is applied to fit the proposed image model (see Fig. 4.16(c)). The healthy retina yields the following estimated parameters (see also the results presented in the left column of Fig. 4.16(d),(e)) : the center coordinates are $\{l_c; m_c\} = \{100; 94\}$, the radius estimated value is $r_0 = 33.4$, and the spread parameter is $\sigma = 5.9$. The second image yields the following estimated parameters (see also the results presented in the right column of Fig. 4.16(d),(e)) : the center coordinates are $\{l_c; m_c\} = \{99; 100\}$, the radius estimated value is $r_0 = 43.5$, and the spread parameter is $\sigma = 4.7$. The spread parameter is larger in the case of the healthy retina. This indicates a reduced center region and slowly varying gray level values in the neuroretinal rim in Fig. 4.16(b), left column : the retina is healthy. The spread parameter is smaller in the case of Fig. 4.16, right column. This indicates a wide center region and rapidly varying gray level values in the neuroretinal rim in Fig. 4.16(b), right column : the retina is non-healthy. Chan and Vese method distinguishes the neuroretinal rim in Fig. 4.16(f) left column, but not in the right column.

– Example 2 : fire detection

We consider the image of Fig. 4.17, which concerns fire front detection : fire propagates from two center points, forming two circles because the wind is not strong. We aim at localizing the regions where trees are still burning, to know in advance where the fire will extend. We process the Cr channel of the YCbCr representation, which permits to get rid of the smoke (see Fig. 4.17(b)). To fit the proposed model, a soft threshold is applied (see Fig. 4.17(c)). The center coordinates are estimated blindly through signal generation on left and bottom linear antennas. The radius and spread values are estimated successively with the proposed methods. Results are displayed in Figs. 4.17(d),(e),(f) including Chan and Vese approach. The estimated parameters are as follows : for the first fire on the left, the center coordinates are $\{l_c; m_c\} = \{70; 73\}$, the radius estimated values is $r_0 = 59$, and the spread parameter is $\sigma = 6.0$; for the second fire on the right, the center coordinates are $\{l_c; m_c\} = \{169; 171\}$, the radius estimated values is $r_0 = 26$, and the spread parameter is $\sigma = 2.6$. The radius value informs about how far the fire front progressed from the source. The spread parameter informs about the surface which is still burning. Chan and Vese method delimitates the fire

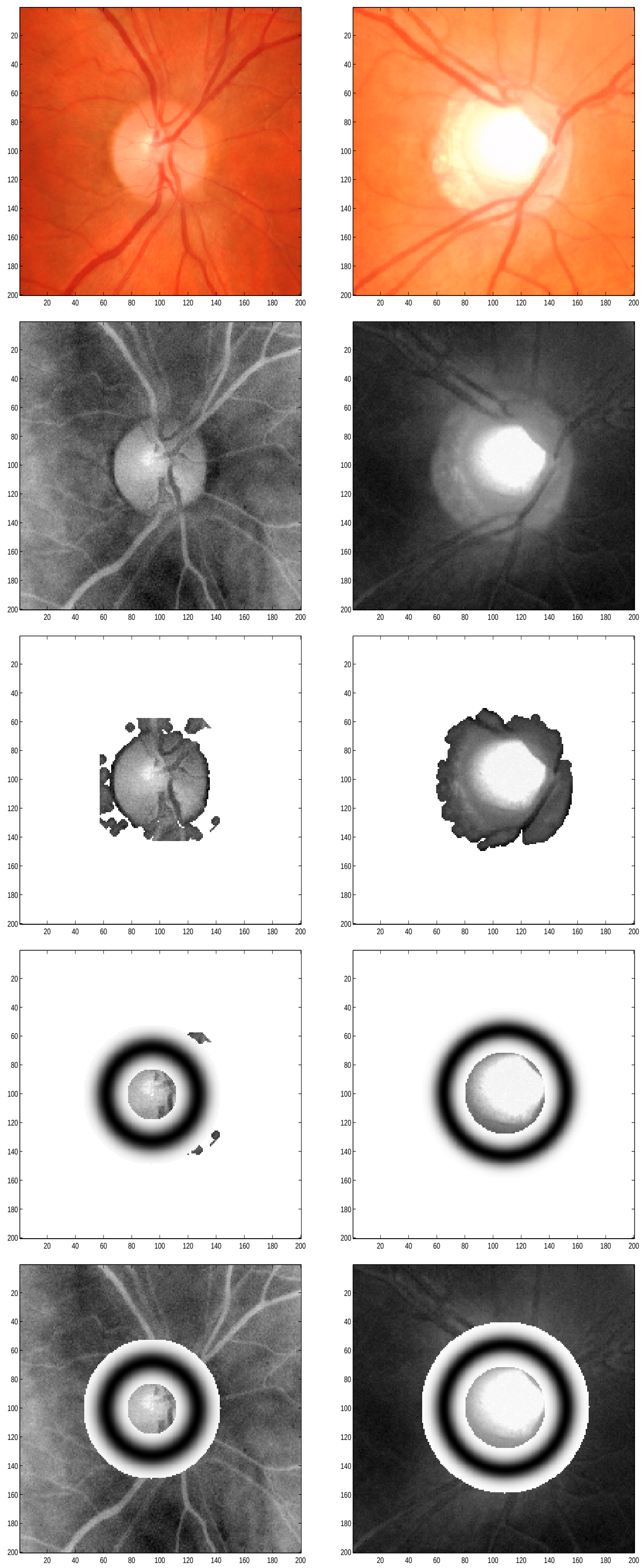

(a)

(b)

(c)

(d)

(e)

(f)

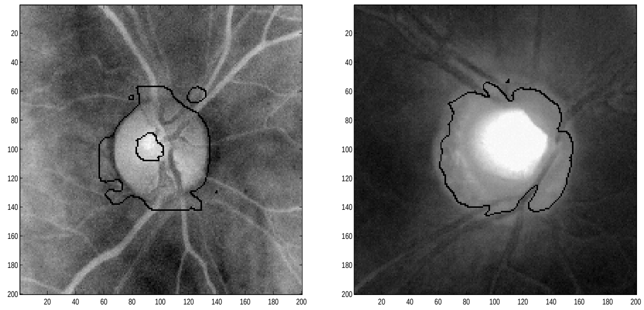

Figure 4.16 — Retina without (left) and with glaucoma (right) : (a) initial color image ; (b)Cb Channel from the image YCbCr representation ; (c) processed image ; (d) and (e) proposed method ; (f) Chan and Vese

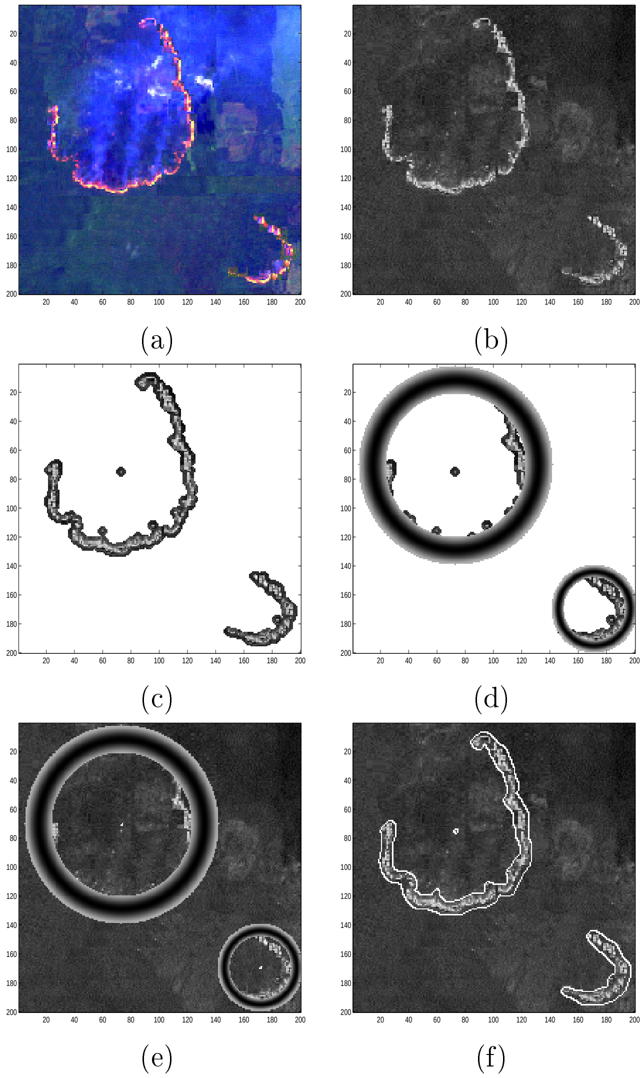

Figure 4.17 — Fire detection : (a) initial color image ; (b)Cr Channel from the image YCbCr representation ; (c) processed image ; (d) and (e) proposed method ; (f) Chan and Vese

front but does not provide the distance to the fire source.

– Example 3 : light beam

In this experiment, we consider two images which are a measurement of spatial light intensity. We aim at studying the effect of the Dove prism on the width of an optical beam. Dove prisms are being extensively used in many physical settings that make use of the OAM (orbital angular momentum) of light (see [105] and references therein). The use of Dove prisms with highly focused beams requires the use of some correcting elements whose characteristics can be determined though the influence of the Dove prism.

Fig. 4.18(a) show two typical spatial shape measurements from light beams, the Dove prism being removed at the left column or present at the right column. The beams which are presented are supposed to be highly focused. The experiment that we propose aims at checking that the Dove prism reduces the radius and spread of the light beam when the beam is highly focused. We also aim at calculating in what extent the characteristics of the beam are modified.

The estimated parameters are as follows :

Tableau 4.2 — Estimated parameter for light beam

	center	radius	spread
(a)	$\{149; 154\}$	52.7	12.2
(b)	$\{145; 151\}$	34.9	8.8

The results obtained show that the left column of the image contain the wide beam obtained without the Dove prism, and the right column of the image contain the straight beam obtained with the Dove prism.

As shown in Table 4.2, the image (a) contains a beam with a radius which is 33% and a spread which is 27% smaller as the beam in the image (b). We deduce from these blind measurements that the image (b) was obtained with a Dove prism.

By computing blindly the radius and spread of a light beam without and with Dove prism permits to evaluate the influence of this prism. As a consequence, the adequate compensating schemes, such as appropriate combinations of cylindrical lenses [105], can be chosen and used to compensate for the Dove prism.

We notice that the proposed model is general enough so that the proposed method should be adapted to various application domains. Moreover, it is not necessary to change the parameters of the proposed methods when slight changes in the image characteristics occur. On the contrary, the comparative Chan and Vese method is more sensitive the parameter tuning.

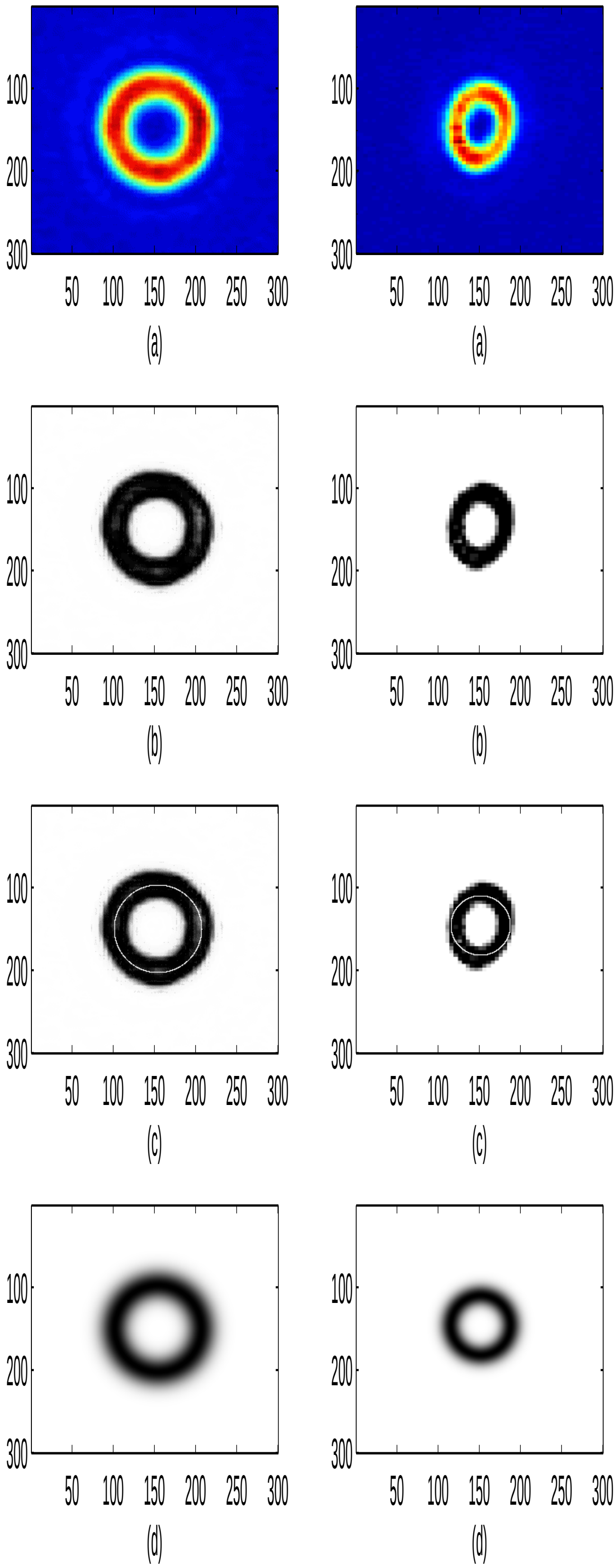

Figure 4.18 — Beam obtained without (left column) and with (right column) a Dove prism : (a) Color image ; (b) Processed image ; (c) Superposition processed image and center circle ; (d) Final result obtained with the proposed methods

4.5 Conclusion

To solve the issue of blurred linear contour, blurred triangular contour and circular contour characterization, we propose an innovative model for these contours, involving few parameters. We adapt appropriate signal generation schemes on either linear or circular antenna, and derive the signal models in each case. We propose the signal models, which fit the subspace-based methods coming from array processing. A signal preprocessing and subspace-based methods yield either the orientation and offset for blurred linear contours, or the radius of a blurred circular contour. Then, appropriate criteria and an optimization strategy yield the contour spread : we adapt the global optimization method DIRECT to characterize blurred linear contours and Newton method to characterize a blurred circle. For blurred triangular contour, a subspace-based method DSPE is applied to estimate the orientation and spread parameter for blurred triangular contour, and we adopt a variable speed generation scheme to estimate all offset values. The proposed methods are successfully applied to hand-made and real-world images and compared with a level set approach, leading to low parameter bias. Not only the mean position of a contour is retrieved, but also the spread parameter which characterizes the gray level variations aside the contour mean position.

Conclusions and perspectives

Conclusions

THIS dissertation is devoted to the detection and the characterization of contours in images by the adaptation of array processing methods. This work presents an original approach for contour segmentation, where we use the concept of "virtual antenna" : "virtual" sensors are associated with directions for signal generation out of the image. Contours in images correspond to sources, and the image background corresponds to the propagation medium. Based on the principles of electromagnetic wave propagation, the array signals are generated from an image. When rectilinear or circular contours are present in the image, the generated signals follow an array processing model. From a theoretical viewpoint, the steering matrix and the source vector in general depend on the parameters which characterize the contours.

From this, we propose to transfer subspace-based methods in array processing to the estimation of the parameters of contours in images, by an original principle of signal generation out of an image. Among these methods one distinguishes those exploiting second-order statistics and those exploiting higher-order statistics. The methods based on second- and higher-order statistics are used successfully in the field of array processing for the fast, accurate, and robust (to noise) estimation of source parameters, and for source separation. On the one hand, we exploit the second-order statistics of the signals by estimating their covariance matrix. The eigenvalue decomposition of the covariance matrix provides a set of eigenvectors which generates the "measurement space". When the signal realizations are independent from noise realizations, one distinguishes in the "measurement space" two subspaces : the signal subspace, and the noise subspace, which are orthogonal. On the other hand, the higher-order statistics of signals are also introduced to improve the results of image recognition, by selecting components of interest in an image database.

- **One-wide pixel contour detection**

For rectilinear contours in images, the steering matrix in the derived model depends on the main orientations of the rectilinear contour, and the source vector is related to their offsets. By the subspace methods based on second-order or higher-order statistics, these parameters can be estimated. We reconstruct the contours by these estimated parameters. For the circular contour, by introducing the linear antenna model and circular antenna model, we analyze the signals received at the side of image. From this, the center coordinates and radii of multiple circles can be computed, so that the circular contours are characterized. When there are concentric circles with close radii, we can use signal generation on a circular antenna and subspace-based methods to estimate their radii. In a correlated noise environment, higher-order statistics are also exploited to improve the estimated results.

For one-pixel wide star-shaped contour, we propose an innovative signal generation approach. Once we get the initialized radius of contours, we model the pixel coordinates in a polar representation as a sum of exponentially damped sinusoids, then we estimate each damped sinusoidal component by subspace-based parameter estimators. After obtaining the respective amplitude, frequency and damping factor of each sinusoidal term, we can reconstruct the star-shaped contour. Considering the noise in images, we further refine the signals which are used for the estimation by solving iteratively a structured total least norm problem.

- **Blurred contour detection**

In real-world conditions, blurred contours often exist in digital images because of acquisition conditions. This issue of blurred contour modeling involves several categories of contour detection methods : levelset methods, mathematical morphology which led to theoretical developments in the domain of fuzzy sets, and to applications in particular for medical 3D image segmentation. Blurred contours in an image have a frontier for which the gradient is non zero and which presents a regular grey level variation. We suppose that the blurred contours can be characterized by few parameters in the given conditions where the variation of the gray level values is described by an exponential function. This facilitates the transfer of array processing methods to the considered parameter estimation issue. Based on the principle of signal generation by linear antenna model or circular antenna model, we generate the array signals from the image, and derive the signal models in each case, which fit the subspace-base methods coming from array processing. To estimate these parameters, we exploit the subspace-based methods and propose the appropriate criteria and optimization strategies, for example, DIRECT global optimization method to characterize blurred linear contours and Newton method to characterize a blurred circle. Different from the existing contour-based or region-based segmentation methods, which in general detect the object edges, our proposed method keep more information, not only the contour edge, but also the gray level variations.

Perspectives for future research

The dissertation aims at answering some problematics of image processing by a novel approach. We establish a connection between high resolution methods in array processing and contour detection in image processing. It shows two main advantages : on the one hand, the connection extends the applications of array processing, on the other hand, the subspace-based array processing methods, using the statistical properties of signals obtained by transformation or reorganization of the data, provide accurate, robust estimation of the parameters of the contours. The theoretical aspect and the applicative aspect are indivisible, to validate the results in a rigorous way. We propose here some research directions for a future extension of this work.

• In the case with correlated noise, we perform the estimation by subspace methods based on higher-statistics, which need the SVD decomposition. This leads to elevate the computational load to a certain extent. To reduce this cost, we consider some improvements, for example, we perform SVD decomposition to slice cumulant matrix instead of the whole cumulant matrix, in Chapter 2. The other subspace-based method can still be investigated to reduce the computation load.

• In Chapter 3, we propose to characterize the highly concave contours in images. The initialization process should be improved to better detect the star-shaped contours. It may be feasible to extend to contours which are not star-shaped. For this, another antenna model could be exploited. More precisely, in the framework of an "evolving" circular antenna model, the circular antenna will have variable center coordinates. The center coordinate values will evolve taking into account the characteristics of the generated signal. Sometimes, especially in presence of disruptive elements such as noise and occlusion, we can also consider shape invariant methods, when a shape prior is known, to enhance the convergence properties of the method. In addition, it will increase the methods robustness to noise, clutter and occlusion.

• In Chapter 4, we model the textured contours as blurred contours. We study the mathematical modeling and the detection of blurred contours by approaches which are inspired by array processing. In our model, we assume that the grey level variations follow a Gaussian distribution. It would be interesting to study the extension to another distribution describing the contour. For the blurred triangular contours, we always suppose that vertices are located at the image boundary. Therefore, the more general case where a truncated triangular contour without the vertex is present in an image should be considered in the future. At the same time, this kind of blurred contour can be also thought as the extension of blurred linear contour. In addition, for blurred circular contours, the optimization method should be studied to estimate effectively the spread parameters of concentric circles.

• In this work, we affixed to the processed image a linear vertical or horizontal or circular antenna. For some special contour detection, the other various positions or shapes of the antenna are of interest. These antenna position or shapes lead to different one-dimensional "shootings" of the contents of the image and to the reconstruction of the image. This will be permitted to perform a detection of 3D object from several two-dimensional shootings. These various antenna positions provide an information concerning the contents of the image : if the generated signal has linear phase, the contour in the image has the same shape as the antenna. This will also enrich the applications in the direction of blind characterization of the content of an image.

ANNEXE A Appendix : Introduction générale

La segmentation d'images a été continuellement améliorée dans les dernières décennies. Le but d'un système d'analyse d'images est de reconnaître des objets dans une scène complexe ou une image. En général, quand les gens sont invités à décrire un contour, ils donnent une liste d'objets ainsi que leurs positions relatives. Donc, l'une des premières étapes dans la compréhension de l'image est la détection des contours des objets présents. Une fois les bords d'un objet détectés, les autres traitements tels que la segmentation des régions, la reconnaissance d'objets tels que des caractères, des défauts ... peut avoir lieu.

La détection de contours consiste à produire une nouvelle image qui, d'une certaine façon, plus souhaitable que l'image de départ. En général, les méthodes de détection de contours doivent être robustes au bruit qui peut être présent dans l'image. Les images proviennent de champs d'application de plus en plus divers, de par la progression observée dans la conception de systèmes d'acquisition tels que les capteurs.

On peut distinguer deux types des méthodes de détection de contours : les méthodes basées sur les régions et celles basées sur les contours. Premièrement, les méthodes de segmentation basées sur les régions visent à distinguer entre les ensembles de pixels de l'image, en se référant à des propriétés telles que la répartition de couleur, la texture, ou la position relative des objets par des outils de morphologie mathématique. La classification non supervisée de pixels en sous-ensembles peut également être effectuée avec les champs de Markov cachés (hidden Markov random fields, ou HMRF). Deuxièmement, les méthodes basées sur les contours visent à détecter l'ensemble des pixels qui délimitent les régions. Plusieurs méthodes appartiennent à cette catégorie : les méthodes des moindres carrés ordinaires ou totaux minimisent la somme des carrés des erreurs à l'égard de mesures. Une des limitations majeures de la plupart des méthodes des moindres carrés est leur sensibilité aux valeurs aberrantes. D'autres méthodes peuvent être utilisées pour la détection de lignes ou de cercles, même dans un environnement bruité. La transformée de Hough et sa version généralisée (GHT) fournissent l'estimation des paramètres de droites ou les coordonnées du centre d'un cercle (lorsque leur rayon est connu).

Le principal inconvénient des méthodes de type de Hough est la charge de calcul, bien que des versions rapides aient été proposées. Les méthodes de type snakes basées sur l'évolution d'un contour, telles que la méthode GVF (Gradient Vector Flow), ont été largement utilisées, pour localiser des bords concaves avec des limites floues. La méthode GVF est limitée par la courbure des contours à retrouver, qui ne doit pas être trop forte. Les méthodes de type Levelset retrouvent en aveugle certains contours, selon les paramètres choisis pour l'évolution du contour actif sur lequel ils sont fondés. Les méthodes de type Levelset ne fournissent pas explicitement les caractéristiques des contours avec des paramètres pré-définis tels que le rayon pour des cercles ou l'orientation pour des lignes. Au contraire, certaines méthodes originales qui sont, elles, paramétriques, telles que la méthode SLIDE, ont été proposées. Elles sont basées sur le transfert des méthodes de traitement d'antenne à la détection de contours.

Une antenne est composée d'un ensemble de capteurs. Chaque capteur reçoit des signaux qui sont supposés être centrés autour d'une fréquence.

Les méthodes de traitement d'antenne ont atteint un niveau de perfectionnement avancé. Elles visent à résoudre des problèmes tels que la détection de directions d'arrivée de fronts d'onde émanant de sources. Elles sont robustes au bruit détériorant ces signaux, en particulier au bruit corrélé. Un principe ingénieux de génération de signal consiste à associer une antenne virtuelle à une image. Ainsi, le contenu de la donnée bi-dimensionnelle qu'est une image est transféré dans un signal unidimensionnel. Les capteurs qui composent l'antenne dans ce principe de génération de signal disposés selon une droite ou un cercle, formant une antenne linéaire ou circulaire. La forme de l'antenne est choisie selon la forme de l'objet à détecter dans l'image.

Le transfert de méthodes provenant du domaine du traitement d'antenne, et dédiées à l'origine à l'estimation de fréquences, est très profitable. De cela, nous exploitons les méthodes de traitement d'antenne pour estimer les paramètres attendus. Lorsque les contours attendus, tels que des lignes ou des cercles, sont présents dans l'image, les signaux générés suivent un modèle de signal du traitement d'antenne : les contours correspondent aux émetteurs de source, le fond de l'image correspond au milieu de propagation, les caractéristiques des contours, comme l'orientation des lignes ou le rayon des cercles, sont des paramètres caractérisant les signaux générés. Un signal généré sur les capteurs peut être divisé en plusieurs sections qui se chevauchent. Ces sections peuvent être considérées comme plusieurs réalisations d'un seul signal aléatoire. Ce type de traitement des données repose, en général, sur le calcul de statistiques d'ordre deux ou de statistiques d'ordre supérieur. Dans le cas où un bruit blanc Gaussien altère l'image, le traitement le plus courant est d'effectuer la SVD (Singular Value Decomposition) de la matrice de covariance des signaux reçus. L'éxécution d'une SVD est la première étape des méthodes par sous-espace, qui peuvent être utilisées pour extraire les paramètres souhaités à partir des signaux traités. Dans le cas où le bruit qui altère l'image est corrélé, les statistiques d'ordre supérieur peuvent être calculées pour supprimer ce bruit.

En particulier, les cumulants d'ordre supérieur à trois suppriment toutes les composantes Gaussiennes, en particulier tout bruit Gaussien.

Les images peuvent souffrir d'autres dégradations que le bruit. A cause du mouvement des objets, du milieu de propagation de la lumière, des changements d'illumination, de la défocalisation, etc., les frontières dans l'image peuvent ne plus être de franches transitions mais plutôt une dégradation progressive des valeurs de niveaux de gris. Ces transitions sont caractéristiques des frontières d'objets. La plupart des méthodes de détection de contours perdent l'information nécessaire à la caractérisation du flou. Pour caractériser des contour précisément, il faudrait, développer des méthodes plus performantes pour améliorer la précision des méthodes de caractérisation du flou et par là même l'exhaustivité des méthodes de caractérisation de contours. L'observation clé lors du calcul de statistiques d'ordre deux et d'ordre supérieur est qu'un sous-espace de faible dimension permet d'extraire l'information utile, en particulier les paramètres de contours. La connaissance, ou l'estimation par des critères statistiques, du sous-espace signal, permet la partition de l'espace des mesures en un sous-espace signal qui contient l'information recherchée, et un sous-espace bruit, qui contient toutes les composantes inutiles des données.

Objectifs et contributions de la thèse

Ce manuscrit se propose de répondre à des problématiques du traitement d'images par une nouvelle approche. Nous établissons une connection entre les méthodes haute résolution du traitement d'antenne et la détection de contour en traitement d'image. L'approche proposée présente deux avantages principaux : d'une part, ce rapprochement étend les applications du traitement d'antenne, d'autre part, les méthodes par sous-espace du traitement d'antenne, qui utilisent les propriétés statistiques des signaux obtenus par la réorganisation des données de l'image, fournissent une estimation précise et robuste des paramètres des contours. Du fait que les aspects applicatifs et théoriques sont indissociables, et qu'il est nécessaire de valider les méthodes proposées de façon rigoureuse, nous appliquons les méthodes proposées à diverses situations qui peuvent être divisées en deux parties : les contours d'une largeur de un pixel -à fort contraste, et les contours flous. Pour ce dernier type de contours, nous proposons un modèle de particulier.

• **Détection des contours à fort contraste**

Lorsque les contours à détecter sont rectilignes, la matrice de transfert dans le modèle de signal dépend de l'orientation du contour, et le vecteur source dépend des offsets. Par les méthodes par sous-espaces fondées sur les statistiques de second ordre et d'ordre supérieur, ces paramètres peuvent être estimés. Nous reconstruisons alors une estimation des contours avec la connaissance de ces paramètres. Lorsque les contours à détecter sont circulaires, en utilisant une antenne linéaire, nous sommes en mesure de retrouver le centre et le rayon de cercles non concentriques. L'antenne circulaire permet de détecter la présence de cercles concentriques et d'en estimer leurs rayons. Les méthodes haute résolution du traitement d'antenne donnent de bons résultats en particulier quand les cercles sont très proches. Lorsqu'un bruit corrélé dégrade l'image, les statistiques d'ordre supérieur sont exploitées pour améliorer les résultats d'estimation.

Pour des contours étoilés d'une largeur de un pixel, nous proposons une variante de la génération de signal sur une antenne circulaire, et un modèle innovant pour les coordonnées des pixels du contour à retrouver. Considérons le cercle "d'initialisation" qui correspond au mieux au contour étoilé recherché. Les coordonnées des pixels d'un contour étoilé sont décomposées de la façon suivante : elles sont la superposition de la valeur du rayon du cercle d'initialisation et d'une somme de sinusoïdes amorties par une fonction exponentielle. Une méthode d'estimation de fréquences évoluée fournit les paramètres (amplitude, fréquence, et facteur d'atténuation) correspondant à ce modèle, ce qui permet de reconstruire le contour étoilé. Afin de prendre en compte la présence de bruit dans les images, nous appliquons un raffinage des signaux qui sont utilisés pour l'estimation en résolvant de façon itérative un problème des moindres carrés totaux structurés.

• **Détection des contours flous**

Dans des conditions réelles, les contours présents dans une image sont souvent flous à cause des conditions d'acquisition. Le problème de la modélisation de contours flous fait intervenir plusieurs catégories de méthodes de détection : les méthodes levelset, la morphologie mathématique, qui a donné lieu à des développements dans la théorie des ensembles flous, et à des applications en particulier pour la segmentation d'images 3D médicales. Les contours flous sont caractérisés par un gradient non nul sur une certaine surface et par une variation régulière des niveaux de gris. Nous supposons que les contours flous peuvent être caractérisés par quelques paramètres. En particulier, nous choisissons une variation exponentielle des valeurs de niveaux de gris. Cela facilite le transfert des méthodes de traitement d'antenne vers ce problème de caractérisation de contours. Selon le principe de la génération de signal sur une antenne linéaire ou circulaire, nous générons des signaux à partir d'une image, pour lesquels les modèles correspondants sont calculés. Nous montrons qu'avec le modèle de contour choisi, ces modèles de signaux suivent ceux attendus en traitement d'antenne. Pour estimer ces paramètres, nous exploitons les méthodes par sous-espaces et proposons des critères appropriés ainsi que des méthodes d'optimisation, comme la méthode d'optimisation globale DIRECT, pour caractériser les contours flous linéaires, et Newton, pour caractériser les contours flous circulaires. En comparaison des méthodes existantes de détection de contours, la méthode proposée fournit plus d'information sur les contours à retrouver, c'est-à-dire, non seulement une frontière mais aussi les variations de niveaux de gris.

Plus spécifiquement, les contributions principales de cette thèse sont les suivantes :

• Dans le domaine du traitement d'antenne, le problème de l'estimation de directions d'arrivée a été largement étudié. En faisant le lien entre la caractérisation de contours dans des images et l'estimation des directions d'arrivée, nous permettons le transfert des outils performants du traitement d'antenne, et montrons que les méthodes qui en découlent améliorent la détection de contour, en termes de temps de calcul et de précision d'estimation.

• Nous considérons la détection de contours rectilignes dans un environnement de bruit corrélé, en adoptant un modèle d'antenne linéaire, et nous fournissons une méthode haute résolution fondée sur les statistiques d'ordre supérieur.

• Nous proposons une approche nouvelle pour estimer les paramètres de droites et de cercles par des antennes linéaire et circulaire. De plus, nous exploitons les statistiques d'ordre supérieur pour estimer le rayon de cercles concentriques dans le cas où le bruit est gaussien corrélé.

• Nous étudions le problème de l'estimation des contours étoilés, et proposons une nouvelle méthode de génération de signal dérivée du paradigme du traitement d'antenne. Ensuite les signaux générés sont décomposés en sinusoïdes amorties. Nous estimons toutes les composantes du signal avec une méthode particulière et ainsi retrouvons le contour.

• Nous proposons un modèle pour les contours flous linéaires, et calculons le modèle de signal qui est valable lorsque les signaux sont générés à partir de l'image sur une antenne linéaire. Nous proposons une méthode par sous-espaces pour estimer l'orientation et l'offset de contours linéaires, et une méthode d'optimisation pour estimer le paramètre d'étendue des contours.

• Pour la première fois, nous calculons un modèle de signal issu du traitement d'antenne, pour les signaux générés à partir d'une image contenant un contour flou triangulaire. Nous exploitons les méthodes du traitement d'antenne qui sont à l'origine dédiées à la caractérisation de sources multiples incohérentes, pour estimer l'orientation et l'étendue des contours, et nous estimons l'offset par un schéma de génération à vitesse variable.

• Nous fournissons un modèle pour un contour circulaire flou à partir de quelques paramètres, qui caractérisent la position moyenne et les variations de niveaux de gris des contours autour de cette position moyenne. Pour caractériser les contours flous circulaires, nous proposons une méthode de traitement d'antenne pour retrouver la position moyenne du contour et le paramètre d'étendue par la méthode d'optimisation de Newton.

Plan du manuscrit

Ce manuscrit est divisé en quatre chapitres.

Le **Chapitre 1** rappelle le concept de base de la segmentation d'images et de la détection de contours en traitement d'images. Il présente plusieurs méthodes existantes. Ensuite le traitement d'antenne est présenté brièvement : nous présentons le problème de l'estimation de directions d'arrivée avec des statistiques d'ordre deux et des statistiques d'ordre supérieur. A partir de ces principes théoriques, nous montrons comment le traitement d'image et le traitement d'antenne peuvent être connectés l'un à l'autre. Ensuite, nous présentons trois méthodes d'optimisation parmi celles qui sont les plus importantes de façon générale mais surtout pour la suite du manuscrit : la méthode de Newton, la méthode de la descente de gradient, et DIRECT (DIviding RECTangles).

Le **Chapitre 2** est dédié à la détection de droites dans une image perturbée par un bruit Gaussien. Nous présentons un principe spécifique pour transposer le problème de la détection de contours en un problème de traitement d'antenne. La méthode existante de caractérisation de droites "SLIDE" (Subspace-based LIne Detection) conduit à des modèles dans lesquels l'orientation et l'offset de lignes droites sont les paramètres à estimer. Il a été prouvé que les cumulants d'ordre supérieur à trois de toute variable aléatoire Gaussienne sont nuls. Ainsi, tout bruit Gaussien peut être supprimé par le calcul de cumulants d'ordre supérieur. Pour supprimer le bruit, nous améliorons la méthode existante SLIDE en exploitant les statistiques d'ordre supérieur. Pour cela, nous présentons les méthodes dérivées de MUSIC et TLS-ESPRIT, dans lesquelles sont introduits les cumulants d'ordre quatre. Ces méthodes permettent d'estimer l'orientation de droites, les offsets de ces droites étant estimés par l'"extension de la transformée de Hough". En particulier, nous considérons aussi la matrice tranche de cumulant qui remplace avantageusement la donnée complète des cumulants en accélérant l'algorithme. Les méthodes proposées fonctionnent de façon aveugle pour l'estimation des orientations et des offsets des droites.

Le **Chapitre 3** introduit un nouveau modèle d'antenne circulaire et adapte un schéma de génération à vitesse variable, qui conduit à partir d'une image contenant un cercle à un signal à phase linéaire. A partir de cela, nous pouvons estimer des valeurs proches de rayon par des méthodes haute résolution dans une image dégradée par un bruit blanc ou un bruit corrélé, comme dans le **Chapitre** 2. En utilisant le modèle d'antenne linéaire, nous calculons les coordonnées du centre de tous les cercles. Ensuite, pour le cas plus général de contours fortement concaves, nous exploitons un modèle de sinusoïdes amorties. Et puis une méthode d'estimation de fréquences est utilisée pour estimer les coordonnées polaires des pixels des contours. De plus, nous raffinons les signaux générés par la méthode d'optimisation STLNB de façon à ce qu'ils soient plus proches du modèle de sinusoïdes amorties qui leur est attribué. Ceci permet d'améliorer la qualité de l'estimation lorsque le niveau de bruit est élevé.

Le **Chapitre 4** résout le problème de l'estimation de contours flous linéaires, triangulaires, et circulaires. Pour la première fois, nous proposons un modèle innovant pour ces contours, impliquant peu de paramètres. Pour les contours flous linéaires et triangulaires, ce sont l'orientation, l'offset central, et l'étendue ; pour les contours flous circulaires, ce sont les coordonnées du centre, le rayon, et l'étendue. Ensuite, nous utilisons les schémas de génération de signal appropriés sur des antennes linéaire et circulaire, et obtenons les modèles de signal correspondants dans chaque cas. Ces modèles correspondent à ceux des méthodes par sous-espaces du traitement d'antenne. Un pré-traitement des signaux et les méthodes par sous-espaces conduisent soit à l'orientation et à l'offset de contours flous linéaires, soit au rayon des contours flous circulaires. Ensuite, des critères appropriés et une méthode d'optimisation conduisent à l'étendue du contour : nous adaptons la méthode d'optimisation globale DIRECT pour caractériser les contours flous linéaires et la méthode de Newton pour caractériser un cercle flou. Pour les contours flous triangulaires, une méthode par sous-espaces appelée DSPE (Distributed Source Parameter Estimator) est appliquée pour estimer l'orientation et l'étendue des contours flous triangulaires, et nous adoptons un schéma de génération à vitesse variable pour estimer les valeurs d'offset. Les méthodes proposées sont appliquées avec succès à des images artificielles et à des images réelles. Les méthodes proposées sont comparées à une approche par levelset. Elles conduisent, en particulier, à de faibles biais d'estimation.

ANNEXE B

Appendix : Publications

- Haiping Jiang, Julien Marot, Caroline Fossati, and Salah Bourennane. *Circular Contour Retrieval in Real-World Conditions by Higher Order Statistics and an Alternating Least Squares Algorithm*. EURASIP Journal on Advances in Signal Processing. Minor revision. 2011.

- Haiping Jiang, Julien Marot, Caroline Fossati, and Salah Bourennane. *Strongly concave contour star-shaped contour characterization by algebra tools*. Signal Processing. Accepted. October 2011.

- Haiping Jiang, Julien Marot, Caroline Fossati, and Salah Bourennane. *Fuzzy Triangle Contour Characterization by Subspace Based Methods of Array Processing*. Proceedings of the 6th IEEE Sensor Array and Multichannel Signal Processing Workshop, Israel, October 2010.

- Haiping Jiang, Julien Marot, Caroline Fossati, and Salah Bourennane. *Fuzzy contour characterization by subspace based methods of array processing and DIRECT method*. Proceedings of the 18th European Signal Processing Conference (EUSIPCO-2010), pp. 1344-1348, Aalborg, Denmark, August 2010.

- Haiping Jiang, Salah Bourennane, and Caroline Fossati. *High-Resolution Algorithm for Image Segmentation in the Presence of Correlated Noise*. Journal of Electrical and Computer Engineering, Volume 2010, Article ID 630768, 6 pages, 2010.

- Xin Jin, Haiping Jiang, Jinlong Hu, Yao Yuan, Cuicui Zhao and Jinglin Shi. *Maximum Data Rate Power Allocation for MIMO Spatial Multiplexing Systems with Imperfect CSI*. Proceedings of the 69th IEEE Vehicular Technology Conference, VTC2009-spring, Barcelona, April 2009.

List of figures

List of tables

Bibliography

[1] Robert M. Haralick and Linda G. Shapiro, "Computer and Robot Vision," vol. 1, Addison-Wesley Longman Publishing Co., MA, 1992.

[2] S. Bileschi and L. Wolf, "A unified system for object detection, texture recognition, and context analysis based on the standard model feature set," *British machine Vision Conference (BMVC)*, 2005.

[3] R. M. Haralick, K. Shanmugam, and I. Dinstein, "Textural features for image classification," *IEEE Transactions on Systems, Man, Cybernetics*, vol. 3, no. 6, pp. 610-621, Nov. 1973.

[4] Z. Tu, X. Chen, A. L. Yuille, and S.-C. Zhu, "Image parsing : Unifying segmentation, detection, and recognition," *Proceeding of the ninth IEEE International conference on Computer Vision*, vol. 2, no 63, 2003.

[5] L. Benyoussef, C. Carincotte, and S. Derrode, "Extension of higher-order HMC modeling with application to image segmentation," *Digital Signal Processing*, vol. 18, no 5, pp. 849-860, Sept. 2008.

[6] C. Carincotte, S. Derrode, and S. Bourennane, "Unsupervised change detection on SAR images using fuzzy hidden Markov chains," *IEEE Transactions on Geoscience and Remote Sensing*, vol. 44, no. 2, pp. 432-441, Feb. 2006.

[7] J. Illingworth and J. Kittler, "A survey of the Hough transform," *Computer Vision Graphics Image Processing*, vol. 44, pp. 87-116, 1988.

[8] D. H. Ballard, "Generalizing the Hough transform to detect arbitrary shapes," *Pattern Recognition*, vol. 13, no. 2, pp. 111-122, 1981.

[9] M. Kass, A.Witkin, and D. Terzopoulos, "Snakes : Active contour models," *International Journal of Computer Vision*, vol. 1, no. 4 pp. 321-331, 1988.

[10] C. Xu and J.L. Prince, "Snakes, shapes, and gradient vector flow," *IEEE Transactions on Image Processing*, vol. 7, no. 3, pp. 359-369, Mar. 1998.

[11] X. Xie, M. Mirmehdi, "RAGS : region-aided geometric snake," *IEEE Transactions on Image Processing*, vol. 13, no. 5, pp. 640 - 652, 2004.

[12] J. F. Aujol, G. Aubert, and L. Blanc-Féraud, "Wavelet-based level set evolution for classification of textured images," *IEEE Transaction on Image Processing*, vol. 12, no. 12, pp. 1634-1641, Dec. 2003.

[13] K. Imen, R. Fablet, J. -M. Boucher, and J.-M Augustin, "Region-based segementation using texture statistics and level-set methods," *Proceeding of IEEE International Conference on Acoustic, Speech and Signal Processing*, Apr. 2006, no. 2, pp. 693-696.

[14] H. K. Aghajan and T. Kailath, "SLIDE : Subspace-based line detection," *IEEE Transactions on Pattern Analysis and Machine Intelligence*, vol. 16, no. 11, pp. 1057-1073, Nov. 1994.

[15] J. Sheinvald and N. Kiryati, "On the magic of SLIDE," *Machine Vision and Applications*, vol. 9, no. 5-6, pp. 251-161, 1997.

[16] H. K. Aghajan, "Subspace thechniques for image understanding and computer vision," Phd thesis, Standford University, Califonia, USA, Nov. 1995.

[17] H. K. Aghajan, and T. Kailath, "A suspace fitting approach to super resolution multiline fitting and straight edge detection," *Proceeding of the IEEE International Conference on Acoustic, Speech and Signal Processing*, vol. 3, 1992.

[18] H. K. Aghajan and T. Kailath, "Sensor array processing techniques for super resolution multi-line-fitting and straight edge detection," *IEEE Transactions on Image Processing*, vol. 2, no. 4, pp. 454-465, Oct. 1993.

[19] B. Porat and B. Friedlander, "Direction finding algorithms based on high-order statistics," *IEEE Transaction on Signal Processing*, vol. 39, no. 9, pp. 2016-2024, Sept. 1991.

[20] H. H. Chiang and C. L. Nikias, "The ESPRIT algorithm with high order statistics," *Procceding of Workshop Higher Order Spectral Anal*, (Vail, CO), pp. 163-168, June 1989.

[21] Zineb Saidi and Salah Bourennane, "Cumulant-based coherent signal subspace method for bearing and range estimation," *EURASIP Journal on Advances in Signal Processing*, vol. 2007, article ID 84576, 9 pages, 2007.

[22] J. Marot and S. Bourennane, "Subspace-based and DIRECT algorithms for distorted circular contour estimation," *IEEE Transactions on Image Processing*, vol. 16, no. 9, pp. 2369-2378, Sept. 2007.

[23] R. O. Schmidt, "Multiple emitter location and signal parameters estimation," *IEEE Transaction on Acoustics, Speech, and Signal Processing*, vol. 4, no. 3, pp. 276-280, 1983.

[24] P. Milanfar, G. Verghese, W. Karl, and A. Willsky, " Reconstructing polygons from moments with connections to array processing," *IEEE Transactions on Signal Processing*, vol. 43, pp. 432-443, Feb. 1995.

[25] M. Elad, P. Milanfar, and G.H. Golub, "Shape from moments-an estimation theory perspective," *IEEE Transactions on Signal Processing* , vol. 52, pp. 1814-1829, Jul. 2004.

[26] G.H. Golub, P. Milanfar, and J. Varah, "A stable numerical method for inverting shape from moments," *SIAM Journal on Scientific Computing*, vol. 21, no. 4, pp. 1222-1243, Dec. 1999.

[27] J.F. Canny, "A computational approach to edge detection," *IEEE Transactions on Pattern Analysis and Machine Intelligence*, vol. 8, no. 6, pp. 679-698, 1986.

[28] W. Frei and C. Chen, "Fast boundary detection : A generalization and a new algorithm," *IEEE Transactions on Computers*, vol. 26, no. 2, pp. 988-998, 1977.

[29] T. Folsom and R. Pinter, "Primitive features by steering, quadrature and scale," *IEEE Transactions on Pattern Analysis and Machine Intelligence*, vol. 20, no. 11, pp. 1161-1173, 1998.

[30] P. Perona and J. Malik, "Scale-space and edge detection using anisotropic diffusion," *IEEE Transactions on Patten Analysis and Machine Intelligence*, vol. 12, no. 7, pp. 629-639, July 1990.

[31] T. F. Chan and L. A. Vese, "Active contours without edges," *IEEE Transactions on Image Processing*, vol. 10, no. 2, pp. 266-277, Feb. 2001.

[32] T. F. Chan and L. A. Vese, "A multiphase level set framework for image segmentation using the Mumford and Shah model," *International Journal of Computer Vision*, vol. 50, no. 3, pp. 271-293, 2002.

[33] W. Gander. G. H. Golub, and R. Strebel, "Least-squares fitting of circles and ellipses," *BIT*, vol. 34, no. 4, pp. 558-578, 1994.

[34] J. Illingworth and J. Kittler, "The adaptive Hough tranform," *IEEE Transaction on Pattern Analysis and Machine Intelligence*, vol. 9, no. 5, pp. 690-698, Sept. 1987.

[35] N. Kiryati and A. M. Bruckstein, "On navigating between freinds and Foes," *IEEE Transactions on Pattern Analysis and Machine Intelligence*, vol. 13, no. 6, Jun. 1991.

[36] R. O. Duda and P. E. Hart, "Use of the Hough transform to detect lines and curves in pictures," *Communications of Association for Computing Machinery*, vol. 15, no. 1, pp. 11-15, 1972.

[37] M.-A. Charmi, S. Derrode and F. Ghorbel, "Fourier-based geometric shape prior for snakes," *Pattern Recognition Letters*, vol. 29, no. 7, pp. 897-904, May 2008, doi :10.1016/j.patrec.2008.01.011

[38] J. A. Sethian, "Level set methods and fast marching methods," *Cambridge University Press*, New York, 1999.

[39] C. Li and C. Xu, "Distance regularized level set evolution with application to image segmentation," *IEEE Transactions on Image Processing*, vol. 19, no. 12, pp. 3243-54, Dec. 2010.

[40] T. Lei and J. Udupa, "A sensor array processing approach to object region detection," *IEEE Transactions on Biomedical Engineering*, vol. 48, no. 11, pp. 1319-1325, Nov. 2001.

[41] M. Viberg, "Subspace fitting concepts in sensor array processing," *Signal Processing*, vol. 19, no. 4, pp. 345, Apr. 1990.

[42] T. Trump, B. Ottersten, "Estimation of nominal direction of arrival and angular spread using an array of sensors," *Signal Processing*, vol. 50, no. 1-2, pp. 57-69, Apr. 1996.

[43] H. Chen, J. Zhao, "Coherent signal-subspace processing of acoustic vector sensor array for DOA estimation of wideband sources," *Signal Processing*, vol. 85, no. 4, pp. 837-847, Apr. 2005.

[44] M. A. Hasan, "DOA and frequency estimation using fast subspace algorithms," *Signal Processing*, vol. 77, no. 1, pp. 49-62, Aug. 1999.

[45] S. Bourennane, C. Fossati, and J. Marot, "About noneigenvector source localization methods," *EURASIP Journal on Advances in Signal Processing*, vol. 2008, Article ID 480835, 13 pages, 2008. doi :10.1155/2008/480835.

[46] F. Gini, M. Montanari, L. Verrazzani, "Maximum likelihood, ESPRIT, and periodogram frequency estimation of radar signals in K-distributed clutter," *Signal Processing*, vol. 80, no. 6, pp. 1115-1126, June 2000.

[47] M. A. Altinkaya, H. Deliç, B. Sankur, E. Anarim, "Subspace-based frequency estimation of sinusoidal signals in alpha-stable noise," *Signal Processing*, vol. 82, no. 12, pp. 1807-1827, Dec. 2002.

[48] H. Chen, S. Van Huffel, A. van den Boom, and P. van den Bosch, "Subspace-based parameter estimation of exponentially damped sinusoids using prior knowledge of frequency and phase," *Signal Processing*, vol. 59, no. 1, pp. 129-136, May 1997.

[49] J. R. Deller Jr., J. H. Hansen, and J. G. Proakis, "Discrete-time processing of speech signals", *IEEE Computer Society Press*, 1999.

[50] J. Jensen, S.H. Jensen, E. Hansen, "Exponential sinusoidal modeling of transitional speech segments," *Procceing of IEEE International Conference On Acoustics, Speech, and Signal Processing*, vol. 1, pp. 473-476, Mar. 1999.

[51] K. Abed-Meraim, and Y. Hua, "Multi-line fitting and straight edge detection using polynomial phase signals," *The 31st Asilomar Conference on signal, Systems and Computers*, Vol. 2, 1997.

[52] K. Abed-Meraim, and A. Beghdadi, "Multi-line Fitting Using Polynomial Phase Transforms and Downsampling", in *Proc. of IEEE International Conference on Acoustices, Speech, and Signal Processing*, vol. 3, pp. 1701-1704, Salt Lake City, May. 2001.

[53] R. Roy and T. Kailath, "ESPRIT : Estimation of signal parameters via rotational invariance techniques," *IEEE Transactions on Acoustics, Speech, and Signal Processing*, vol. 37, pp. 984-995, July 1989.

[54] J. He, Z. Liu, "Two-dimensional direction finding of acoustic sources by a vector sensor array using the propagator method", *Signal Processing*, vol. 88, no 10, pp. 2492-2499, Oct. 2008.

[55] M. Schumermans, P. Lemerling, L. De Lathauwer, and S. Van Huffel, "The use of total least squares data fitting in the shape-from-moments problem," *Signal Processing*, vol. 86, no. 5, pp. 1109-1115, May 2006.

[56] S. Bourennane and J. Marot, "Estimation of straight line offsets by a high-resolution method," *IEE Vision Image and Signal Processing*, vol. 153, no. 2, pp. 224-229, Apr., 2006.

[57] J. Marot and S. Bourennane, "Array processing and fast optimization algorithms for distorted circular contour retrieval," *EURASIP Journal on Advances in Signal Processing*, vol. 2007, Article ID 57354, pp. 1-13, 2007.

[58] H. Krim and M. Viberg, "Two decades of array signal processing research : the parametric approach," *IEEE Signal Processing Magazine*, no. 13, vol. 4, pp. 67-94, Jul. 1996.

[59] S. Haykin, J. P. Reilly, V. Kezys, and E. Vertatschitsch, "Some aspects of array signal processing," *IEE Proceedings-F*, no. 139, vol. 1, pp.1-26, Feb. 1992.

[60] S. Haykin, J. Litva, and T. J. Shepherd (Eds.), "Radar array processing," Springer-Verlag, Berlin, 1993.

[61] D. H. Johnson and D. E. Dudgeon, "Array signal processing : Concepts and techniques", Prentice-Hall, Inc., Englewood Cliffs, NJ, 1993.

[62] N. Yuen and B. Friedlander, "DOA estimation in multipath : an approach using fourth-order cumulants," *IEEE Transactions on Signal Processing*, vol. 45, no. 5, pp. 1253-1263, 1997.

[63] K. Abed-Meraim, H. Maître and P. Duhamelm, "Blind multichannel image restoration using subspace-based method," *Proceedings of International conf. on Acoustics Systems and Signal Processing*, Hongkong, Apr. 2003.

[64] A. Zoubir, Y. Wang, and P. Charge, "Efficient subspace-based estimator for localization of multiple incoherently distributed sources," *IEEE Transactions on Signal Processing*, vol. 56, no. 2, pp. 532-42, Feb. 2008.

[65] A. Zoubir and Y. Wang, "Robust generalised Capon algorithm for estimating the angular parameters of multiple incoherently distributed sources," *Signal Processing, IET*, vol. 2, no.2, pp. 163-168, Jun. 2008.

[66] S. Valae, B. Champagne, and P. Kabal, "Parametric localization of distributed sources," *IEEE Transactions on Signal Processing*, vol. 43, no. 9, pp. 2144-2153, Sept. 1995.

[67] E. Gonen and J. M. Mendel, "Applications of cumulants to array processing–Part III : blind beamforming for coherent signals," *IEEE Transactions on Signal Processing*, vol. 4, no. 9, pp. 2252-2264, 1997.

[68] B. Porat and B. Friedlander, "Direction finding algorithms based on higher-order statistics," *IEEE Transactions on Signal Processing*, vol. 39, no. 9, pp. 2016-2023, 1991.

[69] J. M. Mendel, "Tutorial on higher-order statistics (spectra) in signal processing and system theory : theoretical results and some applications," *Proceedings of the IEEE*, vol. 79, no. 3, pp. 278-305, 1991.

[70] N. Yuen and B. Friedlander, "Asymptotic performance analysis of blind signal copy using fourth-order cumulants," *International Journal on Adaptive Control and Signal Processing*, pp. 239-265, Mar. 1996.

[71] D. R. Jones, C. D. Perttunen, and B. E. Stuckman, "Lipschitizian optimization without the Lipschitz constant," *Journal of Optimization Theory and Application*, vol. 79, no. 1, Oct. 1993.

[72] D. E. Finkel, "DIRECT optimization algorithm user guide," *Technical Report CRSC-TR03–11*, Mar. 2003.

[73] H.K. Aghajan, B.H. Khalaj, and T. Kailath, "Estimation of multiple 2-D uniform motions by SLIDE : Subspace-based line detection," *IEEE Transactions on Image Processing*, vol. 8, no. 4, pp. 517-526, Apr. 1999.

[74] R. O. Schmidt, "Multiple emitter location and signal parameter estimation," *IEEE Transactions on Antennas and Propagation*, vol. 34, no. 3, pp. 276-280, March 1986.

[75] J. Marot and S. Bourennane, "Propagator method for an application to contour estimation," *Pattern Recognition Letters*, vol. 28, no. 12, pp. 1556-1562, Sept. 2007.

[76] S. Bourennane and J. Marot, "Coutour estimation by array processing methods," *EURASIP Journal on Applied Signal Processing*, vol. 2006, Article ID 95634, pp. 1-15, 2006.

[77] P. R. Thrift and S. M. Dunn, "Approximating point-set images by line segments using a variation of the Hough tranform," *Computer Vision Graphics Image Processing*, vol. 21, pp. 383-394, 1983.

[78] H. Jiang, S. Bourennane and C. Fossati, "High-resolution algorithm for image segmentation in the presence of correlated noise," *Journal of Electrical and Computer Engineering*, vol. 2010, Article ID 630768, 6 pages, 2010.

[79] M. Wax and T. Kailath, "Detection of signals by information theoretic criteria," *IEEE Transactions on Acoustics, Speech, and Signal Processing*, vol. 33, no. 2, pp. 387-392, 1985.

[80] J. Borkowski, B. J. Matuszewski, J. Mroczka, and L. K. Shark, "Geometric matching of circular features by least-squares fitting," *Pattern Recognition Letter*, no. 23, pp. 885–894, 2001.

[81] S. H. Chiu and J. J. Liaw, "An effective voting method for circle detection," *Patten Recognition Letters*, no. 26, pp. 121-133, 2005.

[82] S. Bourennane and J. Marot, "Line parameters estimation by array processing methods," *IEEE International Conference on Acoustics, Speech, and Signal Processing*, vol. 4, pp. 965-968,Mar. 2005.

[83] J. Marot and S. Bourennane, "Array processing for intersecting circle retrieval," *Proceeding of* 16^{th} *European Signal processing Conference*, 5 pages, Aug. 2008.

[84] S. Van Huffel, H. Park, and J. B. Rosen, "Formulation and solution of structured total least norm problems for parameter estimation," *IEEE Transactions Signal Processing*, vol. 44, pp. 2464-2474, Oct. 1996.

[85] R. Takiyama, N. Ono, "A least square error estimation of the center and radii of concentric arcs," *Pattern Recognition Letters*, vol. 10, no. 4, pp. 237-242, Oct. 1989.

[86] H. Jiang, J. Marot, C. Fossati, and S. Bourennane, "Strongly concave contour star-shaped contour characterization by algebra tools", *Signal Processing*, Accepted, Sept. 2011.

[87] S.M.R. Dehak, I. Bloch, and H. Maitre, "Spatial reasoning with incomplete information on relative positioning," *IEEE Transactions on Pattern Analysis and Machine Intelligence*, vol. 27, no. 9, pp. 1473 - 1484, 2005.

[88] I. Bloch, "Fuzzy relative position between objects in image processing : a morphological approach," *IEEE Transactions on Pattern Analysis and Machine Intelligence*, vol. 21, no. 7, pp. 657 - 664, 1999.

[89] S. Gao and T. D. Bui, "Image segmentation and selective smoothing by using mumford-shah model," *IEEE Transactions on Image Processing*, vol. 14, no. 10, pp. 1537-1549, Oct. 2005.

[90] S. Krinidis and V. Chatzis, "Fuzzy energy-based active contours," *IEEE Transactions on Image Processing*, vol. 18, no. 12, pp. 2747 - 2755, 2009.

[91] K.P. Philip, E.L. Dove, D.D. McPherson, N.L. Gotteiner, W. Stanford, and K.B. Chandran, "The fuzzy Hough transform-feature extraction in medical images," *IEEE Transactions on Medical Imaging*, vol. 13, no. 2, pp. 235 - 240, 1994.

[92] N. Kiryati and A. M. Bruckstein, "What's in a set of points ? [straight line fitting]," *IEEE Transactions on Pattern Analysis and Machine Intelligence*, vol. 14, no. 4, pp. 496-500, Apr. 92.

[93] S. Bourennane, C. Fossati, and J. Marot, "Contour estimation in image using virtual signal," *Optical Engineering*, Opt. Eng. 49, 057002, May 2010.

[94] M. Lynch, O. Ghita, and P.F. Whelan, "Segmentation of the left ventricle of the heart in 3-D+t MRI data using an optimized nonrigid temporal model," *IEEE Transactions on Medical Imaging*, vol. 27, no. 2, pp. 195 - 203, 2008.

[95] J. Lowell, A. Hunter, D. Steel, A. Basu, R. Ryder, E. Fletcher, and L. Kennedy, "Optic nerve head segmentation," *IEEE Transactions on Biomedical Engineering*, vol. 23, no. 2, pp. 256 - 264, 2004.

[96] R. Bock, J. Maier, L. G. Nyul, J. Hornegger, and G. Michelson, "Glaucoma risk index : Automated glaucoma detection from color fundus images," *Medical Image Analysis*, vol. 14, pp. 471-481, Jan. 2010.

[97] P. Tsakanikas and E. S. Manolakos, "Active contours based segmentation of 2DGE proteomics images," *The 16th European Signal Processing Conference*, Lausanne, 2008.

[98] H. Jiang, J. Marot, C. Fossati, and S. Bourennane, "Fuzzy contour characterization by subspace based methods of array processing and DIRECT method," in *The 18th European Signal Processing Conference*, 5 pages, Aug. 2010.

[99] H. Jiang, J. Marot, C. Fossati, and S. Bourennane, "Fuzzy triangle contour characterization by subspace based methods of array processing," in *Procceding of IEEE Workshop on Sensor Array and Multichannel Signal Processing*, Israël, Oct. 2010.

[100] H. Jiang, J. Marot, C. Fossati, and S. Bourennane, "Circular contour retrieval in real-world conditions by higher order statistics and an alternating least squares algorithm," *EURASIP Journal on Advances in Signal Processing.* Minor revision. 2011.

[101] H. Chao, W.S. Kerwin, T.S. Hatsukami, H. Jenq-Neng, and Y. Chun, "Detecting objects in image sequences using rule-based control in an active contour model," *IEEE Transactions on Biomedical Engineering*, vol. 50, no. 6, pp. 705 - 710, 2003.

[102] F. Sachse, G. Seemann, B. Delhay, P. Clarysse, and I. Magnin, "Locally adapted spatio-temporal deformation model for dense motion estimation in periodic cardiac image sequences," *Functional Imaging and Modeling of the Heart, Lecture Notes in Computer Science*, Springer Berlin / Heidelberg, pp. 393-402, 2007.

[103] P. Vandewalle, L. Sbaiz, J. Vandewalle, and M. Vetterli, "Super-resolution from unregistered and totally aliased signals using subspace methods," *IEEE Transactions on Signal Processing*, vol. 55, no. 7, part 2. pp. 3687 - 3703, Feb. 2007.

[104] M. Frikel and S. Bourennane, "High-resolution methods without eigendecomposition for locating the acoustic sources," *Applied Acoustics*, vol. 52, no. 2, pp. 139-154, 1997.

[105] N. Gonzalez, G. Molina-Terriza, J. P. Torres, "How a Dove prism transforms the orbital angular momentum of a light beam," *Optical Express*, vol. 14, no. 20, pp. 9093-9102, Oct. 2006.

RÉSUMÉ :

La description de formes est un objectif important de la vision par ordinateur et du traitement d'image, en particulier, pour les contours linéaires, triangulaires et circulaires. L'objectif visé par cette thèse est d'aboutir à des méthodes de détection et de caractérisation de contours en exploitant les méthodes haute résolution du traitement d'antenne, qui sont fondées sur des méthodes à sous-espaces. Nous adaptons un formalisme original pour générer des signaux qui suivent un modèle du traitement d'antenne en simulant la propagation d'une onde. Un modèle pour une image conduit à un modèle adéquat pour le signal généré à partir de cette image sur des capteurs virtuels, et les méthodes haute résolution du traitement d'antenne sont adaptées pour estimer les paramètres de contours. En particulier, le cas où l'image est dégradée par un bruit corrélé est considéré, et des statistiques d'ordre supérieur sont adaptées pour estimer les paramètres des contours. Ensuite, nous considérons l'estimation de contours étoilés en émettant l'hypothèse que les coordonnées radiales des pixels du contour s'expriment comme une somme de sinusoïdes amorties. En partant d'un cercle d'initialisation, la méthode proposée estime les déviations des coordonnées radiales des pixels autour du cercle d'initialisation, avec une méthode qui est robuste au bruit et aux fortes concavités. Nous incluons une étape de raffinement fondée sur une méthode d'optimisation, qui améliore l'adéquation des signaux générés au modèle proposé. Finalement, des contours flous sont étudiés. Ils sont modélisés par une distribution Gaussienne de niveaux de gris. Un modèle de signal correspondant à un contour flou est calculé. Ainsi, nous proposons une approche nouvelle pour détecter des contours flous par les méthodes à sous-espaces du traitement d'antenne. Des algorithmes d'optimisation sont aussi adaptés pour estimer certains paramètres des contours, tel que l'étendue.

TITRE : DÉTECTION ET CARACTÉRISATION DE CONTOURS DANS DES IMAGES PAR LES MÉTHODES À SOUS-ESPACES

ABSTRACT :

Shape description is an important goal of computational vision and image processing, especially for linear, triangular and circular features. This thesis aims mainly at detecting and characterizing contours by exploiting high resolution subspace-based methods. We adapt an original formalism to generate array signals from an image by simulating wave propagation. After modelling the image data, subspace-based high-resolution methods are used for estimating the parameters. In particular, the environment with correlated Gaussian noise is considered, and higher-order statistics methods are proposed to estimate contour's parameters. Then, we discuss the problem of recovering a star-shaped contour with the assumption that the contour coordinates can be decomposed into damped sinusoids. Starting from an initialization circle, the proposed method estimates the deviations of the pixel coordinates around an initialization circle with a method which copes with noise and strongly concave contours. We include a refinement step based on an optimization method which improves the adequation of the collected signals to the proposed model. At last, blurred contours with Gaussian distribution of grey level value are also investigated. We derive a signal processing model out of an image which contains a blurred contour, and provide a new viewpoint to detect blurred contours for the first time by subspace-based methods of array processing. Optimization algorithms are also adapted to estimate the parameters.

DISCIPLINE : Optique, Photonique et Traitement d'Image.

MOTS-CLÉS : Contour, Détection, Caracterisation, Haute résolution, Cumulants, Contour flou, Traitement d'antenne, Optimisation, Contour linéaire, Contour triangulaire, Contour circulaire, Approximation.

Adresse :

Institut Fresnel, UMR CNRS 6133, Ecole Centrale Marseille et Université Paul Cézanne (Aix-Marseille III),
D.U. de Saint Jérôme, 13397 Marseille - France.